Stellar Winds in Interaction

Proceedings of the international ProAm workshop on stellar winds
Convento da Arrábida, Portugal 2010 May 29 - June 2

Editors: Thomas Eversberg & Johan H. Knapen

Contents

Preface: Stellar Winds in Interaction

December 1, 2010

We are presently in the "Golden Age of Astronomy". Professional telescopes reached the 10 m limit and semi-conductors displaced chemicals-based data acquisition in the form of photographic plates. This also influences amateur astronomy. Technical equipment becomes much cheaper and telescope apertures of the order of 40 cm are no longer an exception. The amateur can thus in principle use the same technologies as the professional astronomer and since the early 1990s many advanced amateur astronomers have discovered the field of stellar spectroscopy.

There is an important gap in professional astronomy which can be filled by amateur astronomers and their smaller telescopes. Some stellar phenomena need longer time coverage, of order, e.g., some weeks. This is especially valid for binary stars. One such interesting target is WR 140, a WR+O binary with a highly eccentric orbit and a period of about 8 years. The observation of its periastron passage in the visible wavelength range is valuable for measurements in other wavelength domains to understand the wind-wind interaction of both components and the global geometry and physics of the system. For this and some other massive star targets, a group of amateur and professional astronomers wrote a successful proposal for 116 nights at the 50 cm Mons telescope at Teide observatory on Tenerife, supported by the Instituto de Astrofísica de Canarias (IAC). The group of observers was a mix of enthusiastic astronomers from various professions (e.g., physicists, a physics student, a chemist, a physician, a schoolboy, a pilot) but they all have been experienced observers. A concluding meeting for first-hand presentations took place at the Convento da Arrabida, an old monastery close to Lisbon in Portugal, from May 29 to June 2, 2010. Many campaign participants came together and discussed results of X-ray, visual, IR and radio observations, as well as aspects of future ProAm campaigns. These proceedings contain the written version of most of the presentations at the workshop, and highlight some of the initial results of our campaign.

As a direct consequence of our meeting we established the new ProAm Convento Group (www.stsci.de/convento) which will support future collaborations between amateur and professional astronomers.

Thomas Eversberg

Tony Moffat

Berthold Stober

Lothar Schanne

Hot colliding winds and the 2009 campaign on WR140

Anthony F. J. Moffat

Département de physique, Université de Montréal,
and Centre de Recherche en Astrophysique du Québec,
C.P. 6128, Succ. Centre-Ville, Montréal, QC, H3C 3J7, Canada

Abstract: WR140 (WC7pd + O5) is often considered to be the archetype of hot, luminous colliding-wind binaries, with strong cyclic high-energy and dust-formation events. The challenge is that this system is quite extreme, with a long period (nearly an integral 7.94 years) and high eccentricity (e = 0.88). Most of the action thus occurs during the relatively short several-month interval of close periastron passage, which in the most recent 2009 January passage occurred during the northern winter months when this summer Cygnus star was least favourably placed in the sky for groundbased observation. To meet this challenge, various multiwavelength campaigns were organized at different sites and from space, mainly within several months of periastron passage 2009. Of particular interest to this workshop was the MONS optical spectroscopic effort, involving both amateur and professional astronomers at the MONS site on Tenerife from 2008 December through 2009 March. I will describe WR140 in terms of the general phenomenon of hot colliding winds and leave the new campaign details to other speakers at this workshop.

1 Preamble

Among high-energy phenomena in the Universe, colliding winds (CWs) occupy a prominent place. While they are not in the highest-energy category (MeV and higher, e.g. gamma rays) associated with relatively rare events such as supernovae (SNe) and gamma-ray bursts (GRB), CWs produce energies in the several keV range (e.g. X-rays, corresponding to temperatures of several tens of million Kelvins) as stellar winds at velocities of order 1000 km/s collide head-on. They are quite common, occurring in essentially all binaries (themselves very frequent) containing massive stars with strong, fast winds and in young regions of high stellar density, where multiple winds collide to produce hot intra-cluster gas. This article deals only with binaries.

2 Massive stars

What is meant by a "massive" star? Normally one takes massive stars to be those stars with initial masses above 8 M_{Sun}. Such stars can, in their cores, nuclearly "burn" H into He, He to C, etc., and finally ending up with Fe, at which point no more energy can be extracted from this process and they end their lives violently as core-collapse supernova (ccsn) (or even earlier as pair-instability supernova - pisn - for the most massive objects). The former (ccsn) leave neutron stars (NS)or black holes (BH, for more massive progenitors), while the latter (pisn) blows the whole star apart. What distinguishes massive from other stars, besides their hot temperatures (during most of their lifetime) and extremely

high luminosities, is their ability to drive off matter in the form of strong stellar winds. While the Sun has a prominent wind of particles with typical speeds of c. 500 km/s, its mass-loss rate is relatively low [c. 10^{-14} M_{Sun}/yr]. Only massive stars can produce high-speed (up to 5000 km/s), dense outflows [up to 10^{-4} M_{Sun}/yr], driven by the radiation pressure of their extreme luminosities. Hence, despite their rarity, massive stars are the main drivers of the ecology of the Universe, via both stellar winds during their whole lifetimes with an ever richer mix of heavier elements the more the star evolves, and their SN explosions. Normally, the winds are strongest towards the end of their evolution, just before the SN explosion. This occurs during the core He-burning Wolf-Rayet (WR) stage (subsequent rapid core burning even up to Fe can also be occurring without being noticed at the stellar surface before it is too late), which lasts about 10% of the star's whole lifetime. For WR stars the mass-loss rates are typically at least an order of magnitude higher than their core H-burning O-star progenitors. Within the WR stage, the WN phase reveals H-burning products (mainly He and N) in its wind, while the subsequent WC or WO phase reveals C- and O-rich winds from core He-burning.

3   Massive binaries

The majority (possibly even the entirety at birth) of massive stars are found in multiple systems, with binaries the most frequent and most stable configuration. Among these massive binaries, one recognizes two grand classes (Vanbeveren, Van Rensbergen & De Loore 1998): (1) non-interacting, with initial periods $P \geq P_{\text{c}} = 10$ years, and (2) interacting, with $P \leq P_{\text{c}}$. The former (1) behave essentially like two single stars, such that neither star in the binary expands enough in its evolution to spill over its Roche lobe overflow (RLOF) onto the companion. The latter (2) can produce RLOF (with some complications, e.g. stars above initial mass ~ 25 M_{Sun} never reach the large red supergiant stage, maxing out as much smaller LBVs, so Pc for them could be much smaller than 10 years), sooner for shorter initial periods, and even a common-envelope configuration for systems with the shortest periods and high mass ratios. But all massive binary systems can, in principal, produce CWs, which is the subject of the rest of this article, although the impact diminishes roughly as the inverse separation of the two stars.

It is interesting to ponder what one would miss if it weren't for massive binaries, particularly of the interacting kind. Following Moffat (2008) these include: enhanced stellar X-rays, non-thermal radio emission, WR dust spirals, inverse mass-ratios, very rapid stellar spin, rejuvenation & blue stragglers, enhanced dense-cluster dynamics, massive runaways, intermediate- & supermassive-BHs, gamma-ray bursts (GRB), and facilitating obtaining certain stellar parameters such as masses and sizes. Clearly the gain in information far exceeds a factor two, i.e. merely going from one to two stars!

As an example of the first phenomenon, X-rays are produced by shock thermalization of plasma flows, with $kT \sim m_p v^2/2$ (k is the Boltzmann constant, T the temperature, m_{p} the proton mass, v the velocity of the gas that is stopped). This yields $T \sim 10^5$K for $v \sim 100$ km/s (e.g. internal shocks in hot winds) and $T \sim 10^7$ K for $v \sim 1000$ km/s (e.g. CWs in hot, luminous binaries). As for GRB, all extremely rare although detectable throughout the Universe, those of long duration are believed to involve a SN of type Ic (i.e. lacking H and He) in a rapidly rotating WC/O star, possibly spun up in a very short-period binary. Short GRB likely occur during the rapid final merging of a NS+NS or NS+BH system, resulting ultimately from previously exploded massive stars.

4   Colliding winds

In the simple case of two massive, hot luminous stars with winds in a binary, it is inevitable that the two winds will collide, no matter what the separation . For two spherically symmetric, uniform winds, the resulting collision will produce a shock cone defined primarily by a contact surface, where the rate of momentum transfer of each star's wind cancels vectorally. On either side of this surface, there will be a shock front of hot plasma associated with each star. The shape of the contact surface can be calculated algebraically (e.g. Usov 1992; Canto, Raga & Wilkin 1996) or numerically (e.g. Stevens et al. 1992 - see Fig. 1); basically it resembles a hyperbolic cone of rotation, rounded off at the apex, with its axis in the orbital plane pointing towards the star with the stronger wind. The cone opening angle depends in a predictable way on the ratio of the rate of momentum transfer of each star's wind, at the moment of contact (usually at terminal speed except in very close systems). The shape of the cone will change if the winds are not spherically symmetric, but we will not worry about that for the moment.
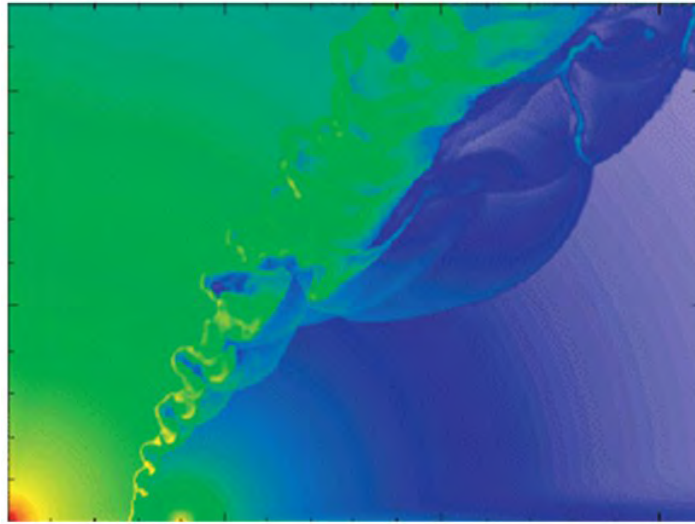

Figure 1: Numerical simulation of a WR (centred at left corner) + O (centred at 4th tick to the right) CW system (Pittard priv. comm.). Density decreases from red, yellow, green to blue.

The evidence for the existence of CWs has been somewhat slow in coming. However, we now know that CWs produce excess X-rays of higher energy than the stellar winds (although sometimes difficult to detect against the stars' own X-ray emission), non-thermal radio emission (from relativistic acceleration of electrons in the CW shocked region in a locally produced magnetic field), and excess line emission in the UV/optical/NIR (and even X-ray lines!). The strongest effects are seen in binaries containing at least one WR star, due to the very dense winds of these stars. The excess emission appears to fall off directly as the inverse of the orbital separation for large separations, where the interaction is adiabatic. For closer systems, where radiative effects are more prominent, the fall-off with separation is faster. Originally, X-ray and radio imaging was unresolved, but this is changing (to great benefit of constraining the geometry of the cones and the emission mechanism) with better telescopes (e.g. Chandra's 0.5 arcsec resolution or VLBI imaging). In the UV/optical/NIR, spectroscopy is not yet spatially resolved, although the spectroscopic Doppler effect effectively yields a kind of poor-man's resolution.

In some cases, one sees IR emission from warm carbon-based dust when the WR star is a carbon-rich WC. In the case of established binarity for many of these "dustars", the dust must somehow be formed in the CW shock zone, where compression factors are high and shielding from the lethal dust-

busting UV radiation occurs. But the exact process of dust formation remains a mystery, so any leads would be useful.

In fact, there are two classes of WC stars that form C-based dust: A. - WC+O binaries with WC of any subtype, although not all WC binaries do it. B. - cool WC stars (usually WC9, but also a few WC8), whose binary nature is suspected in a number of cases, but not yet firmly established as a unique source in all cases. Recent high spatial resolution work in the NIR/MIR has revealed that many dustars are surrounded by resolved pinwheels, clearly the result of hot emitting dust flowing out and cooling down along the shock cone, which is wrapping up as the binary turns. When the orbit is highly elliptic, as in the frequent case of long periods $\geq$ a year, the resulting spirals, although repeating faithfully from one turn to the next, appear broken in symmetry (see Fig. 2). One way to explain this is via misaligned axisymmetric CWs, which would lead to four directions of enhance dust, much as one sees in certain systems (Moffat, in prep.).
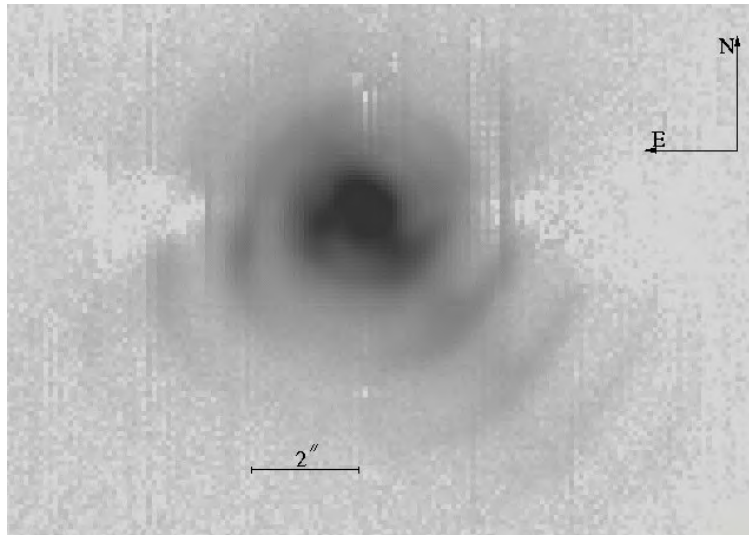

Figure 2: WC9d star WR112 imaged in the MIR, showing 5 successive dust spirals, although broken several times in azimuthal distribution (Marchenko & Moffat 2007).

5 The case of WR 140

Located in the Cygnus direction of the Milky Way at a distance of just under 2 kpc, WR140 = HD193793, WC7pd + O5 (with "p" referring to the WR star's peculiarly broad emission lines for its subtype and "d" referring to its dust-making), is the brightest WR star in the northern sky, whose binarity defied detection for many years until finally in the 1980s its long ($P = 7.94$ year), highly elliptical ($e = 0.88$) orbit was discovered. This allowed for a clear explanation of the NIR/MIR dust "event" first discovered in 1977, coinciding with the time just after periastron passage when the winds collide with the greatest force. Indeed, the next IR events repeated in 1985 and 1993, so a multi-wavelength campaign was organized to study the nest 2001 periastron passage (where most of the action occurs) in great detail. This included observational campaigns in the NIR, MIR, radio, X-ray and optical, all most intensely for several months on either side of periastron passage in mid February - a difficult time in mid winter to observe a summer object of modest declination (+40 degrees)! Of particular interest from that campaign and other recent data are: the high-resolution NIR/MIR images showing expanding arcs that repeat in the previous ejection (Williams et al. 2009); a resolved bow-shock head in non-thermal radio emission (see Fig. 3) coming up to, but dying away

as self absorption occurs near periastron (Doughtery et al. 2005); a general $\sim 1/D$ increase in X-ray flux towards and away from periastron, but with a narrow dip in X-ray flux just after periastron when the O-star eclipses the strongly X-ray emitting bow-shock head (Pollock et al. 2005); detection for the first time of optical emission-line excess in the density-sensitive line of CIII 5696A and the low-ionization line of HeI 5876A, giving constraints on the shock-cone properties, not to mention a vastly improved radial velocity (RV) orbit of both stars (see Fig. 4), along with mass-estimates of 50 and 19 $M_{\rm Sun}$ for the O and WR components, respectively (Marchenko et al. 2003). Optical broad-band monitoring also revealed several week-long, $\sim$0.1 mag deep dips over the 2-5 month interval after periastron; their colour dependence constrained the dust to be unexpectedly fine, with typical grain size 0.07 micrometres.
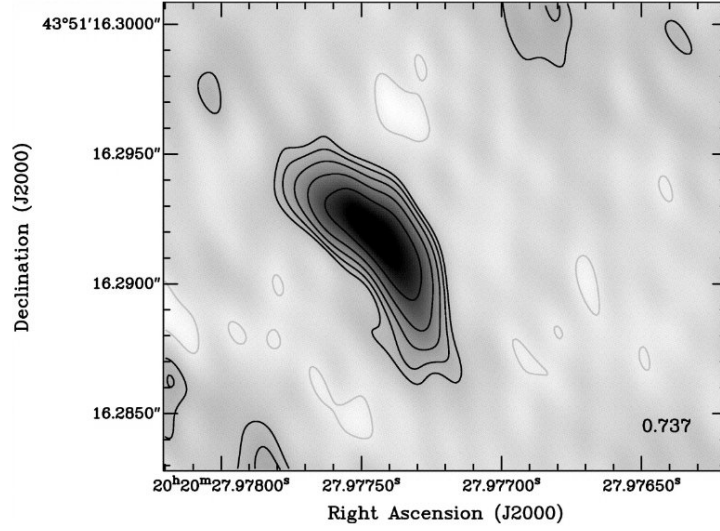

Figure 3: VLBI imaging snapshot of WR140 of the resolved bowshock head in non-thermal radio emission (Dougherty et al. 2005).
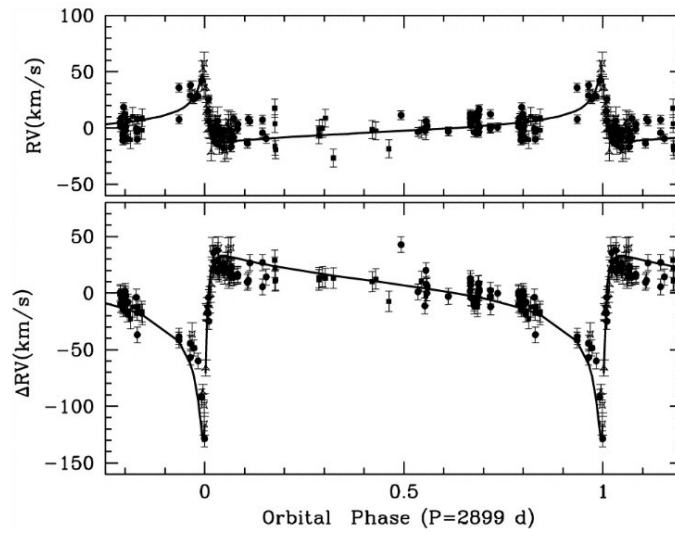

Figure 4: RV orbits of the two components (O star above, WR star below) of WR140 from the 2001 campaign (Marchenko et al. 2003).

6   Need for another WR140 campaign around periastron passage

While the 2001 campaign was a success, we were still working somewhat blindly and it did raise several questions. Most of all, we were amazed at how short the interval of optical emission-line excess was, leading to only a few points on the critical interval of ~2 months on either side of periastron. More intense coverage would be necessary in the next (2009) campaign to provide better constraints. It would also be useful to know if the dust dips in the optical light curve 2-5 months after periastron repeat exactly as before or are a stochastic phenomenon. We also needed denser IR coverage to constrain the shock-cone geometry, without which it will be difficult to trace the dust formation. Perhaps WR140 will eventually solve this infamous problem, given its high eccentricity and thus ability to probe CWs at a vast range of separations in the same system. Denser coverage is also required in X-ray imagery and spectroscopy and in radio imaging at multi frequencies.

Due to the near integer period in years of WR140, the 2009 periastron passage in mid January provided the same challenges as that of 2001. Basically, from the ground one will only be able to observe WR140 for a small portion of the night, the more periastron is approached from either side (evening just after sunset or morning just before sunrise). Therefore, to fill the rest of the night in the MONS campaign, we monitored other luminous hot stars that are known to vary on timescales (days-weeks) unique to such a campaign. These will be reported in later publications.

7   Conclusions

WR140 shows clear, intense CW action at all wavelengths during a short interval of its long orbit, centred on or slightly after periastron passage. Other articles in this series following this one will discuss the results found so far in the 2009 campaign.

References

Canto, J., Raga, A.C., Wilkin, F.P. 1996, ApJ, 469, 729

Dougherty, S.M., Beasley, A.J., Claussen, M.J., Zauderer, B.A., Bolingbroke, N.J. 2005, ApJ, 623, 447

Marchenko, SV, Moffat, A.F.J., et al. 2003, ApJ, 596, 1295

Marchenko, S.V., Moffat, A.F.J. 2007, in Massive Stars in Interactive Binaries, ASPC 367, p.213

Moffat, A.F.J. 2008, in Massive Stars as Cosmic Engines, proc. IAU Symp 250, p. 119

Pollock, A.M.T., Corcoran, M.F., Stevens, I.R., Williams, P.M. 2005, ApJ, 629, 482

Stevens, I.R., Blondin, J.M., Pollock, A.M.T. 1992, ApJ, 386, 265

Usov, V.V. 1992, ApJ, 389,635

Vanbeveren, D., Van Rensbergen W., De Loore, C. 1998, The Brightest Binaries, ApSpScRev, 232

Williams, P.M., Marchenko, S.V., Marston, A.P., Moffat, A.F.J., Varricatt, W.P., Dougherty, S.M., Kidger, M.R.,
        Morbidelli, L., Tapia, M. 2009, MNRAS, 395, 1749

The WR 140 periastron passage 2009: first results from MONS and other optical sources

R. Fahed[1], A. F. J. Moffat[1], J. Zorec[2], T. Eversberg[3], A. N. Chené[4],
F. Alves*, W. Arnold*, T. Bergmann*, L. F. Gouveia Carreira*, F. Marques Dias*,
A. Fernando*, J. Sanchez Gallego*, T. Hunger*, J. H. Knapen*, R. Leadbeater*,
T. Morel*, G. Rauw*, N. Reinecke*, J. Ribeiro*, N. Romeo*,
E. M. dos Santos*, L. Schanne*, O. Stahl*, Ba. Stober*, Be. Stober*,
N. G. Correia Viegas*, K. Vollmann*, M. F. Corcoran*, S. M. Dougherty*,
J. M. Pittard*, A. M. T. Pollock*, and P. M. Williams*

[1] Université de Montréal, Montréal, Canada
[2] Institut dastrophysique de Paris, Paris, France
[3] Schnörringen Telescope Science Institute, Köln, Germany
[4] Herzberg Institute of Astrophysics, Victoria, Canada
* MONS pro-am collaboration

Abstract: We present the results from the spectroscopic follow-up of WR140 (WC7 + O4-5) during its last periastron passage in January 2009. This object is known as the archetype of colliding wind binaries and has a relatively large period ($\sim$ 8 years) and eccentricity ($\sim$ 0.89). We provide updated values for the orbital parameters, new estimates for the WR and O star masses and new constraints on the mass-loss rates.

1   Introduction

WR140 is a very eccentric WC7+O5 colliding-wind binary (CWB) system with an eccentricity of 0.89 and a long period of 7.94 years. It is also the brightest Wolf-Rayet star in the northern hemisphere and is considered as the archetype of CWB. We present here the results from a spectroscopic follow-up, unique in time coverage and resolution. The observation campaign was a worldwide collaboration involving professional and amateur astronomers and took place during a period of 4 months around periastron passage in January 2009.

2   Observations

Among the amateur data, we first have the MONS project: under the leadership of Thomas Eversberg, a German amateur astronomer who has founded his own astronomical observatory (the Schnörringen

Table 1: List of the different sources in the 2009 campaign.

Observatory	Dates	Wavelength Range (Å)	Resolution (Å/ pixel)	Number of spectra
Tenerife	1.12.08 - 23.03.09	5530-6000	0.35	34
OHP	12.12.08 - 23.3.09	4000-6800	0.01	63
DAO	22.4.08 - 9.1.09	5350-5900	0.37	13
OMM	5.7.09 - 8.8.09	4500-6000	0.63	18
Robin Leadbeater	10.12.07 - 20.3.09	5600-6000	0.68	38
Berthold Stober	26.8.08 - 29.2.09	5500-6100	0.53	12

Telescope Science Institute), a LHIRES spectrograph was installed on a telescope now owned by the Instituto de Astrofísica de Canarias (IAC), but previously by the University of Mons (Belgium) and which is used mainly for pedagogical purposes. The 50 cm telescope is located at the Teide observatory of the IAC in Tenerife. During four months, data have been acquired with this instrument. Other amateurs contributed using their own personal instruments in Portugal, Germany and England.

The professional data were obtained with the echelle spectrograph SOPHIE at the Observatoire de Haute Provence (OHP), at the Dominion Astrophysical Observatory (DAO) and at the Observatoire du Mont Mégantic (OMM). A list of the data sources and characteristics of the campaign is presented Table 1.

3   Radial velocities

The WR star radial velocities were measured by cross correlation with a reference spectrum and the O star radial velocities by measuring the centroid of the photospheric absorption lines (see Fig. 1). We notably find a higher eccentricity than previously published ($e = 0.896 \pm 0.002$ cf. 0.881 ± 0.005 from Marchenko et al. 2003 = M03) and update the value for the period (2896.5 ± 0.7 d instead of 2899.0 ± 1.3 d).

4   Excess emission

The presence of a shock cone around the O star induces an excess emission that we measured on the C III 5696 flat-top line. This excess emission appears first, just before periastron passage, on the blue side of the line, and then moves quickly to the red side, just after periastron passage, before it disappears (Fig. 2). We fitted the radial velocity and the width of this excess as a function of orbital phase using a simple geometric model (Luehrs 1997) taking into account the half opening angle of the shock cone θ, the velocity of the fluid along the cone v_{strm}, the orbital inclination i and an angular shift due to Coriolis forces $\delta\phi$ (see Fig. 3). The result of this fit is shown in Fig. 4. We find a value for the inclination of $52° \pm 8°$ (cf. $58° \pm 5°$ from Dougherty et al. 2005), which yields the following estimate for the stellar masses : $M_{\mathrm{WR}} = 18.4 \pm 1.8\, M_\odot$ and $M_{\mathrm{O}} = 45.1 \pm 4.4\, M_\odot$ (cf. $19\, M_\odot$ and $50\, M_\odot$ from M03). From the half opening angle of the shock cone (Canto et al. 1996), we also find a wind momentum ratio $\eta = 0.028 \pm 0.009$.
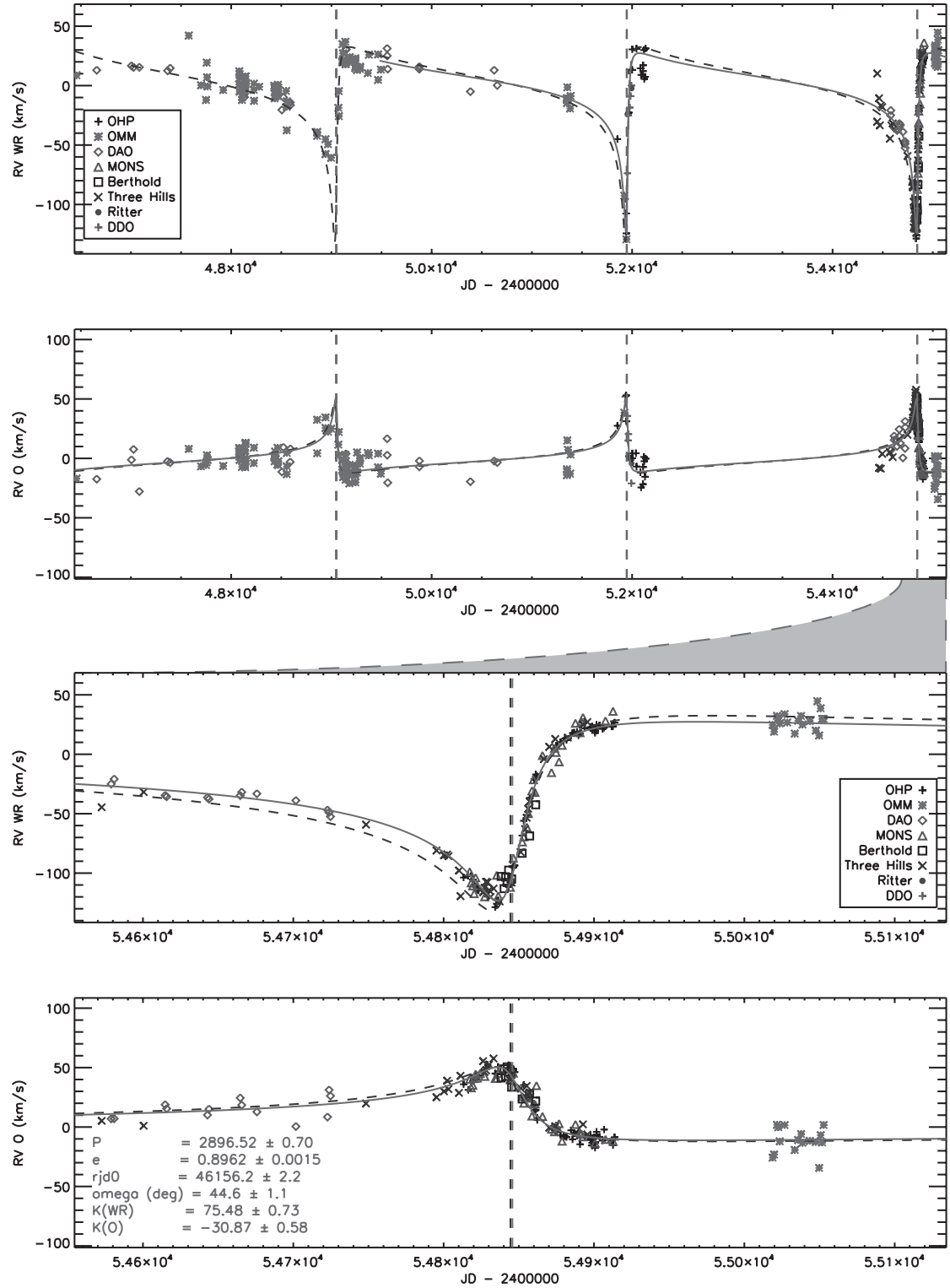
Figure 1: (Top two panels) Measured radial velocities of the WR star and of the O star together with the fit for the orbital solution (full line). We included data from the last periastron campaign in 2001 (M03). The black dashed line is the orbital solution from M03. The dashed vertical lines show the position of the periastron passage. (Bottom two panels) Same plots but zoomed in on the 2009 campaign. The best fit parameters are indicated in grey.
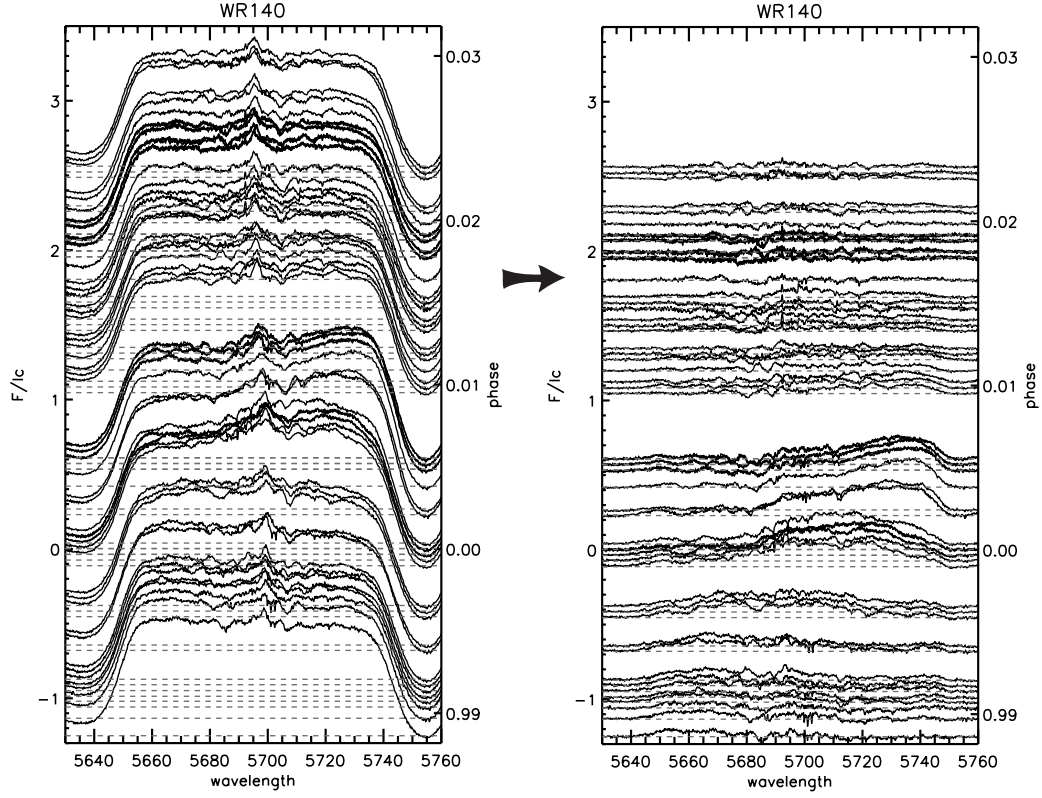
15

Figure 2: (Left) The CIII 5696 flat top line as a function of the orbital phase. (Right) Excess emission as a function of the phase, obtained by substraction of a reference profile, unaffected by wind collision.
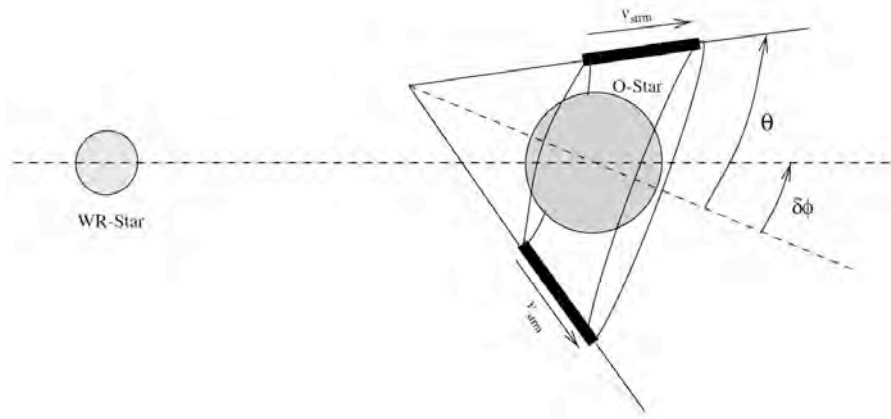

Figure 3: Schematic view of the geometric model by Luehrs (1997). The full width and radial velocity of the excess will then be given by : $\mathrm{FW_{ex}} = C_1 + 2\,v_{\mathrm{strm}}\sin(\theta)\sqrt{1 - \sin^2(i)\cos^2(\phi - \delta\phi)}$ and $\mathrm{RV_{ex}} = C_2 - v_{\mathrm{strm}}\cos(\theta)\sin(i)\cos(\phi - \delta\phi)$
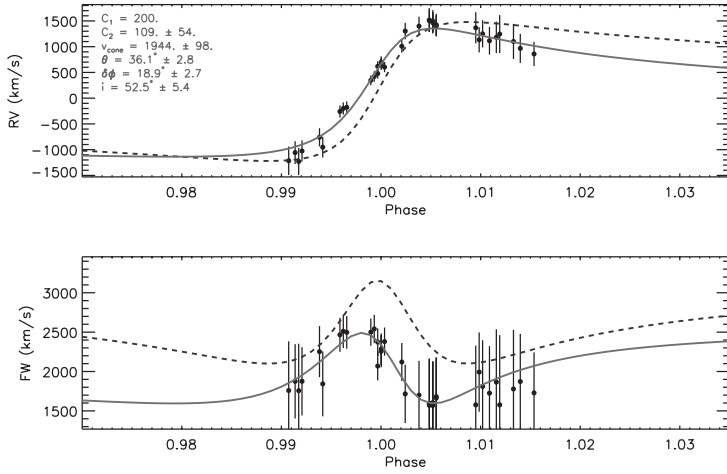
Figure 4: Fit of the radial velocity and width of the excess using the Luehrs (1997) model (full grey line). The black dashed line shows the solution from M03.
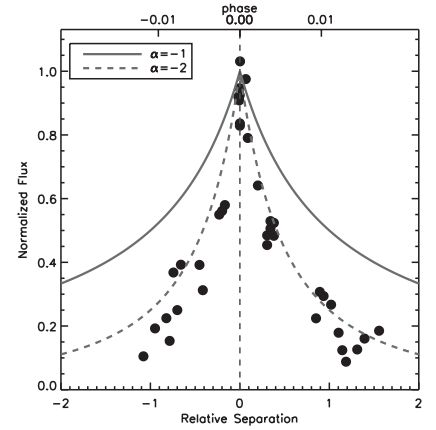

Figure 5: Normalized flux of the excess as a function of the relative separation of the two stars ($[d - d_{\min}]/d_{\min}$). The full line shows a d^{-1} dependancy, expected for an adiabatic emission process. The dashed line shows a d^{-2} dependency, possibly more in line with an isothermal process.

5 Conclusion

The 2009 periastron campaign on WR140 provided updated values for the orbital parameters, new estimates for the WR and O star masses and new constraints on the mass-loss rates. However, our capability to measure the shock cone parameters with confidence and to understand its underlying physics is limited by the over simplistic approach of our model. A more sophisticated theoretical investigation should be done. Meanwhile, the d^{-2} dependency of the excess, shown in Fig. 5, strongly suggests that some kind of isothermal process is involved here. Links with observations in other spectral domains (X-ray, infrared, and radio) will certainly provide valuable clues about the physics. Finally, we will attempt to isolate the WR spectrum from the O-star spectrum from our data in order to identify the spectral type of the latter more precisely. We also have some photometric and spectropolarimetric data to analyse to complete our view of this system.

References

Canto, J., Raga, A.C. & Wilkin, F.P., 1996, ApJ, 469, 729

Dougherty, S.M., Beasley, A.J., Claussen, M.J., Zauderer, B.A. & Bolingbroke, N.J., 2005, ApJ, 623, 447459.

Luehrs, S., 1997, PASP, 109, 504513.

Marchenko, S.V., Moffat, A.F.J., Ballereau, D., Chauville, J., Zorec, J., Hill, G.M., Annuk, K., Corral, L.J., Demers, H., Eenens, P.R.J., Panov, K.P., Seggewiss, W., Thomson, J.R. & Villar-Sbaffi, A., 2003, ApJ, 596, 12951304.

Remi Fahed

Ann & Tony Moffat

WR 140 in the Infrared

Peredur Williams

Institute for Astronomy, Royal Observatory, Edinburgh, UK

Abstract: Observations in the infrared have played a significant rôle in the development of our understanding of WR 140. Two sets of observations are described here: the changing profile of the 1.083-μm He I line observed for the 2009 campaign to study evolution of the wind-collision region near periastron passage, and multi-wavelength photometry and imaging of the dust made by WR 140 in previous periastron passages.

1   Introduction

In his contribution, Tony Moffat has described the properties of WR 140 (= HD 193793) and the motivation for the 2009 campaign. Fundamental to colliding-wind binaries is the power in their winds. The WC7 and O5 stars in WR 140 have fast (~ 3000 km^{-1}) winds carrying $\sim 2 \times 10^{-5}$ and $\sim 2 \times 10^{-6} M_\odot$ y^{-1} mass-loss respectively. The kinetic powers of these winds are in excess of 10^4 and $10^3 L_\odot$. Of these, $\sim 3 \times 10^3 L_\odot$ is dissipated where the winds collide (the wind-collision region, WCR), leading to shock-heating and compression of the plasma, X ray emission, synchrotron radio emission, changes to the profiles of some emission lines and condensation of 'dust' (really something like soot) in the shock-compressed wind. Of these effects, dust formation was certainly the most unexpected. The 1977 dust formation episode from WR 140 was independently discovered (Williams et al. 1977, 1978) at the 1.5-m Infrared Flux Collector (now the Carlos Sánchez Telescope) at Izaña on Tenerife – only a short distance from the Mons telescope.

From 1977 to the 2001 periastron, the thermal emission from dust made by WR 140 was tracked with infrared photometers at a variety of wavelengths between 1 and 20 μm and, in the years following the 2001 dust-formation episode, with infrared cameras which imaged the dust clouds. These observations have been published, but I will summarise the most recent work (Williams et al. 2009) to show how much we can learn from observing in this wavelength domain.

For the 2009 campaign, we (Watson Varricatt, Andy Adamson and the author) extended the observations of the 1.083-μm He I line taken around the 2001 periastron passage (Varicatt, Williams & Ashok 2004). This line has a P Cygni profile, with a flat-topped emission component like the λ5696 Å C III line observed in the optical campaign, and develops a strong sub-peak near periastron passage. Its absorption component varies as we observe the stars through different parts of the wind. The new observations were taken in 2008 with UIST on the United Kingdom Infrared Telescope (UKIRT) at a resolution of 200 km s^{-1} and comprise five spectra extending the coverage to earlier phases ($\phi =$ 0.93–0.95) and nine spectra near $\phi = 0.99$, when the WR 140 system was changing very rapidly.

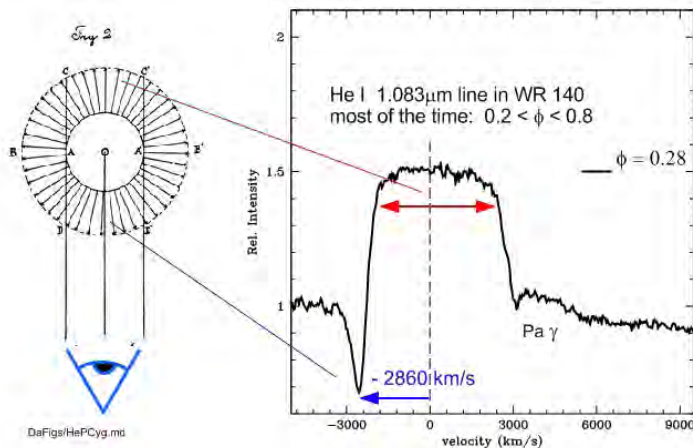Figure 1: P-Cygni profile of the He I 1.083-μm line for *most* of the orbit. The weak emission feature marked Paγ more probably comes from the hydrogenic He II and C IV transitions at this wavelength.
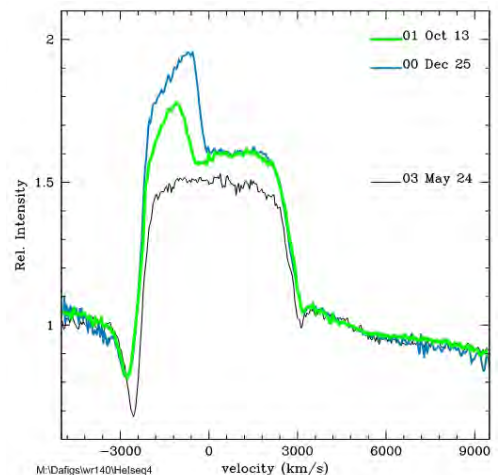

Figure 2: Profiles of the 1.083-μm line showing development of the sub-peak at phases 0.96 and 0.986.

2 Geometry of the WCR from the 1.083-μm He I line profile

Spectra of WR 140 in the region of the 1.083-μm He I line are shown in Figs 1[1] and 2. The first spectra of this line in WR 140 were taken in a programme to measure stellar wind terminal velocities, v_∞, and not near periastron. The profiles in Fig. 2 come from the study by Varricatt et al., and show rapid development of the sub-peak as WR 140 approached the 2001 periastron.

The WCR (Fig. 3) lies where the dynamic pressures of the WC7 and O5 stellar winds balance. Its shape can be calculated (e.g. Cantó, Raga & Wilkin 1996) from the ratio of the momenta of the two stellar winds, $\eta = (\dot{M}v_\infty)_{O5}/(\dot{M}v_\infty)_{WC7}$, and is closer to the O5 star because its mass-loss rate and wind momentum are much lower than that of the WC star. At large distances from the stars, the WCR can be approximated by a cone (opening angle θ), which is twisted to form a spiral in the orbital plane by the orbital motion. The pitch angle of the spiral depends on the ratio of the transverse velocity of the stars in their orbit relative to stellar wind velocities. In an elliptical orbit like that of WR 140, this ratio varies significantly (factor > 15), so the breadth of the spiral varies hugely round the orbit—a bit like a snake which has swallowed a large animal.

The WC7 and O5 stellar winds are shocked on each side of the WCR in regions which are wide if the shocks are adiabatic (most of the time in the case of WR 140) but very thin if the shocks are radiative (only around periastron). These shocks compress the winds, which flow along the WCR (only that of the WC7 star is shown in the figure). The compressed wind accelerates from the stagnation point to an asymptotic value, V_{flow}, on the 'conical' region of the WCR, and can be calculated from the stellar winds following Cantó et al. (1996). It is in the compressed WC7 stellar wind, comprising mostly helium and carbon ions, that we believe the He I and C III sub-peak emission features form.

What we observe in the line profile, in terms of sub-peak emission and absorption of the underlying stars, depends on our line of sight, which makes an angle ψ with the axis (WC7–O5) joining the stars. This viewing angle ψ varies round the orbit as $\cos\psi = -\sin i \sin(f + \omega)$, where ω is determined from the RV orbit, the inclination, i, comes from other observations, e.g. an astrometric orbit, and f is the true anomaly, the P.A. of the stars in their orbit. Owing to the high eccentricity of

---

[1]The sketch of an expanding stellar envelope showing where the absorption and emission components are formed dates from the first published interpretation of such a profile, in a nova spectrum in 1804, by Jakob Halm, of the Royal Observatory Edinburgh.
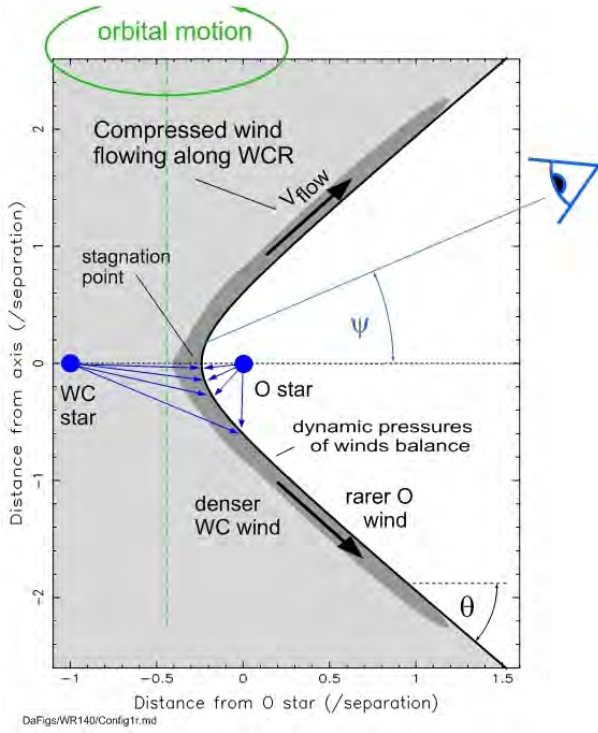
Figure 3: A slice through the WCR perpendicular to the orbital plane. The stars and WCR rotate about the vertical axis.
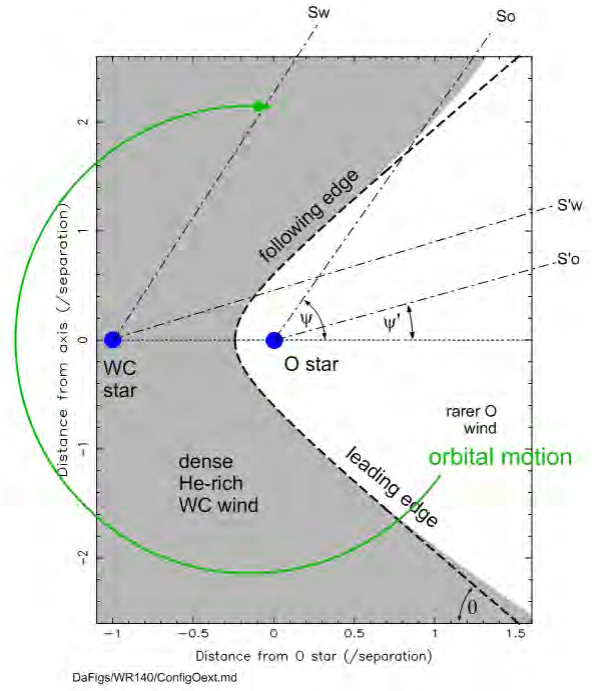

Figure 4: A view of the WCR in the plane including the observer, showing how the lines of sight to the stars vary with orbital phase.

the orbit, the variation of f with phase is very sensitive to the elements of the RV orbit. Work for this contribution used those of Marchenko et al. (2003), and some of the results may be different when they are re-calculated using the definitive orbit from the 2009 campaign.

The strength of the 1.083-μm absorption varies significantly (Figs 2 and 5). The underlying continuum comes from both the WC7 and O5 stars. In Fig. 4 we see the WCR from a different viewpoint: above the plane including the observer, to show how our sightlines S′o and So to the O5 star and S′w and Sw to the WC7 star change with the orbital motion. The WCR is asymmetric: as we move away from the stars, it lags behind the WC–O axis and cone because of the orbital motion, eventually to form the variable-width spiral. The stars and WCR move clockwise in this figure, so progressively later sightlines to the observer occur in the opposite sense. We see that the WC7 star is always viewed through some of its own wind, nearest the star. As this star is also the fainter component in the one-micron region, most of the variation observed in the 1.083-μm line absorption component must come from the variation in absorption to the O5 star. When the viewing angle is small, near conjunction (ψ' in Fig. 4), the O5 star is seen through its own wind (sightline S′o), which has one-tenth the density of the WC7 wind and a significantly lower helium abundance, so the absorption is at its lowest. This can be seen in Fig 5, where the absorption is least near conjunction (O5 star in front) and barely changes when we observe it through the O5 stellar wind alone between the first observation and $\phi = 0.985$, when it suddenly rises sharply. This must be the phase at which the following edge of the WCR crosses our sightline to the O5 star (Figs 4 and 6, i.e. when the viewing angle, $\psi \simeq \theta$, the cone angle, and we begin to observe the O5 star through the more opaque WC7 stellar wind. Modelling the sharp increase of absorption ('eclipse') must take account of the twisting of the WCR from the orbital motion, but we have a robust measure of the opening angle, θ = 50° using the Marchenko et al. (2003) RV orbit and i from Dougherty et al. (2005). This implies a wind-momentum ratio $\eta = 0.10$ and a comparable mass-loss ratio, given the similarity of the wind
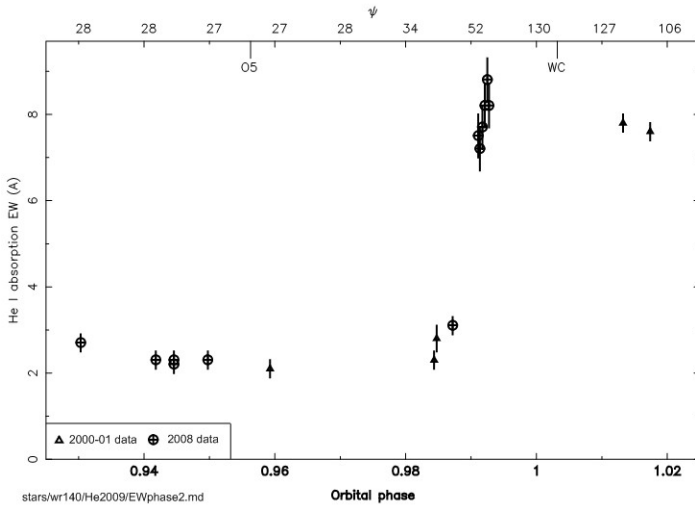
Figure 5: EW of absorption component as a function of phase near periastron. On top are the viewing angle, ψ, and phases of conjunction, 'O5' and 'WC', in front.
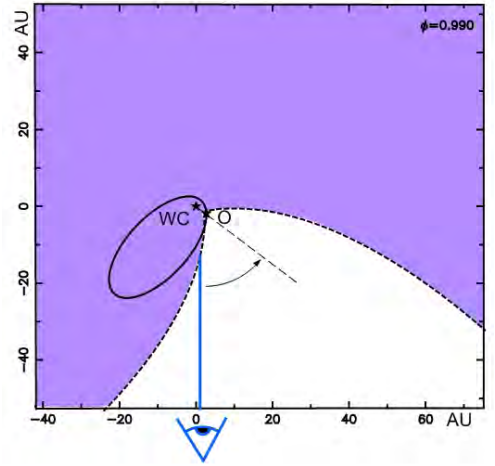

Figure 6: Sketch of the system at lower scale than Fig. 4 for beginning of eclipse at $\phi = 0.990$.

velocities.

Spectra from the 2009 campaign showing the subpeak evolution are shown in Figs 7 and 8. The first spectrum shows a blue-shifted symmetric profile, which barely changed as the system moved through conjunction (July and August spectra, not shown here). In December, the profile had shifted, broadened and become asymmetrical. Modelling these changes requires knowledge of the geometry of the WCR, to be derived from the stellar winds, the orbit and the changes in the absorption component, the bulk velocity of the compressed flow (e.g. calculated following Cantó et al. 1996) with the addition of an appropriate amount of turbulence, and then the line emissivity within the WCR, hopefully from the ever more sophisticated colliding wind models being calculated.

For a first pass, we can use the simplified geometry introduced by Lührs (1997), which considers only the conical region of the WCR, defined by θ, where the compressed flow velocity has reached its asymptotic value, V_{flow}. This requires only two parameters, which can be constant round the orbit, and has the further advantage that there is no need to know the location of the line emission or its spatial variation in the WCR. The down-wind spiral shape is modelled with a single tilt angle applied to the whole structure. This model has been successfully applied to model the sub-peaks in several system, mostly having almost circular orbits. The observed radial velocities of the sub-peak centre, RVc, and extent, ±RVext, can be related to the orbit via the viewing angle, ψ: RVc= $V_{\text{flow}} \cos(\theta) \cos(\psi)$ and RVext= $V_{\text{flow}} \sin(\theta) \sin(\psi)$.

We apply this to WR 140 using our value of θ from the absorption profile and V_{flow} calculated following Cantó et al. (1996) and show the variation of RVc, RVc+RVext and RVc−RVext with phase together with RVc and extents (vertical bars) from our observed profiles in Fig 9. The RVc curve reproduces the observed central velocities reasonably well, but overestimates the RV extents before periastron, and underestimates them afterwards. But when we come to calculate a line profile using the same model for the WCR, the fit (Fig. 10) is poor. Tuning parameters of the model does not improve the fit; nor is the twisting of the WCR from orbital motion likely to help: at $\phi = 0.94$, the transverse velocity is less than 2% of the wind velocities, and even less at earlier phases, which define the spiral at the time of observation[2].

---

[2]Because the shape of the WCR in the orbital plane depends on the ratio of transverse to wind flow velocities at preceeding phases, the shapes of the WCR at a particular phase interval before and after periastron will *not* be the same.
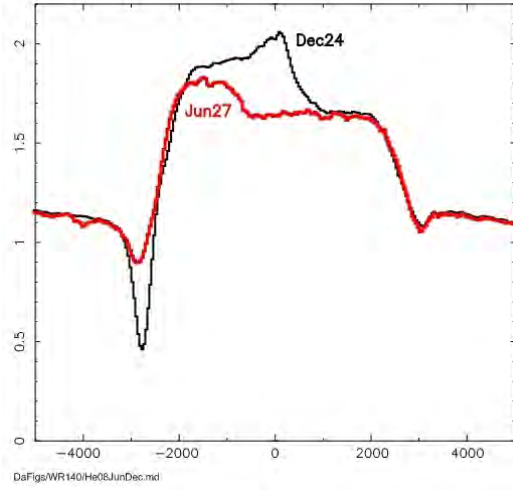
Figure 7: Spectra observed on 2008 June 27 and Dec. 24 showing change of sub-peak profile as well as its movement to more positive velocity.
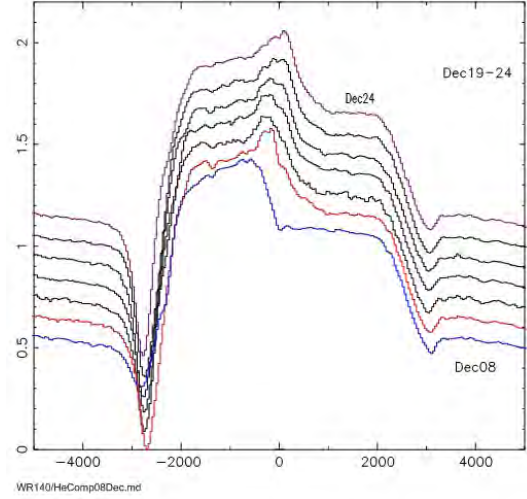

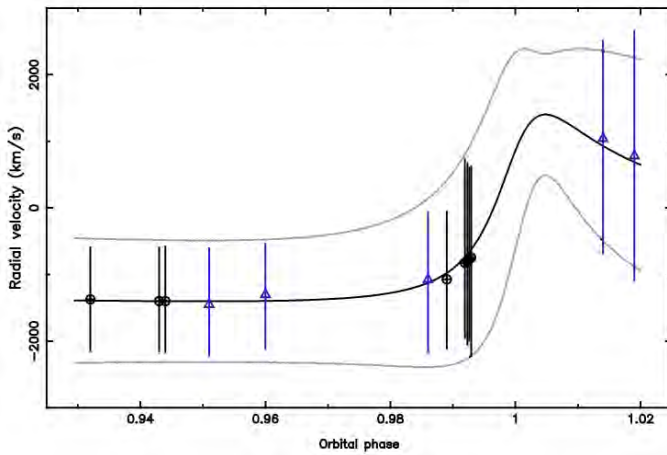Figure 8: Montage of spectra showing evolution of sub-peak profile in 2008 December.

Figure 9: Measured central velocities ($\oplus$, $\triangle$) and extents (vertical bars) of He I sub-peaks compared with RVc and RVc$\pm$RVext from a Lührs (1997) model.
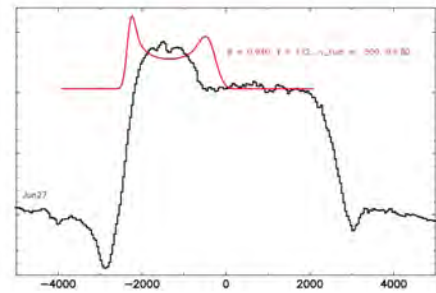

Figure 10: Model profile for sub-peak profile formed in a thin shell with same parameters. Central velocities match, but the profiles are totally different.
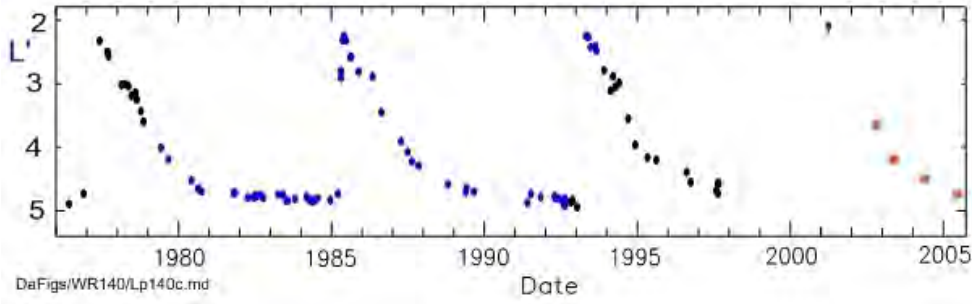
Figure 11: Light curve of WR 140 in L' (at 3.8μm); data points in orange are from IR images; others from photometers on UKIRT (blue) or the IRFC/TCS, SPM, TIRGO, and Calgary telescopes or published data (black).

Models including sub-peak line formation from the curved portion of the WCR, where wind is still accelerating, are more promising but require knowledge of the line emissivity with distance from the stagnation point, which requires detailed modelling of conditions in the WCR.

Returning to the observational data, it will be most interesting to compare the profiles of the 1.083-μm He I subpeaks with those observed on the 5696 Å C III line. Do the lines have similar profiles and central velocities? Is the variation of their intensity with, say, stellar separation the same? This will tell us whether they are formed in the same region of the WCR. These profiles and line shifts should also be compared with those the X-ray lines observed at high resolution (e.g. Pollock et al. 2005 and the present campaign) to build a self-consistent model of the WCR.

3 Infrared emission from dust made by WR 140

A dust grain located near a hot star with a strong stellar wind like WR 140 experiences three effects: heating by the stellar radiation, accelerative force from the stellar radiation and collision from ions in the stellar wind. The heated grain re-radiates at long wavelengths with a spectrum determined from the Planck function for its temperature and the wavelength-dependent grain emissivity law. There have been many laboratory experiments to make analogues of astronomical grains and measure their optical properties, and the best fits to WR star dust spectra come from amorphous carbon grains. Their emissivity laws have approximately the same wavelength dependence in the infrared, $\kappa \propto \lambda^{-1.1}$, so the grain temperature can be determined observationally. The spectrum of even a relatively small amount ($10^{-9} M_\odot$) of dust can readily be distinguished from that of a hot stellar wind using infrared observations at a few wavelengths between 1 and 10 μm, and the grain temperature and, less certainly, total mass of dust measured. From the grain's temperature, we can determine its distance from the star by considering the balance between its radiative heating and re-radiation because the heating depends on the geometric dilution of the stellar radiation field at the grain's distance. The equilibrium temperature T_{g} of a grain of radius a located at a distance r from a star of temperature T_* and radius R_* is related to these quantities through their Planck mean absorption cross-sections $\overline{Q}(a,T)$ appropriate to the grain or stellar temperature:

$$4\pi a^2 \overline{Q}(a, T_{\mathrm{g}}) T_{\mathrm{g}}^4 = \pi a^2 \overline{Q}(a, T_*) \frac{4\pi R_*^2 T_*^4}{4\pi r^2}$$

For small amorphous carbon grains relevant to WR dust, $\overline{Q}(a, T) \propto aT$, and we get a handy relation between the equilibrium temperature of a grain and its distance from a star: $T_{\mathrm{g}} \propto r^{-2/5}$. If the grain is too close to the star, its equilibrium temperature would be too high and it will evaporate;
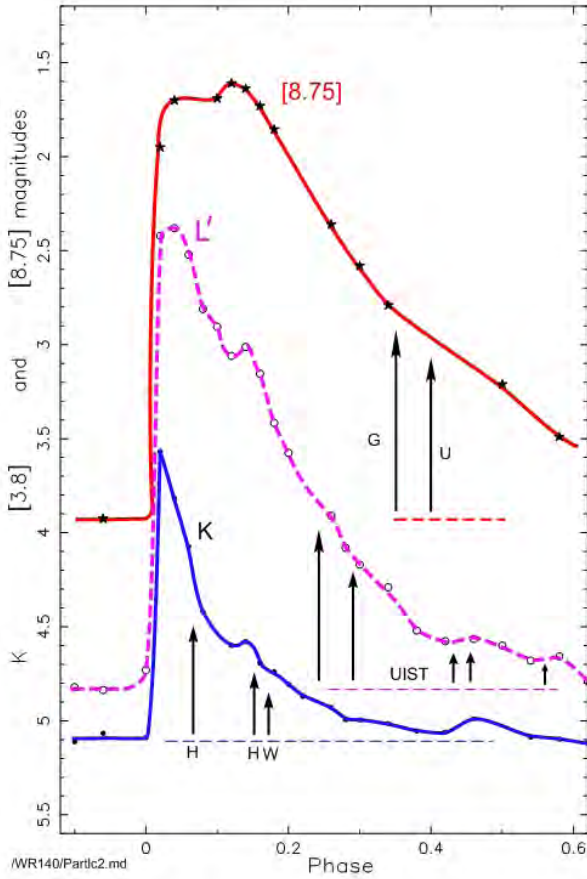
24

Figure 12: Light curves at 8.75μm, 3.8μm (L') and 2.2μm (K) near maximum, showing also phases of imaging observations (see text).
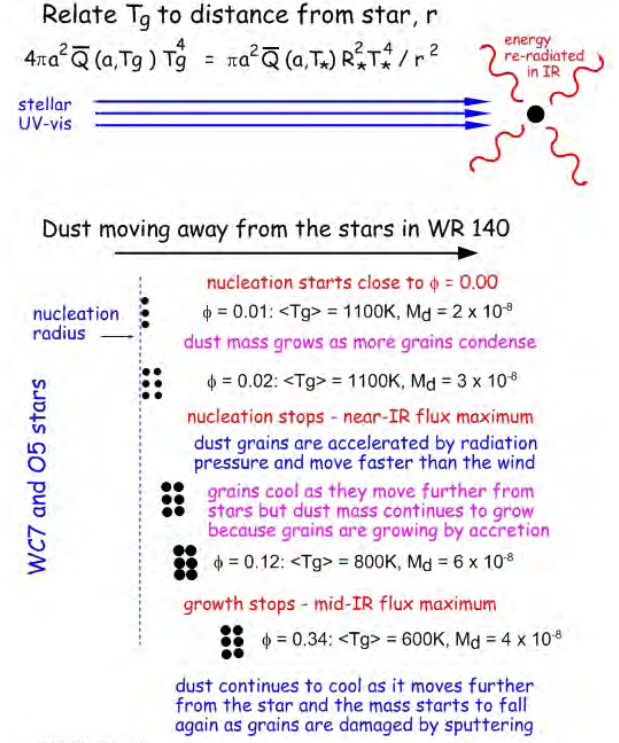

Figure 13: Cartoon of processes affecting the dust grains in the wind of WR 140

the corresponding distance is the closest at which grains can survive and is sometimes considered to be that at which they condense, the 'nucleation radius'. A grain moving away from a star with the stellar wind, say, will inevitably cool and its infrared emission will fade. It follows that if we observe constant infrared emission from a WR star, as is sometimes the case, the dust being taken away in the wind must be being replenished by the formation of new grains at the same rate.

In the case of WR 140, the L' light curve (Fig 11) shows repeated episodes of dust formation ($\Delta L'$ = 2.5), followed by fading of the emission as the grains move away from the stars. The wavelength of this curve (3.8 μm) is optimal for studying WR dust formation because the emission by newly formed dust having $T_{\mathrm{g}} \sim 1000 - 1200$ K peaks in this wavelength region, while the flux from the stellar photosphere and wind have fallen off sufficiently by this wavelength for the dust emission to be conspicuous. This light curve and those in H and K, give periods of 2905 ± 10 d, 2905 ± 8 d and 2900 ± 10 d, respectively, consistent with the RV orbit (2899 ± 1.3 d).

As the fading of the IR emission is caused by cooling of the dust as it moves away from the stars, we expect light curves at shorter wavelengths to have steeper delines than those at long wavelengths, and this is largely observed (Fig. 12), where we see the fading in K is steeper than that in L' while that at 8.75μm is less steep. But if this was the whole story, the light curves at all wavelengths would start fading at the same time, while the observations show that the flux maxima occur later at longer wavelengths; the 12.5-μm and 19.5-μm light curves resemble the 8.75-μm curve, and are even less steep.

From the multi-wavelength data, we can form spectral energy distributions (SEDs) for particular
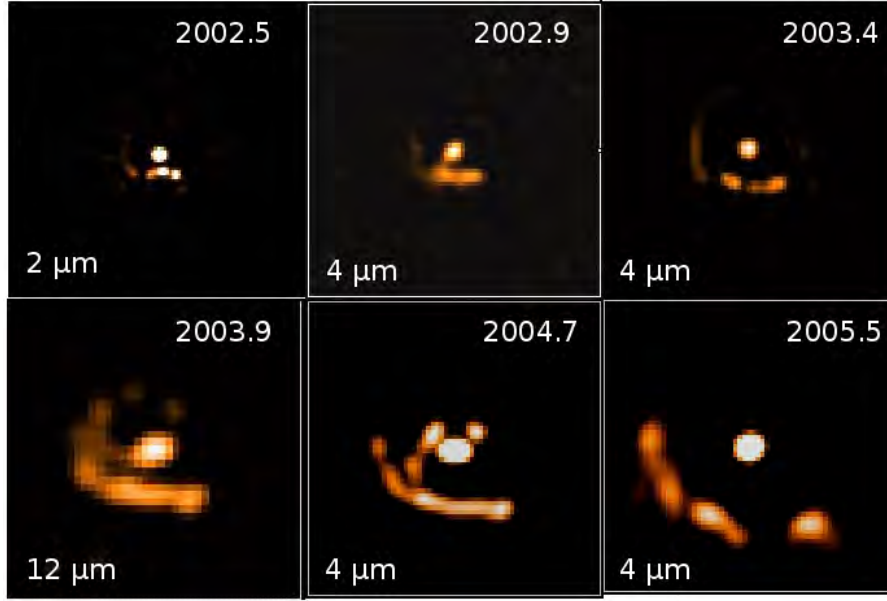
Figure 14: Infrared images of WR 140 all on the same scale, $4''$ square, with North at the top, East to the left, with dates and wavelengths of observations.

phases and model them to determine grain temperature and dust mass. The photometry tracks the integrated dust emission, so the temperature is an average, $\langle T_g \rangle$, of those of grains at different distances from the stars. Fits to the 1.6- to 19.5-μm and 1.6- to 12.5-μm data at phases 0.01 and 0.02 gave $\langle T_g \rangle \simeq 1100$ K and dust masses $M_d = 2 \times 10^{-8}$ and 3×10^{-8} $M_\odot$, respectively. The approximate constancy of $\langle T_g \rangle$, and therefore radiative-equilibrium distance from the stars, r, at these phases while the dust mass increased can be interpreted as continued condensation of new dust grains at a fixed distance from the stars, the 'nucleation radius'. At $\phi = 0.00$, we have only $JHKL'$ data and the fit to them gives $M_d \simeq 2 \times 10^{-10}$ $M_\odot$, so it is evident that dust formation had just begun at periastron. By $\phi = 0.03$, the $JHKL'$ magnitudes were fading and $\langle T_g \rangle$ was falling, indicating that no new dust was condensing to replenish the dust carried away with the wind. From $\phi = 0.03$ to $\phi = 0.12$, the near-IR flux fell while the mid-IR flux rose to maximum (Fig. 12). The model fits to the SEDs show that the dust mass doubled to 6×10^{-8} $M_\odot$ while $\langle T_g \rangle$ fell to 800 K at $\phi = 0.12$. This shows that the increase of dust mass was caused by the growth of the recently formed grains at their radiative equilibrium temperature rather than by the condensation of fresh grains at $T_g \simeq 1100$ K. This is summarised in a cartoon in Fig. 13. The grains can grow by implantation of carbon ions they collide with in the wind, and this process is greatly helped if the grains are forced to move through the wind by radiation pressure – which they certainly experience. Evidence for larger grains made in WR 140 comes from the eclipses observed in the optical light curves between phases 0.020 and 0.055 by Marchenko et al. (2003).

The K and L' light curves show an inflexion at $\phi = 0.14$, suggesting a short-lived increase in dust emission. The H photometry does not show any interuption in its fading at this phase, suggesting that the brightening at K and L' does not come from the condensation of new, hot dust but from a temporary increase in the growth rate of the grains already condensed.

After $\phi = 0.14$, the fading continues at all wavelengths and the dust cools as expected. The total mass, however, falls from its maximum of 6.5×10^{-8} $M_\odot$ to less than 3×10^{-8} $M_\odot$. It suggests that, as grains move through the wind, the rate of destruction by thermal sputtering eventually overtakes that of growth by implantation of carbon ions and grains are destroyed.

The light curves give valuable information on the integrated properties of the dust, including its
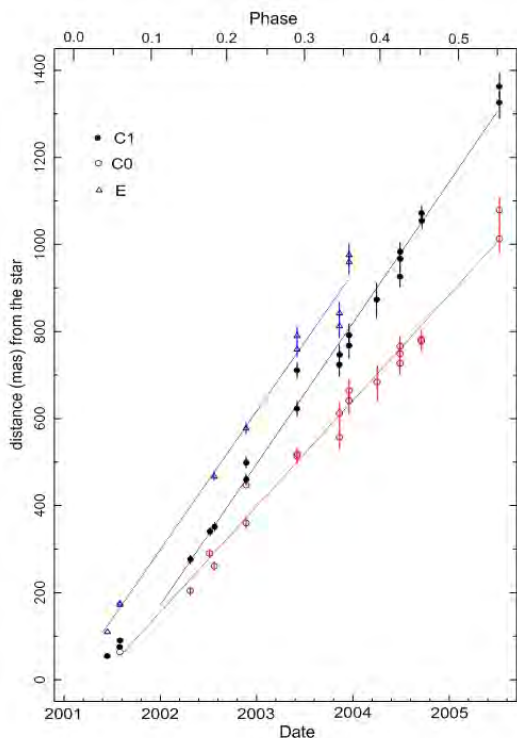
Figure 15: Radial distances (mas) of dust features (see text) against date and phase.
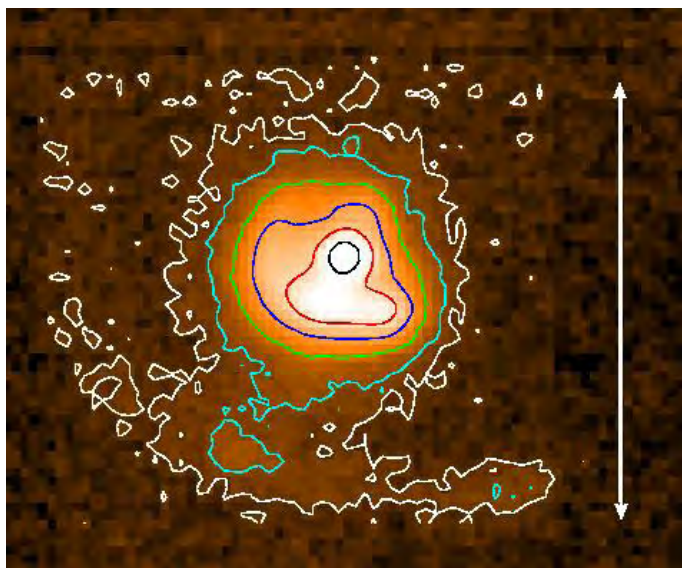

Figure 16: Combined 2003 November+December 12.5-μm image (5″ scale marker) at a more sensitive intensity scale than Fig. 14 to show the faint emission from the 1993 dust-formation episode to the south-east and south-west of the 2001 dust feature.

radial expansion, and are nicely complemented by imaging observations, which map the dust on the sky and allow us to relate it to the orbit. The dust emission by WR 140 was first imaged in 2001 (phases 0.04 and 0.06) by Monnier, Tuthill & Danchi (2002) with the Keck telescope. More images at wavelengths between 2.2 μm and 12.5 μm were observed in a multi-site campaign by Sergey Marchenko, Tony Marston, Tony Moffat, Watson Varricatt and the author using the Hale 5 m telescope, William Herschel Telescope (WHT), UKIRT and Gemini North with infrared cameras and, in some cases, adaptive optical systems. As the dust cooled, it was necessary to observe it at longer wavelengths. Details are given by Williams et al. (2009). The phases of the observations are marked on the light curves closest in wavelength to the images in Fig. 12 with 'H' (Hale), 'W' (WHT), 'U or UIST' (UKIRT) and 'G' (Gemini). A montage of images, all on the same scale, is presented in Fig. 14. We see dust features to the S and E of the stars (which are not resolved), expanding away from them. The features look like clumps but are better described as concentrations in extended emission with brightness enhanced by the maximum-entropy reconstruction processing of the images. (The two compact features close to the stars in the 2004.7 image are instrumental artefacts.)

The positions of persistent features, 'C' at the west end of the 'bar' to the south of the stars, 'C0' at the east end of the 'bar' and 'E' in the feature to the east, have been measured. The position angles of each are constant, showing radial motion, and the distances are plotted against date and phase in Fig. 15. Within the errors, the proper motions are constant, suggesting that the dust is moving into a 'clean' environment, presumably cleared by the O5 and WC stellar winds. Some of the long-wavelength images (Fig. 16) show dust features corresponding to 'C' and 'C0' but much further away—at distances which fit the extrapolated proper motions derived from the 2001 dust and their formation in the previous, 1993, periastron passage!

The constancy of the proper motions seems surprising given that the grains must experience radiation pressure: a 100 Å grain located 100 AU from the O5 and WC stars will gain 100 km s^{-1} in

velocity within one week. But as a grain accelerates to move faster than the wind, it experiences supersonic drag, which increases with the square of the velocity relative to the wind until the radiation pressure is balanced by the drag and the grain has a constant, 'drift', velocity relative to the wind. The expansion velocity of the dust is then the sum of V_{flow}, inherited from the compressed wind, and the drift velocity. Projection of the proper motions back to the stars suggests that feature 'E' was formed about 136 d (0.05 P) before 'C' and 'C0'.

The images allow us to separate photometry of the dust features from that of the stars and, when we have images at two wavelengths (e.g. 3.6 μm and 3.99 μm on UKIRT or 7.9 μm and 12.5 μm on Gemini), we can determine infrared colours. The results show that the dust features are 'redder' than the stars in ([3.6]–[3.99]), as expected from heated dust and stellar wind emission, but 'bluer' in ([7.9]–[12.5]). The latter may be surprising but is correct: at the time of the observations, the dust emission peaked at a wavelength shorter than 7.9 μm, and the Rayleigh-Jeans tail of the Planckian dust spectrum is steeper than the spectrum of the free-free emission from the stellar wind.

Relation of the dust maps to the projected orbit is difficult. From combination of their radio images with the RV orbit, Dougherty et al. (2005) derived i and Ω, orienting the orbit on the sky. They noted that the O5 star was NW of the WC7 star at the time of periastron, and commented on the paucity of dust in that direction given that the base of the WCR (i.e. the open end), where dust was expected to form, would have been pointing in that direction. Owing to the high orbital eccentricity, however, the position angle of the WCR changes very rapidly around periastron passage (e.g. the P.A. of the O5 star relative to the WC star moves through three-quarters of its orbit in only 0.04 P. These ranges are very sensitive to the orbital eccentricity itself, because it is so high, and account for the spreading of the dust around much of the orbit despite the short duration of dust formation. Also, the density along the dust plume varies sharply with P.A. Even if dust forms at a constant rate, the density on the sky of dust condensed from the compressed wind originating at periastron is more than ten times lower than that originating at phase 0.02, where the WCR sweeps round more slowly, and the dust is spread less thinly than nearer periastron.

Models for the dust emission have been constructed using the orbit, timing of dust formation from the IR light curves, V_{flow} and the shape of WCR from the winds, populating the down-stream WCR with dust. This is projected on the sky to get images for comparison with the observed images. The model images are very sensitive to the orbital elements, especially eccentricity, and the fits are improved by dropping the assumption that the wind densities in the WCRs are uniform around their axes and having higher densities on the 'trailing edge in the plane, which is consistent with with some models of WCRs. This also accounts for the lower proper motion of one of the dust features ('C0', Fig. 15).

Successful modelling of the dust formation by WR 140 is the biggest test of the colliding-wind dust-formation paradigm because we know so much about this system; if we cannot model it, we cannot claim to understand dust formation by the CWBs. And, in any fitting process, we should remember the words of John von Neumann (as quoted by Enrico Fermi) "with four parameters I can fit an elephant and with five I can make him wiggle his trunk."

Acknowledgements

References

Cantó J., Raga A. C., Wilkin F. P., 1996, ApJ, 469, 729

Dougherty S. M., Beasley A. J., Claussen M. J., Zauderer A., Bolingbroke N. J., 2005, ApJ 623, 447

Lührs S., 1997, PASP, 109, 504

Marchenko S. V., et al., 2003, ApJ, 596, 1295

Monnier J. D., Tuthill P. G., Danchi W. C., 2002, ApJ, 567, L137

Pollock A. M. T., Corcoran M. F., Steven I. R., Williams P. M.,2005, ApJ 629, 482

Varricatt W. P., Williams P. M., Ashok N. M. 2004, MNRAS, 351, 1307

Williams P. M., Stewart J. M., Beattie D. H., Lee T. J., 1977, IAU Circ. 3107, 2

Williams P. M., Beattie D. H., Lee T. J., Stewart J. M., Antonopolou E., 1978, MNRAS 185, 467

Williams P. M., Marchenko S. V., Marston A. P., et al. 2009, MNRAS 395, 1749

Peredur Williams & Robin Leadbeater

The Orbit and Distance of WR 140

S. M. Dougherty[1,2], V. Trenton[1,3], A. J. Beasley[4]

[1] NRC-HIA DRAO, Penticton, BC, Canada
[2] Institute for Space Imaging Science, University of Calgary, AB, Canada
[3] University of Prince Edward Island, Charlottetown, PEI, Canada
[4] National Ecological Observatory Network, Boulder, Colorado, USA

Abstract: A campaign of 35 epochs of milli-arcsec resolution VLBA observations of the archetype colliding-wind WR+O star binary system WR 140 show the wind-collision region (WCR) as a bow-shaped arc of emission that rotates as the highly eccentric orbit progresses. The observations comprise 21 epochs from the 1993-2001 orbit, discussed by Dougherty et al. (2005), and 14 epochs from the 2001-2009 orbit, and span orbital phase 0.43 to 0.95. Assuming the WCR is symmetric about the line-of-centres of the two stars and "points" at the WR star, this rotation shows the O star moving from SE to E of the WR star between these orbital phases. Using IR interferometry observations from IOTA that resolve both stellar components at phase 0.297 in conjunction with orbital parameters derived from radial velocity variations, the VLBA observations constrain the inclination of the orbit plane as $120° \pm 4°$, the longitude of the ascending node as $352° \pm 2°$, and the orbit semi-major axis as 9.0 ± 0.1 mas. This leads to a distance estimate to WR 140 of 1.81 ± 0.08 kpc. Further refinements of the orbit and distance await more IR interferometric observations of the stellar components directly.

1 Introduction

The 7.9-year period WR+O system WR 140 (HD 193793) is the archetype of colliding wind binary (CWB) systems. It is comprised of a WC7 star and an O4-5 star in a highly elliptical orbit ($e \approx 0.88$), where the stellar separation varies between ~ 2 AU at periastron to ~ 30 AU at apastron. This highly eccentric orbit clearly modulates the dramatic variations observed in the emission from the system, from X-ray energies to radio wavelengths (Williams et al. 1990). Perhaps the most dramatic variations are observed at radio wavelengths, where there is a slow rise from a low state close to periastron of a few mJy, to a frequency-dependent peak in emission of 10's of mJy between orbital phase 0.65 to 0.85, before a precipitous decline immediately prior to periastron (see Fig. 1). A number of attempts to model these variations have been made (e.g. Williams et al. 1990; White & Becker 1995) with limited success, though advances in our understanding of WCRs are being made (e.g. Pittard & Dougherty 2006; Pittard, these proceedings). Accurate orbital parameters are critical inputs to these models.

Many of the orbital parameters in WR 140, in particular the orbital period (P), epoch of periastron passage (T_o), eccentricity (e), and the argument of periastron (ω) have been established by others (see Marchenko et al. 2003 and references therein), and refined most recently in an extensive observing
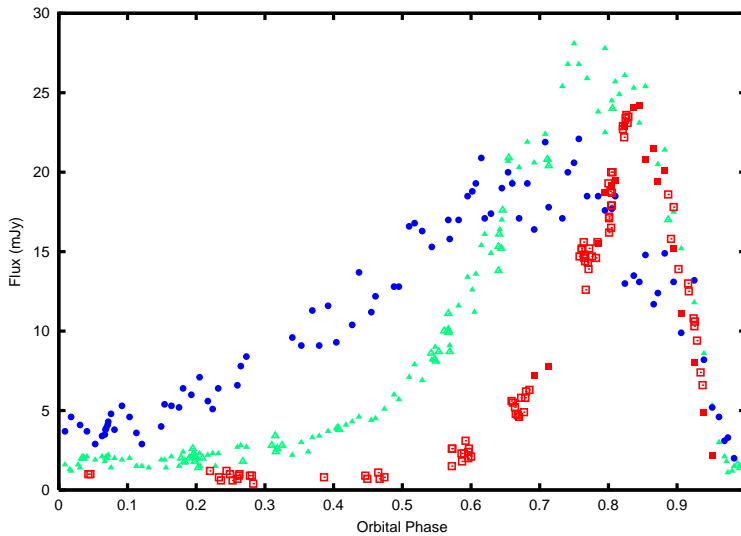
Figure 1: Radio emission from WR 140 at 15 (blue circles), 5 (green triangles), and 1.6 GHz (red squares) as measured with the VLA (solid) and WSRT (open). Data taken from Williams et al. (1990) and White & Becker (1995).

campaign during the 2009 periastron passage. However, the orbital inclination (i), semi-major axis (a), and the longitude of the ascending node (Ω) require the system to be resolved into a "visual" binary. The two stellar components in WR 140 have been resolved using the Infra-red Optical Telescope Array (IOTA) interferometer at a single epoch (Monnier et al. 2004). This single observation sets the scale and orientation of the orbit since it constrains potential families of solutions for (i, a, Ω). Further epochs of IOTA observations have been completed, but until analysis is complete, the VLBA observations of the WCR offer the only means to determine the orbit direction and constrain i, and hence Ω and a.

An initial analysis of 21 epochs of VLBA observations taken between 1999 and 2000 (orbital phase 0.74 to 0.95) was described in Dougherty et al. (2005). The work presented in this paper is an amalgamation of those observations with an additional 14 observations obtained between 2004 to 2008, that extended the orbital phase coverage from 0.43 to 0.96. A re-analysis of the earlier observations with the new data leads to tighter constraints on the derived orbit parameters.

2   VLBA observations of WR 140

WR 140 was observed with the VLBA at 8.4 GHz at 35 epochs between orbital phase 0.43 and 0.97. A selection of images are shown in Fig. 2. The 8.4-GHz emission is clearly resolved, with a bow-shaped emission region observed at many epochs. This shape is anticipated for a WCR from model calculations (see, e.g., Eichler & Usov 1993; Dougherty et al. 2003; Pittard et al. 2006). The WCR rotates from "pointing" NNW to W over the observed orbital phases. This rotation is key to determining the orbit of WR 140. Assuming the arc of emission is symmetric about the line-of-centres and points towards the WR star, the O star is to the SSE of the WCR at epoch 0.43, and approximately to the E at phase 0.96.
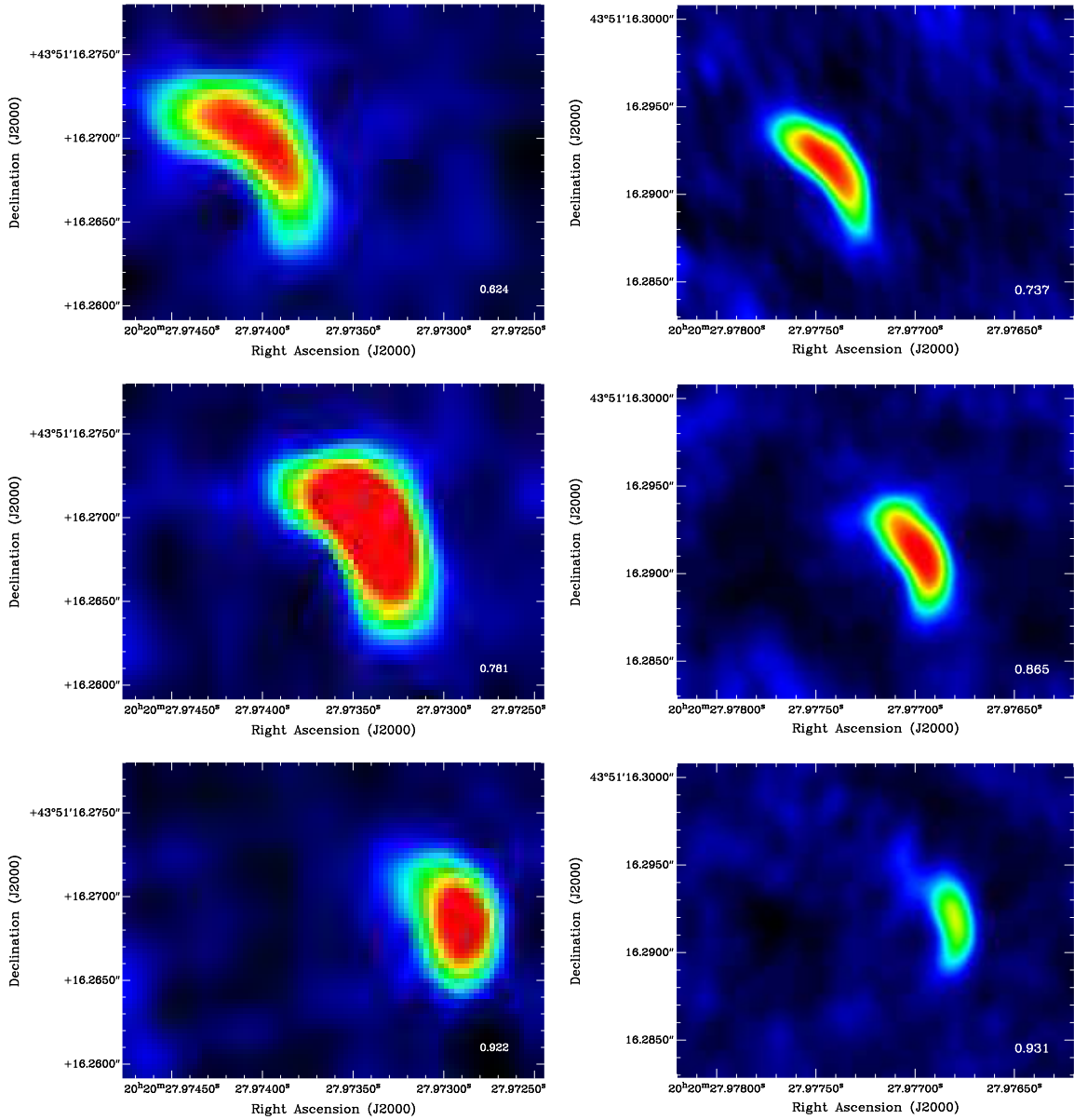
Figure 2: VLBA 8.6-GHz images of WR140 at phases 0.62, 0.74, 0.78, 0.87, 0.92, and 0.93 from the 1993-2001 orbit (phases 0.74, 0.87 and 0.93—taken from Dougherty et al. 2005) and the 2001-2009 orbit. The synthesized beam is $2.0 \times 1.5 \, \text{mas}^2$ in the 1993-2001 orbit, and approximately $1.3 \times$ that for the latest observations. Note change in RA and Dec between the images taken from the 1993-2001 orbit and the recent orbit. Rotation and proper motion of the WCR are evident during both orbits.

3   Deriving the Orbit

On June 17, 2003 Monnier et al. (2004) observed WR 140 to have a separation of $12.9^{+0.5}_{-0.4}$ mas at a position angle of $151.7^{+1.8}_{-1.3}$ degrees east of north. Using $P = 2896.6$ days, $T_o = 2446156.3$, $e = 0.897$ and $\omega = 46.8°$, as determined from analysis of observations during the 2009 periastron (Fahed et al., these proceedings), the observation at orbital phase 0.296 restricts potential sets of solutions for i, a and Ω to those shown in Fig. 3 for inclinations in the range $0° < i < 180°$.

The change in the orientation of the WCR with orbital phase gives the inclination since each (i, Ω) solution family provides a unique set of position angles as a function of orbital phase. A weighted
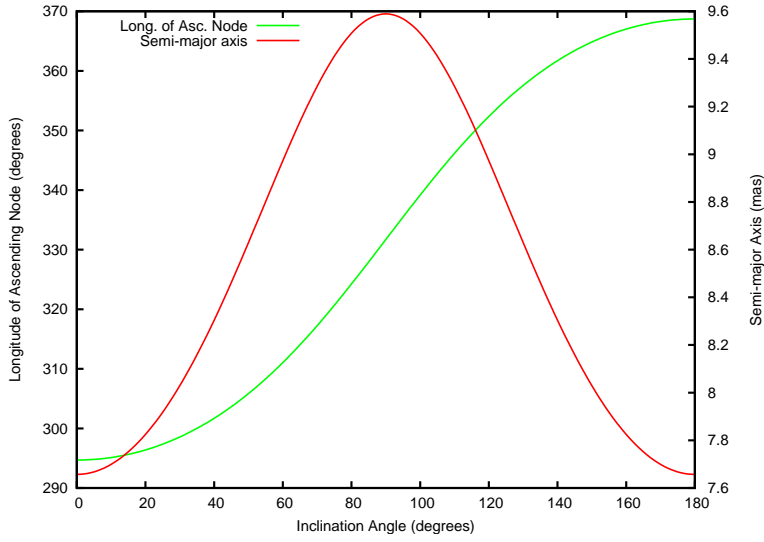
33

Figure 3: Solutions for the longitude of the ascending node (red line) and orbit semi-major axis (green line) as a function of orbit inclination, derived from an IOTA separation and a position angle of the stellar components at orbit phase 0.296 (Monnier et al. 2004). The uncertainty in the IOTA observation gives an error in Ω of closely $\pm 1°$, and in the semi-major axis of ± 0.3 mas.

minimum χ^2 measure between the observed position angle of the line of symmetry of the WCR, and by proxy the line-of-centres of the stars, as a function of orbit phase determined for different sets of (i, Ω) leads to a best-fit solution of $i = 120° \pm 4°$ and $\Omega = 352° \pm 2°$ (Fig. 4). These values lead to a semi-major axis of $a = 8.97 \pm 0.13$ mas.

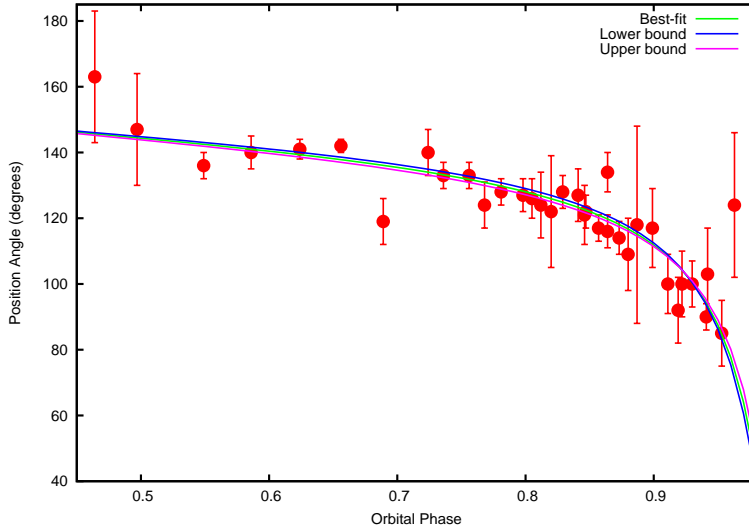Figure 4: The change in the position angle of the axis of symmetry of the WCR as a function of orbital phase. The green line is the weighted best-fit curve of the position angle of the line-of-centres of the two stars as a function of phase, corresponding to $i = 120°$ and $\Omega = 352°$. The other two lines show the fits for $\Delta\chi^2 = \pm 1$, showing the range of potential fits for the quoted uncertainties.

34

4 Distance of WR 140

Stellar distance is one of the more difficult parameters to determine for stars. Marchenko et al. (2003) determined $a \sin i = 14.10 \pm 0.54$ AU from radial velocity observations. From our estimate of i, this gives $a = 16.28 \pm 0.81$ AU. A semi-major axis of $a = 8.97 \pm 0.13$ mas then gives a distance estimate of 1.81 ± 0.09 kpc, consistent with the previous estimate of 1.85 ± 0.16 kpc by Dougherty et al. (2005).

5 Summary

High-resolution radio observations of the WCR in WR140 have provided, to date, the only way to determine the direction and orientation of the orbit, starting from the scale of the orbit as deduced from IR interferometry and orbital parameters from optical spectroscopy. From this work it is possible to determine a precise, and hopefully accurate, distance to WR140.

WR140 is the best colliding-wind binary system for attempts to understand the underlying particle acceleration processes and physics in wind-collision regions, in large part due to the wealth of observational constraints. However, the orbit and distance are critical to modelling the WCR, and further refinements of these parameters await further IR interferometric observations that will resolve the stellar components directly.

Acknowledgments

References

Dougherty, S. M., Beasley, A. J., Claussen, M.J., Zauderer, B.A., Bolingbroke, N. J. 2005, ApJ, 623, 447

Dougherty, S. M., Pittard, J. M., Kasian, L., Coker, R. F., Williams, P. M., & Lloyd, H. M. 2003, A&A, 409, 217.

Eichler, D., & Usov, V. 1993, ApJ, 402, 271.

Marchenko, S. V., et al. 2003, ApJ, 596, 1295.

Monnier, J. D., et al. 2004, ApJ, 602, L57.

Pittard, J. M., Dougherty, S. M., Coker, R. F., O'Connor, E. & Bolingbroke, N. J. 2006, A&A, 446, 1001.

Pittard, J. M. & Dougherty, S. M. 2006, MNRAS, 372, 801.

White, R. L., & Becker, R. H. 1995, ApJ, 451, 352.

Williams, P. M., van der Hucht, K. A., Pollock, A. M. T., Florkowski, D. R., van der Woerd, H., & Wamsteker, W. M. 1990, MNRAS, 243, 662.

Luis Carreira & Alberto Fernando

The X-ray Lightcurve of WR 140

M. F. Corcoran[1,2], A. M. T. Pollock[2], K. Hamaguchi[1,4], C. Russell[5]

[1] CRESST/NASA-GSFC, Greenbelt, MD, USA
[2] Universities Space Research Association, Columbia, MD, USA
[3] European Space Agency, Villanueva de la Cañada, Madrid, Spain
[4] University of Maryland, Baltimore County, Baltimore, MD, USA
[5] University of Delaware, Baltimore, MD, USA

Abstract: WR 140 is a canonical massive "colliding wind" binary system in which periodically-varying X-ray emission is produced by the collision between the wind of the WC7 and O4-5 star components in the space between the two stars. We have obtained X-ray observations using the *RXTE* satellite observatory through almost one complete orbital cycle including two consecutive periastron passages. We discuss the results of this observing campaign, and the implications of the X-ray data for our understanding of the orbital dynamics and the stellar mass loss.

1   Introduction: WR 140 as a "Canonical" System

Although massive stars are the most important objects in the Universe for generation of metals needed for the formation of rocky planets and biological entities, there remain many open questions about these objects, especially concerning how they evolve and die. Understanding this evolutionary process is largely a matter of understanding how these massive stars lose mass and angular momentum. The study of massive binaries is one key since in these systems the fundamental stellar parameters can be directly measured (at least for those fortuitously situated) and because wind-wind (or even wind-star) collisions in these systems provide an in-situ measure of the radiatively driven process which is the major means of mass and angular momentum loss for most of a massive star's natural life.

WR 140 is often termed a "canonical" colliding wind system by stellar astrophysicists. Presumably this is meant in the sense that WR 140 may be used to establish the rule of behaviour of such massive binaries. Physicists refer to canonical pairs of complementary variables and this is at least superficially appropriate for WR 140. A canonical object also suggests a kind of systemic uniqueness, and indeed WR 140 as a system is nearly unique (if uniqueness can be approached in degrees): it's an evolved binary system with an unusually long (7.9 year) period, and it possesses nearly the highest eccentricity of all known stellar orbits (see Williams et al. 1990, and R. Fahed et al., these proceedings). It is well beyond the scope of the current discussion to try to understand how this binary collapsed into this peculiar state (stellar capture? explosive disintegration of a third component?). Nature, however, has kindly provided this laboratory in which the stellar separations and orbital velocities vary by an order of magnitude around the orbit. This allows the patient astronomer to measure the dependence
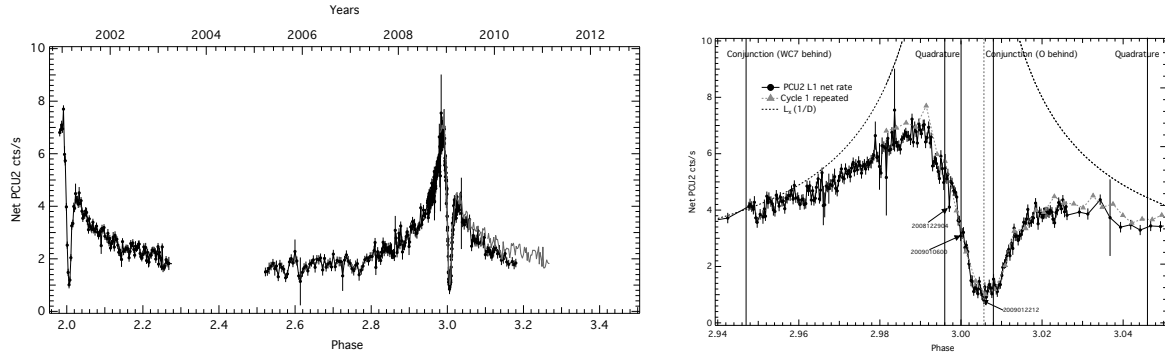
Figure 1: *Left*: The *RXTE* lightcurve of WR 140, December 2000 to June 2010. *Right*: Detailed view of the two minimum observed by *RXTE*. The data in grey represents is the *RXTE* data offset by one orbital period, adopted to be $P = 2897$ days.

of the state of the shock heated gas in the wind-wind collision on the local thermodynamic variables, and to look for the influence of subtle (and sometimes not so subtle) effects due to radiative transfer of photospheric photons winding their way through a complex interacting wind structure, or due to the sudden onset of fluid instabilities. All these things make WR 140 an object of intense interest for observational astronomers of all stripes, stellar evolutionists, hydrodynamicists, and plasma physicists.

2   X-ray Emission from Colliding Wind Binaries Like WR 140

The X-ray band is extremely useful for the study of colliding wind shocks in general and for the study of WR 140 in particular. In WR 140 the stellar winds have terminal speeds $V_\infty \sim 3000$ km s^{-1}. A collision at these speeds produces shock-heated gas at a temperature of

$$T_\mathrm{s} \approx \frac{3}{16}\mu V_\infty^2 R^{-1} \approx 1.51 \times 10^5 (V_\infty/100 \text{ km s}^{-1})^2 \text{ K} \approx 1.3 \times 10^8 \text{ K}$$

(where R is the gas constant and μ the mean molecular weight of the winds), suitably emitting in the X-ray band at energies of 1–10 kilo-electron volts (keV). Because a substantial portion of the stellar winds becomes involved in the shock, the amount of X-ray emission generated is substantial and observable with modern X-ray satellite observatories. WR 140 was first detected as an X-ray bright source on 1984 May 19 by the *EXOSAT* observatory (Pollock 1985), and has been observed many times subsequently by X-ray observatories like *ROSAT*, *ASCA*, *XMM*, *CHANDRA*, and *RXTE*.

3   *RXTE* Observations

The *Rossi X-ray Timing Explorer* (*RXTE*, Bradt et al. 1993), launched in December 1995, is a satellite observatory that flexibly observes variable X-ray emitting cosmic objects on timescales of microseconds to years. The workhorse instrument, the Proportional Counter Array (PCA), is sensitive to X-rays emitted in the 2–60 keV band, which includes the 10–20 million K emission generated within WR 140's wind-wind collision shock. The first observation of WR 140 by *RXTE* was obtained on 2000 December 9, just 53 days before periastron passage, and *RXTE* observed the system about once per week up to about 778 days past periastron passage. Observations resumed on 2005 March 8, just past apastron of the stellar orbits, and continue up through the time of this writing, at a variable cadence of a few observations per month to one observation per day during the most recent periastron passage in 2009 January.
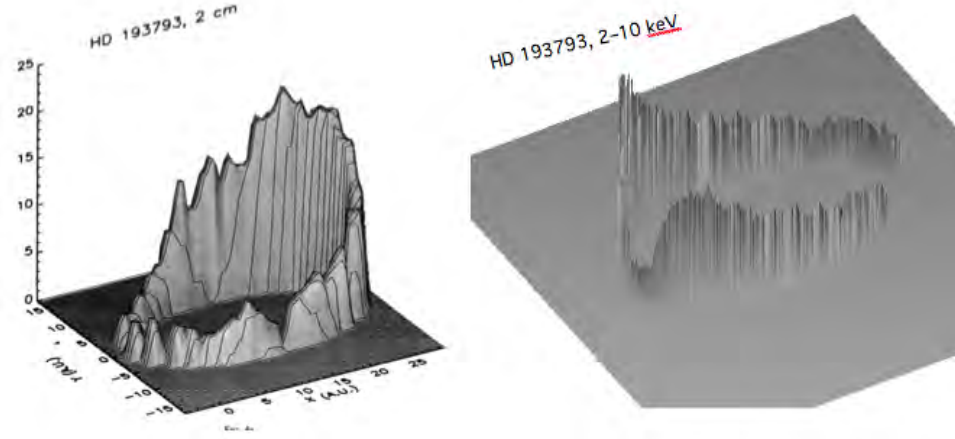
Figure 2: Comparison of the orbital variation of the 2 cm radio flux (from White & Becker 1995) and the 2–10 keV X-ray flux.

Figure 1 shows the WR 140 *RXTE* lightcurve as a function of phase ϕ (where $\phi = 0$ is periastron passage) and time in years. The general characteristic is a gradual increase in X-ray brightness as the stars approach periastron, followed by a rapid decline to a brief minimum state, a quick recovery followed by a gradual decline in brightness. It's worth noting that there is no rapid ($\sim$weeks) variations ("flaring") of the X-ray brightness as seen in WR 140's "sister star" η Car just prior to the start of its X-ray minimum. As shown in Fig. 1, the X-ray minima from the two orbits observed by *RXTE* agree very well with each other in terms of brightness variability, depth and duration. There may, however, be slight variations in the level of X-ray brightness between the two cycles. Figure 1 also shows a curve which represents a $1/D$ variation, where D is the separation between the two stars. Near X-ray minimum the X-ray brightness curve does not follow a $1/D$ variation as it would if the colliding wind shock were adiabatic and there were no line-of-sight absorption variations. We also note that X-ray minimum apparently precedes O-star conjunction (i.e. the time in the orbit when the O star is behind the WR star) by about 6 days. Figure 2 compares the orbital variation of the 2 cm radio flux with the 2–10 keV X-ray flux. As can be seen from this figure, both the radio flux and X-ray flux show minima near periastron passage/O star conjunction when the colliding wind shock is viewed through the thick wind of the WC7 star. The radio decline is much more gradual than the X-ray minimum and in fact just before periastron passage the radio emission is in its minimum state while the X-ray emission is still increasing. The X-ray recovery from minimum is much more rapid than the radio recovery. The radio emission reaches a maximum intensity near apastron when the colliding wind shock moves out from behind the radio photosphere of the system.
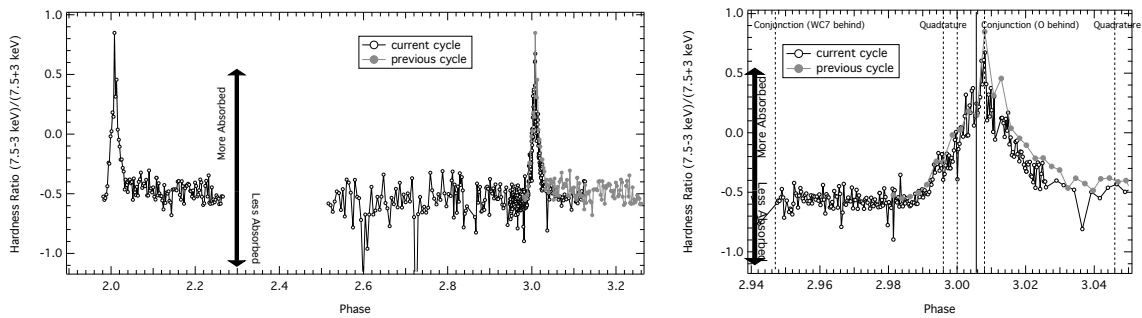

Figure 3: WR 140 hardness ratio (HR) variation as measured by the *RXTE* PCA, where HR is the flux at 7.5 keV minus the flux at 3 keV divided by their sum. *Left*: Complete HR curve. *Right*: Detailed view near periastron passage. The thick verticle line just after $\phi = 3.0$ marks the phasing of the minimum X-ray brightness.

39

Changes in the X-ray spectrum occur in concert with the observed 2–10 keV flux variations. These spectral variations have been seen by *EXOSAT*, *ROSAT*, and *ASCA*, but the *RXTE* observations provide a more complete view of how the spectrum changes around the orbit. Because the *RXTE* PCA has rather poor energy resolution, we choose to characterise these spectral variations as changes in X-ray hardness rather than attempting to fully model the spectra. Figure 3 shows the hardness ratio variations as seen by *RXTE*, along with a detailed view of the changes near periastron passage. In this figure the data in grey are data from the previous cycle advanced by 1 period. In contrast to the X-ray flux variation, the X-ray hardness reaches an extremum at O-star conjunction, as expected if the hardness maximum signals the time of maximum X-ray absorption.

4   Modelling

The first calculations of the level of X-rays to be expected from the wind-wind shock in colliding wind binaries were by Cherepashchuk (1976) and Prilutskii & Usov (1976). Recent modelling efforts have included numerical 3-D hydrodynamic simulations of the wind-wind interaction (Parkin & Pittard 2008, Okazaki et al. 2008). Figure 4 shows a density slice through the orbital plane for a 3-D smooth particle hydrodynamics (SPH) simulation using the Okazaki SPH code (see, for example, Okazaki et al. 2008) for WR 140. Four snapshots are shown: near X-ray maximum; near periastron; near X-ray minimum; and near O-star conjunction (maximum X-ray hardness). The axes are marked in units of the orbital semi-major axis a. The black arrow in the first image shows the observer's line of sight projected onto the orbital plane.
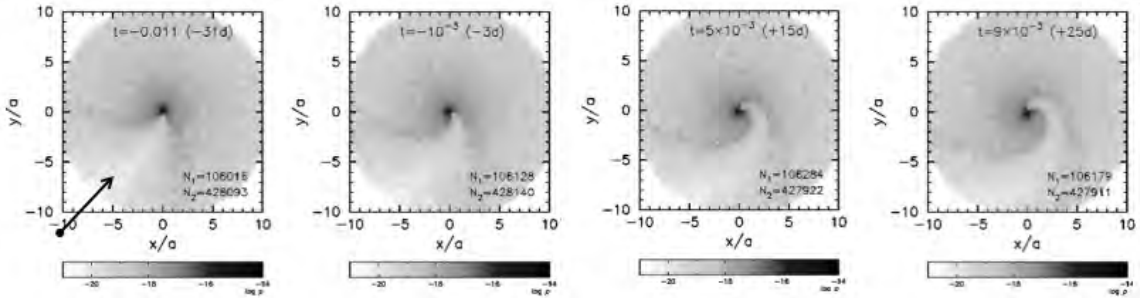

Figure 4: A density slice through the orbital plane for a 3-D SPH simulation for WR 140. Four snapshots are shown, from left to right: near X-ray maximum; near periastron; near X-ray minimum; and near O-star conjunction (maximum X-ray hardness). The black arrow in the first image shows the observer's line of sight projected onto the orbital plane.

X-ray maximum occurs when the projected line of sight passes near the middle of the low density region of the O star's wind, channeled by the boundary of the colliding wind shock. As the stars revolve in their orbit the bow shock around the O star twists behind the companion and gets increasingly obscured by the wind of the WR star through X-ray minimum. At conjunction the X-ray hardness reaches a maximum; this suggests that only the highest-energy photons can penetrate through the thick wind of the WC7 star at this phase.

Figure 5 shows an attempt to model the X-ray lightcurve using the SPH model. The model shown is somewhat artificial in that it assumes a mono-energetic point source of X-rays located at the stagnation point of the flow. The X-rays produced by this point source are absorbed by the distorted wind structure of the WC7 star which is simulated by the SPH model. As seen in Fig. 5 this reproduces quite well the variation seen in the *RXTE* lightcurve. However, more realistic models under development, in which the X-rays are produced by a distribution of hot gas extended along the wind-wind collision shock, and using a more realistic temperature distribution, do not reproduce the X-ray behaviour as well as the point source model. This "distributed-emission" model is still under investigation.
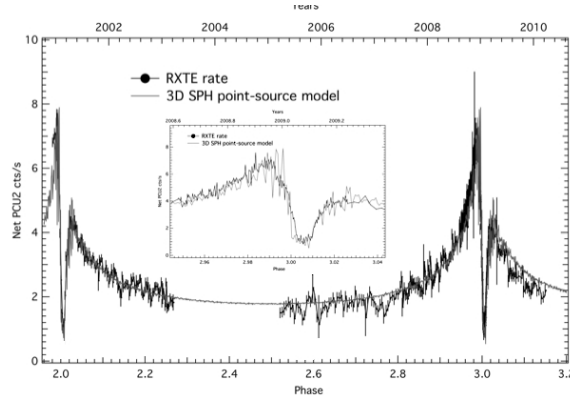
Figure 5: An X-ray lightcurve from the SPH model compared to the *RXTE* fluxes.

5   Conclusion

The *RXTE* monitoring of WR 140 confirms that the X-ray emission varies in a predictable way which is mostly consistent over the two orbital cycles studied. Far from periastron the X-ray emission mostly follows a $1/D$ law expected from an adiabatic shock, though strong deviations are seen near periastron, not all of which can be explained by absorption in the wind of the WC7 star. Matching the X-ray minimum from 2001 to the 2009 minimum suggests that the X-ray period is $P = 2897$ days, about 2 days shorter than the period proposed by Marchenko et al. (2003). The X-ray data confirm that WR 140 is a good laboratory for the study of the phenomena associated with strong shocks in the astrophysical environment.

Acknowledgements

References

Bradt, H. V., Rothschild, R. E., Swank, J. H., 1993, A&AS, 97, 355

Cherepashchuk, A. M., 1976, Soviet Astronomy Letters, 2, 138

Marchenko, S. V., Moffat, A. F. J., Ballereau, D., et al., 2003, ApJ, 596, 1295-1304

Okazaki, A. T., Owocki, S. P., Russell, C. M. P., Corcoran, M. F., 2008, MNRAS, 388, L39-L43

Parkin, E. R., Pittard, J. M., 2008, MNRAS, 388, 1047-1061

Pollock, A. M. T., 1985, Space Science Reviews, 40, 63

Prilutskii, O. F., Usov, V. V., 1976, Soviet Astronomy, 20, 2

Williams, P. M., van der Hucht, K. A. Pollock, A. M. T., Florkowski, D. R., van der Woerd, H., Wamsteker, W. M., 1990, MNRAS, 243, 662

White, R. L., Becker, R. H., 1995, ApJ, 451, 352

Eva Santos, Nelson Viegas & Remi Fahed

Theory and Models of Colliding Stellar Winds

J. M. Pittard

School of Physics and Astrophysics, University of Leeds, United Kingdom

Abstract: I discuss some of the important aspects of the phenomena of colliding winds in massive binary star systems with a particular focus on WR 140.

1   Introduction

Luminous stars are able to drive powerful winds which, while ploughing into their surroundings, may also cause significant mass loss and thus modify the star's evolution. Determining the rate of mass loss is key to understanding how such stars evolve. Fortunately, in massive binary systems we are able to use the wind of one star as an in-situ probe of the wind of the other star. In addition, the collision of the winds unleashes a broad spectrum of emission revealing the interesting physics of high Mach number shocks, including the acceleration of a small proportion of particles to relativistic energies.

2   The Dynamics of Colliding Wind Binaries

2.1   Instabilities

The nature of the wind-wind collision in colliding wind binaries (CWBs) depends on a number of factors, and displays a huge diversity. For instance, in some systems the winds are of almost equal strength and collide roughly mid-way between the stars. In others, one wind is significantly more powerful than the other and completely overwhelms the weaker wind, causing the collision region to crash onto the surface of the companion star. Hence the nature of the wind-wind collision region (WCR) depends on the wind properties of the system. The thermal behaviour of the WCR also depends on the orbital properties of the system. In short period systems, where the two stars are very close together, the wind-wind collision is likely to be highly radiative. The shock-heated gas therefore cools very rapidly, and a geometrically thin and dense region of gas forms which is prone to severe, and perhaps disabling, non-linear thin-shell instabilities (NTSI, Vishniac 1994)[1]. On the other hand, if the orbital period is long, the shocked gas may behave largely adiabatically, flowing out of the system while still hot. In this case the WCR stays thick and "puffed-up", and is far less affected by disruptive instabilities, although Kevin-Helmholtz instabilities, due to a velocity shear at the contact discontinuity between the winds, may still occur. Where one wind is radiative and the

---

[1]This is the conventional wisdom, but in fact it is not clear exactly what occurs between the stars—e.g. even whether two "winds" are produced—in such an extreme and hostile environment.

other largely adiabatic, a thin dense layer of cooled gas abuts a thicker, hotter, but more rarefied layer which acts like a "cushion" to damp out thin shell instabilities occurring in the dense layer (Vishniac 1983). These differences were illustrated by Stevens et al. (1992) and are reproduced in Fig. 1.
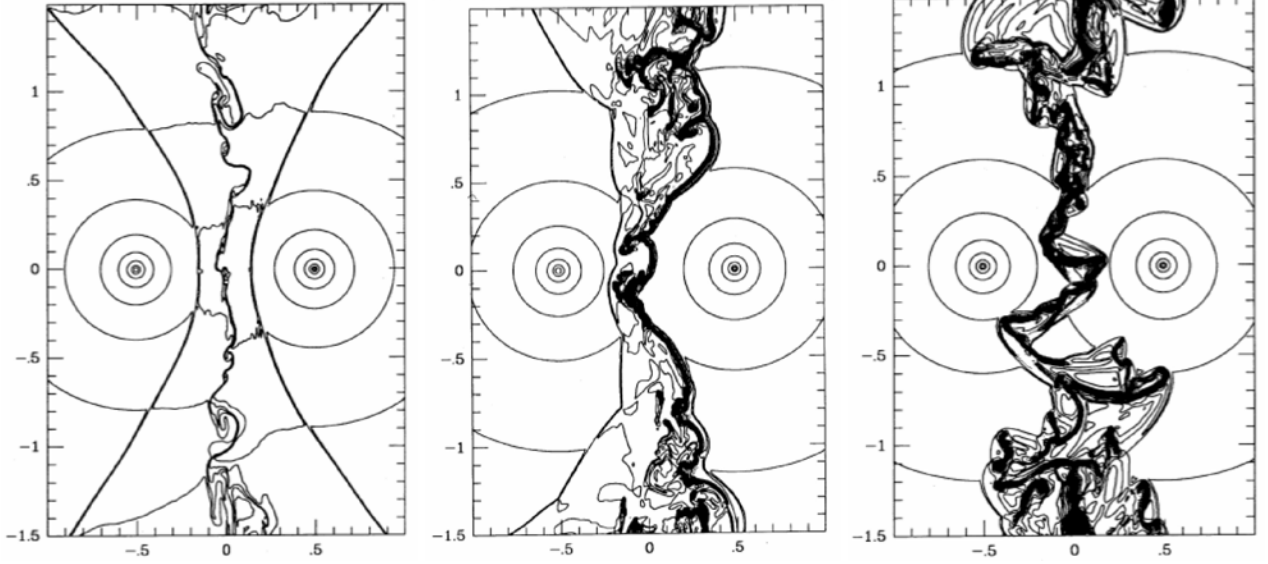

Figure 1: Instabilities in the WCR of CWBs. *Left:* When both sides of the contact discontinuity are largely adiabatic, the WCR is very smooth. *Center:* When one side is radiative, thin shell instabilities occur, but are somewhat limited by the "cushioning" of the hot gas (Vishniac 1983). *Right:* When both sides are radiative, the much stronger and highly non-linear thin shell instability occurs (Vishniac 1994). Adapted from Stevens et al. (1992).

The transition between radiative and adiabatic post-shock regions is conveniently estimated using the value of $\chi \equiv t_{\rm cool}/t_{\rm dyn} \approx v_8^4 D_{12}/\dot{M}_{-7}$, where $t_{\rm cool}$ is the cooling time of the gas, $t_{\rm dyn}$ is a dynamical flowtime which is rather loosely defined but can be taken as either the time for shocked gas at the apex of the WCR to flow a distance $D_{\rm sep}$ downstream, or for the shocked gas from the weaker wind to flow a distance $r_{\rm OB}$ downstream (see Stevens et al. 1992 for these definitions). In the above, v_8 is the wind speed normalised to $1000\ {\rm km\,s^{-1}}$, D_{12} is the stellar separation normalised to $10^{12}\ {\rm cm}$, and $\dot{M}_{-7}$ is the mass-loss rate normalised to $10^{-7}\ M_\odot\,{\rm yr^{-1}}$. Note that this formalism for χ depends on specific assumptions about the post-shock temperature and the morphology of the cooling curve at this point (see Pittard & Stevens 2002). By specifying appropriate values for $\dot{M}_{-7}$, etc., it is possible to determine a separate value of χ for each shocked wind.

One of the reasons why WR 140 is of particular interest is that its highly eccentric orbit results in big, but reproducible, changes in the properties of the WCR, for instance its density. While the shocked O-star wind is largely adiabatic throughout the entire orbit, the same is not true of the shocked WR wind, which though adiabatic at apastron ($\chi_{\rm WR} \sim 50$), has much more significant cooling at periastron ($\chi_{\rm WR} \sim 2$). At this time the shocked gas radiates away all of its energy as it leaves the system, seemingly creating the ideal conditions for dust formation (P. Williams, these proceedings). A signature of this cooling is believed to be seen in the He I 1.083-μm line, which develops a sub-peak on top of its normal flat-topped profile as the stars approach periastron (see Varricatt, Williams & Ashok 2004, and also P. Williams, these proceedings).

The exact thermal behaviour of the shocked gas is impossible to determine without fully three-dimensional numerical simulations, since the value of χ as estimated above is only approximate. A number of other mechanisms can also influence the value of χ. For instance, if the winds are clumpy, which is believed to be the case for hot stars, the cooling and hence χ will be underestimated.

Furthermore, the efficient acceleration of non-thermal particles in the WCR may sap energy from the thermal plasma, again causing it to cool more rapidly. Therefore, values of χ estimated using the above equation should be taken as only a rough guide of the true thermal behaviour.

2.2 Radiative Driving Effects

Systems where the stars are relatively close to each other (i.e. those with short periods and/or highly eccentric orbits) may suffer from interactions between one star's wind and the other star's radiation field. Two scenarios have been determined. In the "radiative inhibition" scenario, the acceleration of one or both winds is inhibited by the radiation field of the other star, thus reducing the speed of the wind(s) before the collision (Stevens & Pollock 1994). Another effect, termed "radiative braking" comes into play in systems where the stronger wind closely approaches the more luminous star (Gayley et al. 1997). This condition is met in many Wolf-Rayet (WR) + O-star binaries. The stronger radiation field may then efficiently couple to the more powerful wind, causing a sudden deceleration or braking. The effect is highly non-linear, and the braking can be so severe that the stronger wind can be prevented from colliding with the surface of the more luminous star even in cases where a normal ram-pressure balance between the winds would not be possible. Neither of these effects is believed to be important in WR 140, since even at periastron the stars are still well separated (see R. Fahed et al., these proceedings), and the WCR is at least several stellar radii from the surface of the O-star despite the large disparity in wind strengths.

2.3 Orbital Effects

The orbit of the stars can also strongly influence the properties and nature of the WCR. The most obvious effect is a spiralling of the WCR as the gas within it flows out of the system. Due to the large computational cost of 3D simulations, it is only recently that the first 3D hydrodynamical models of colliding wind binaries were presented in a refereed journal (Lemaster et al. 2007), and this work lacked several key processes which are important in the short-period systems where the effects of orbital motion are greatest. The most notable omissions were the lack of any treatment for the acceleration of the winds and the cooling of the shocked gas. Shortly afterwards, 3D smoothed-particle hydrodynamics (SPH) simulations of the WCR in the massive binary system η Carinae were presented (Okazaki et al. 2008). Though these models were isothermal, and did not solve for the temperature structure behind the shock, they provided much insight into the dynamics of the WCR in this highly eccentric ($e \approx 0.9$) system. At about the same time, a "dynamic" model was presented by Parkin & Pittard (2008). This model did not solve the hydrodynamic equations, but instead mapped the apex of the WCR (given by the equations in Stevens et al. 1992) into a 3D space. The apex was provided with a time-dependent skew which aimed to reflect the ratio of the wind to orbital speeds, and the gas was assumed to behave ballistically further downstream. Though the resulting dynamics are only representative of the true situation, a comparison against results from a full hydrodynamical calculation revealed that this approach does a more than adequate job in many situations.

The first 3D simulations of CWBs to include orbital motion, the radiative driving of the winds and cooling of the shocked gas were presented by Pittard (2009). Focusing on O+O-star systems, models with circular orbits were presented. Depending on the orbital period (3 d or 10 d) the WCR was either highly radiative or largely adiabatic. In the former, differences in the nature of the instabilities in the leading versus the trailing edge of each "arm" of the WCR are seen. In the latter, the density and temperature of the hot gas changes across the arms. The most interesting behaviour, however, was seen from a system with an eccentric orbit where the stellar separation at periastron was the same as the system with the 3 d orbital period, while the apastron separation was the same as the

system with the 10 d orbital period - this required $e = 0.36$. Most notably, the properties of the WCR exhibited a distinct phase lag compared to those expected from the instantaneous position of the stars, which reflects the recent history of the stellar separation. Hence there were marked differences in the WCR properties when the stars are at identical stellar separations depending on whether the stars are approaching or receding from each other. For instance, the gas in the WCR remains hot until near phase 0.9, after which it collapses into a thin dense sheet which is torn apart by instabilities. Yet it is past apastron before the cold clumps are cleared away from the stars (this long timescale is due to the high inertia of the dense clumps relative to the rarefied gas which flows past them). This process is clearly shown in synthetic images at 1000 GHz (see Fig. 2).
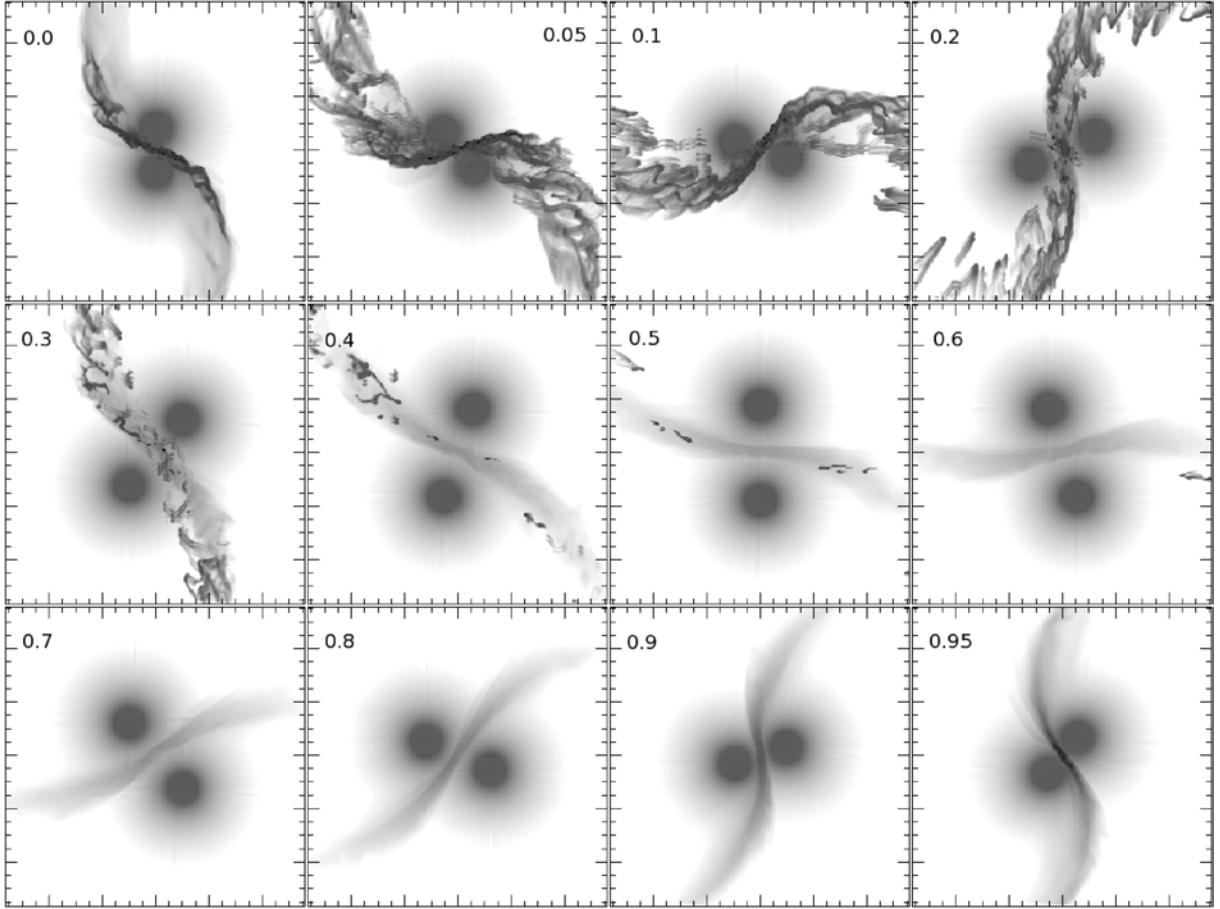

Figure 2: Intensity images at 1000 GHz for an observer viewing an eccentric ($e = 0.36$) O+O-star system with an orbital period of 6.1 d (adapted from Pittard 2010). See Pittard (2009) for details of the hydrodynamical model).

For most of WR 140's orbit, orbital effects are minimal, and the WCR is approximately axisymmetric, with rotational symmetry about the line running through the centres of the stars. However, orbital effects become very significant as the stars swoop through periastron passage. The rapid changes in the positions of the stars induces severe curvature into the WCR, breaking the axisymmetry which exists up until about phase 0.95. One must then be careful when interpreting data using axisymmetric models for the WCR (e.g. the Lührs 1997 model), since this curvature will bias estimates of the opening angle of the WCR, and thus of the momentum ratio of the winds.

2.4 The Effect of Clumpy Winds

Studies of how wind clumping affects the WCR have been presented by Walder (1998), who showed that dense clumps can tip an otherwise marginally adiabatic WCR into a radiative regime. Pittard (2007) examined the effect of clumps on the adiabatic WCR of WR 140 at apastron. If the clumps are not too dense or large (so that they do not punch through the WCR), they can be rapidly destroyed by the vorticity created during their passage through the shocks bounding the WCR. Although the WCR becomes highly turbulent as a result, the overall effect is to smooth out the flow. Thus determinations of the stellar mass-loss rates using the X-ray emission from a WCR may be relatively insensitive to clumping, and thus offer a useful alternative to other methods where this is not the case. The strong turbulence occurring within the WCR also has implications for particle acceleration and the mixing of the winds.

3 Models of WR 140

Due to its interesting behaviour, WR 140 is one of the best studied CWB systems, and this has led to the development of a large number of theoretical models. Each model has typically addressed one aspect of its emission. In the following I summarise the models which have been made of the thermal X-ray and non-thermal radio emission. The latter have also been used to predict the expected flux of the high-energy non-thermal emission, so I will discuss these too. I will not discuss the thermal IR emission from WR 140, which has been extensively studied and modelled by Peredur Williams and collaborators, details of which are given in the contribution by Peredur Williams in these proceedings.

3.1 Thermal X-ray Emission

WR 140 is an exceptionally luminous X-ray source for a colliding wind binary system, with an X-ray luminosity $\sim 4 \times 10^{34}\,\mathrm{erg\,s^{-1}}$. This indicates that, in addition to the strong, dense and fast wind from the Wolf-Rayet star, the companion star must also have a powerful wind (the maximum efficiency for converting wind power into hot shocked gas is obtained when the winds are of equal strength). The X-ray luminosity displays large, phase-repeatable, variations around the orbit. Such variations must reflect the underlying changes occurring to the hot plasma in the WCR, augmented by changes in the circumstellar absorption from the surrounding winds (see, e.g., M. Corcoran et al., these proceedings).

To model the emission from the WCR with hydrodynamic codes, one must resolve the cooling length behind the shock. This is a difficult task when the cooling is very rapid, but perfectly possible for WR 140 since the shocked gas is never strongly radiative. Early predictions for the X-ray spectrum and lightcurve were made by Stevens et al. (1992). The predicted X-ray luminosity scales as D^{-1}, where D is the stellar separation, and there is a deep X-ray minimum as the orbit moves the denser wind of the WR star in front of the apex of the WCR. Prior to this work, a simple point-source model for the X-ray absorption was constructed to compare against the observed absorption of EXOSAT spectra (Williams et al. 1990). Today, observations by the *RXTE* X-ray satellite reveal the X-ray lightcurve in exquisite detail (see M. Corcoran et al., these proceedings). An immediate puzzle is that the expected D^{-1} scaling is not observed—instead the real increase is lower. This has yet to be explained, but may be related to the cooling of the plasma or the acceleration of non-thermal particles within the WCR. Furthermore, models which adopt spatially extended X-ray emission at the WCR are not able to reproduce the deep X-ray minimum (see, e.g., M. Corcoran et al., these proceedings).

Several other models have investigated various physical aspects of the high Mach number shocks found in WR 140. The heating of electrons and ions at the shocks was modelled by Zhekov & Skinner

(2000) who concluded that models where the electrons were heated more slowly than the ions provided better fits to the *ASCA* X-ray data available at the time (see also Pollock et al. 2005). Another process which is likely to have a significant timescale is that of ionisation equilibrium—the initial post-shock plasma is under-ionised for its temperature, and ionisation towards equilibrium proceeds as material flows downstream from the shock and eventually out of the system. This effect is beautifully illustrated in Pollock et al. (2005), where it is seen that the FWHM of various X-ray lines increases with the ionisation potential of the species. This is the opposite trend to that expected from a plasma in collisional ionisation equilibrium (CIE), where the hottest gas and most highly ionised species occur at the apex of the WCR where the shocks are perpendicular to the oncoming winds. Pollock et al. (2005) estimates that the distance for ionisation equilibrium to be established when the stars are at apastron is about 32 AU (i.e. comparable to the orbital separation). Models of X-ray line profiles (see Henley, Stevens & Pittard 2003; Henley et al. 2005, 2008) where the plasma is assumed to be in CIE fail spectacularly when an attempt is made to fit the WR 140 data. This adds further support to the plasma being in non-equilibrium ionisation.

By constructing a number of hydrodynamical models and examining the expected X-ray emission from each, Pittard & Dougherty (2006) determined a range of possible mass-loss rates and wind momentum ratios which were consistent with the observed X-ray flux. The mass-loss rates should be accurate to $\pm 25\%$, with uncertainties due to the ill-determined composition of the WR wind (see Pollock et al. 2005 and Pittard & Dougherty 2006 for more details). Zhekov & Skinner (2000) derived slightly higher mass-loss rates for their adopted wind momentum ratio ($\eta = \dot{M}_{\rm O} v_{\rm O} / \dot{M}_{\rm WR} v_{\rm WR} = 0.0353$) as they assumed relatively low abundances for C and O. Note that previous works have sometimes used mass-loss rates which are inconsistent with the X-ray luminosity (e.g. Dougherty et al. 2005). The values of η investigated by Pittard & Dougherty (2006) spanned the range $0.02 - 0.2$. Larger values of η require relatively smaller values of $\dot{M}_{\rm WR}$ and larger values of $\dot{M}_{\rm O}$. The latest investigation on the sudden increase in the absorption component of the He I 1.083-μm line near periastron implies that $\eta = 0.1$ (see the contribution by Peredur Williams in these proceedings), which in turn implies that $\dot{M}_{\rm WR} \approx 2 \times 10^{-5} \, M_{\odot} \, {\rm yr}^{-1}$ and $\dot{M}_{\rm O} \approx 2 \times 10^{-6} \, M_{\odot} \, {\rm yr}^{-1}$. Further (3D) modelling is needed to test these values.

3.2 Non-Thermal Radio Emission

In the late 1970s and early 1980s the radio emission from WR 140 was determined to be highly variable, with both the flux and the spectral index undergoing significant changes. Over the intervening years further observations in the radio have revealed in exquisite detail phase repeatable light curves and images of the emission from the WCR (see Williams et al. 1990; White & Becker 1995; Dougherty et al. 2005; S. Dougherty et al., these proceedings). Part of the modulation is thought to be caused by the variable circumstellar extinction to the source of the non-thermal (synchrotron) emission (the WCR) as the O-star orbits in and out of the radio photosphere in the dense WR wind. However, the intrinsic non-thermal emission probably also varies around the orbit. Various aspects of the particle acceleration in and non-thermal emission from CWBs were discussed by Eichler & Usov (1993).

Early models of the non-thermal radio emission from CWBs were very simple. It was usually assumed that the observed flux ($S_{\nu}^{\rm obs}$) was a combination of the free-free flux from the spherically symmetric winds ($S_{\nu}^{\rm ff}$), plus the flux from a point-like non-thermal source located at the stagnation point of the WCR ($S_{\nu}^{\rm nt}$). In this model the non-thermal emission is then attenuated by free-free absorption (opacity $\tau_{\nu}^{\rm ff}$) through the surrounding winds:

$$S_{\nu}^{\rm obs} = S_{\nu}^{\rm ff} + S_{\nu}^{\rm nt} \, {\rm e}^{-\tau_{\nu}^{\rm ff}}. \tag{1}$$

While this approach allows simple solutions to the radiative transfer equation (e.g., Williams et al. 1990; Chapman et al. 1999), such models fail to reproduce the spectral variation of the emission with orbital phase. Williams et al. (1990) therefore proposed that in future models of WR 140 the low-opacity "hole" in the dense WR wind created by the O-star's wind should be accounted for. However, White & Becker (1995) pointed out that in WR 140, even the O-star's wind has significant opacity. Together, these works demonstrated the need for more realistic models which account for the spatial extent of the emission and absorption from the circumstellar envelope and the WCR. More realistic models should also account for the effects of various cooling mechanisms (e.g. inverse Compton, adiabatic, etc.) on the non-thermal electron distribution, and also additional absorption mechanisms (e.g., the Razin effect).

The modelling of the non-thermal radio emission from CWBs took a dramatic jump forward when key assumptions in previous models, such as a point-like source of non-thermal emission, and a spherically symmetric, single temperature, surrounding envelope, were removed. This was achieved in Dougherty et al. (2003), where models of the thermal and non-thermal radio emission used 2D, cylindrically symmetric, hydrodynamical simulations, to more accurately describe the density and temperature structure of the system. Sight-lines to the observer could now pass through regions of both high and low opacity. The assumption of a point-source of non-thermal emission was also removed, by treating the emission in a phenomenological way where the local density of non-thermal electrons and the magnetic field strength were related to the local thermal energy density within the WCR. The non-thermal electrons were further assumed to have a power-law distribution, $N(\gamma)d\gamma = C\gamma^{-p}d\gamma$, where γ is the Lorentz factor, C is a proportionality constant which fixes the normalisation, and it was assumed that $p = 2$ (suitable for test particle diffusive shock acceleration, with strong shocks and an adiabatic index equal to $5/3$).

Although this work was not directly applied to WR 140, the results provided a great deal of new insight into the nature of the radio emission from CWBs. An immediate realisation was the potential importance of the Razin effect in attenuating the low frequency synchrotron emission within the WCR. Several key scaling relationships were also established. For instance, in the absence of IC cooling the total synchrotron emission from the entire WCR in adiabatic systems was found to scale as $D^{-1/2}\nu^{-1/2}$ (as a reminder the X-ray emission in the optically thin, adiabatic limit, scales as D^{-1}). In a successive paper, Pittard et al. (2006) investigated the effect of inverse Compton (IC) cooling of the non-thermal electrons as they flowed downstream from their accelerating shocks and out of the system. This work showed that with IC cooling the *intrinsic* luminosity actually *declines* with stellar separation. The effect of the stellar separation on the *thermal* radio flux was also explored. It was discovered that the *thermal* radio emission from the WCR scales as D^{-1}, in an identical way to the thermal X-ray emission. Since this emission is optically thin in systems with an adiabatic WCR, it can mimic a synchrotron component, so that one should rather cautiously interpret data with a spectral index $-0.1 \lesssim \alpha \lesssim 0.5$ (Pittard et al. 2006).

The model of Pittard et al. (2006) was applied to WR 140 in Pittard & Dougherty (2006). Fits were obtained to data at orbital phase 0.837, which is around the peak of the non-thermal radio lightcurve. It was found that the low frequency turndown in the radio spectrum could be explained as either free-free absorption through the surrounding stellar winds, or the Razin effect (see Fig. 3). In the former case it proved impossible to obtain a good fit to the data with $p = 2$. The best fit was obtained with $p = 1.4$, though changes to the assumed magnetic field strength allow some small variation in this value. Such indices can result from the shock re-acceleration process, whereby the non-thermal particles pass through a sequence of shocks (Pope & Melrose 1994), or from 2nd order Fermi acceleration. Either of these processes may be significant in CWBs, since the clumpy nature of the winds means that the WCR is likely to be highly turbulent, with weak shocks distributed throughout it (Pittard 2007). In contrast, fits with the Razin effect dominant do allow $p = 2$, though require a worryingly
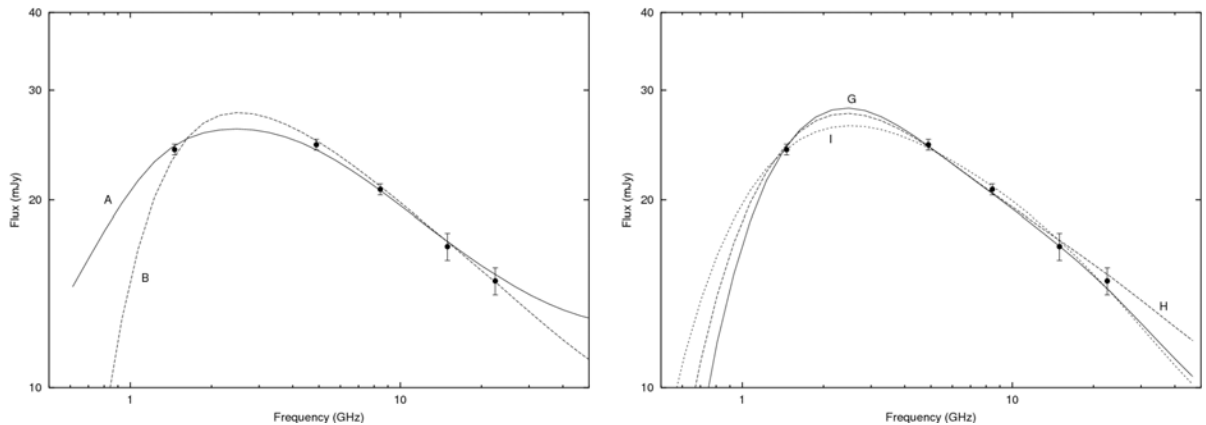
Figure 3: Model fits to the radio data of WR 140 at $\phi = 0.837$. *Left*: Fits where the low-frequency turndown is due to free-free absorption. Models A and B span plausible values of the wind momentum ratio, η. *Right*: Fits where the Razin effect is responsible for the turndown. For further details of the models see Pittard & Dougherty (2006).

high efficiency of electron acceleration. For this reason, fits with free-free absorption dominant were preferred. A wide range of wind momenta could fit the data in this case, though it might be possible to constrain the models with future, high sensitivity VLBA observations.

3.3 Non-Thermal X-ray and γ-ray Emission

The presence of non-thermal electrons and ions should produce non-thermal emission at X-ray and $\gamma-$ray energies via several mechanisms, including the up-scattering of lower energy (e.g., stellar UV) photons (inverse Compton [IC] scattering), relativistic bremsstrahlung, and pion decay. Early predictions for the high-energy non-thermal emission from CWBs were made by Benaglia & Romero (2003). In this work it was assumed that IC scattering was the dominant mechanism. Then the ratio of the luminosity from IC scattering to the synchrotron luminosity is equal to the ratio of the energy density of the target photons, $U_{\rm ph}$, to the magnetic field energy density, $U_{\rm B}$:

$$\frac{L_{\rm ic}}{L_{\rm sync}} = \frac{U_{\rm ph}}{U_{\rm B}}. \tag{2}$$

While very straightforward, the predictive power of this equation is severely curtailed by the fact that the magnetic field strength in the WCR is generally very uncertain. Since $U_{\rm B} \propto B^2$, small changes in the estimated value of B lead to large changes in $L_{\rm ic}$.

In recent years the dramatic sensitivity gains achieved by space-based satellites and ground-based arrays of Cerenkov telescopes have raised the tantalising prospect of the first detection of the non-thermal X-ray and γ-ray emission from CWBs (in fact, we now believe that we have detected the massive CWB η Carinae at γ-ray energies, Abdo et al. 2010; Walter et al. 2010). This, in turn, has led to new theoretical predictions (e.g., Bednarek 2005). The anisotropic nature of the IC process, where the emitted power is dependent on the scattering angle, was considered by Reimer, Pohl & Reimer (2006). This work developed a two-zone model of the non-thermal emission. Particles are accelerated in an inner zone where their spatial diffusion exceeds their motion due to advection with the background fluid. Their energy distribution is self-consistently computed by considering all relevant gain and loss mechanisms. Particles are assumed to be resident within this region until their timescales for advection and diffusion are comparable, after which they are assumed to move into the advection region where they suffer further losses as they flow downstream. Fig. 4 shows the assumed geometry

50

and the resultant non-thermal energy spectra of the electrons and nucleons. The left panel of Fig. 5 shows the predicted IC emission from WR 140 as a function of orbital phase. While Reimer et al. (2006) conclude that while WR 140 should be easily detected with GLAST/Fermi, the high galactic background has meant that unfortunately no detection has yet been made. The change in the IC flux with viewing angle due to anisotropic scattering is likely to be obscured by large variations in the energy density of the stellar radiation fields resulting from the high orbital eccentricity.
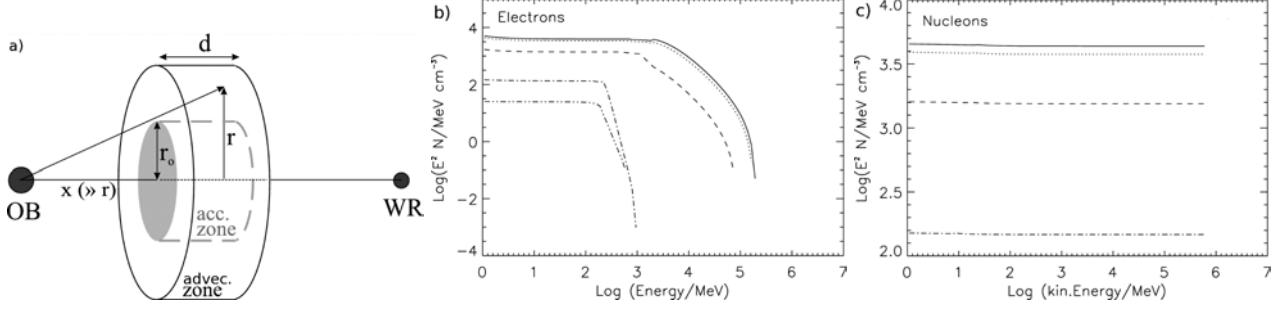

Figure 4: a) Geometry of the 2-zone model in Reimer et al. (2006). b) Evolution of the non-thermal electron spectrum from the inner acceleration zone (*solid line*) as a function of downstream distance in the advection zone. At low energies adiabatic/expansion losses dominate, while at high energies IC losses dominate. c) As b) but for nucleons. Only adiabatic losses occur. See Reimer et al. (2006) for further details.

Pittard & Dougherty (2006) also predicted the non-thermal X-ray and γ-ray emission from WR 140, using fits to the radio and thermal X-ray emission as constraints. The adopted approach was quite different but complementary to that of Reimer et al. (2006)—while the non-thermal particle spectrum was assumed rather than calculated, and the IC scattering was treated as isotropic, it benefitted from a more realistic description of the density and temperature distribution within the system based on the X-ray constraints. Pittard & Dougherty showed that the uncertain particle acceleration efficiency and spectral index have at least as much influence on the predicted flux as the angle-dependence of the IC emission.

The right panel of Fig. 5 shows a predicted spectral energy distribution for WR 140 from one of the models presented in Pittard & Dougherty (2006). Large differences in the predicted γ-ray emission occur depending on whether the low frequency turndown in the radio spectrum results from free-free absorption through the surrounding stellar winds, or from the Razin effect. While Pittard & Dougherty (2006) could not determine the nature of the absorption process from the fits to the radio spectrum, future γ-ray detections will determine the γ-ray flux and spectral index, and thus will also distinguish the nature of the low-frequency turndown. The acceleration efficiency of the non-thermal electrons and the strength of the magnetic field will then both be revealed.

4   Conclusions

Theoretical models of the hydrodynamics of and emission from CWBs, including of WR 140, continue to improve. Hydrodynamical models are becoming more sophisticated, with the first 3D simulations to be published in refereed journals being made in only the last several years. The goal now is to gradually add further important physics, such as non-equilibrium ionisation and electron heating, to these 3D models. Predictions for the non-thermal emission have also progressed, leaving behind some of the assumptions in earlier works. Further progress will be made when the non-thermal particle distribution function is self-consistently solved with an accurate description of the post-shock flow and cooling.
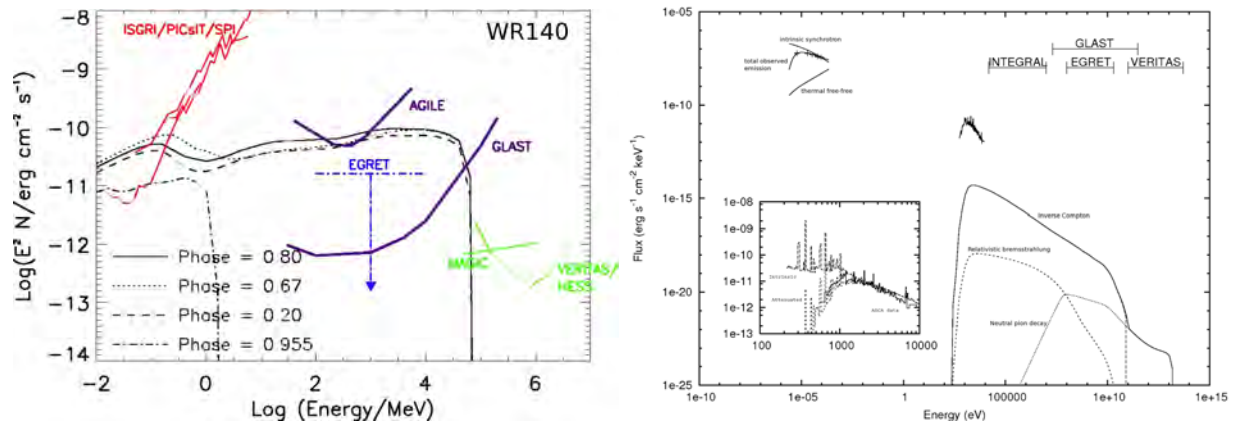
Figure 5: *Left:* Predicted IC spectra for WR 140 at phases 0.2, 0.67, 0.8 and 0.955 from Reimer et al. (2006). γ-ray absorption is not included. *Right:* The radio and non-thermal UV, X-ray and γ-ray emission calculated from model B in Pittard & Dougherty (2006), together with the observed radio and X-ray flux (both at orbital phase 0.837). The model IC (*long dash*), relativistic bremsstrahlung (*short dash*), and neutral pion decay (*dotted*) emission components are shown, along with the total emission (*solid*). See Pittard & Dougherty (2006) for more details.

Acknowledgements

References

Abdo A. A., et al., 2010, arXiv:1008.3235

Bednarek W., 2005, MNRAS, 363, L46

Benaglia P., Romero G. E., 2003, A&A, 399, 1121

Chapman J. M., Leitherer C., Koribalski B., Bouter R., Storey M., 1999, ApJ, 518, 890

Dougherty S. M., Beasley A. J., Claussen M. J., Zauderer B. A., Bolingbroke N. J., 2005, ApJ, 623, 447

Dougherty S. M., Pittard J. M., Kasian L., Coker R. F., Williams P. M., Lloyd H. M., 2003, A&A, 409, 217

Gayley K. G., Owocki S. P., Cranmer S. R., 1997, ApJ, 475, 786

Henley D. B., Corcoran M. F., Pittard J. M., Stevens I. R., Hamaguchi K., Gull T. R., 2008, ApJ, 680, 705

Henley D. B., Stevens I. R., Pittard J. M., 2003, MNRAS, 346, 773

Henley D. B., Stevens I. R., Pittard J. M., 2005, MNRAS, 356, 1308

Lemaster M. N., Stone J. M., Gardiner T. A., 2007, ApJ, 662, 582

Lührs S., 1997, PASP, 109, 504

Okazaki A. T., Owocki S. P., Russell C. M. P., Corcoran M. F., 2008, MNRAS, 388, L39

Parkin E. R., Pittard J. M., 2008, MNRAS, 388, 1047

Pittard J. M., 2007, ApJ, 660, L141

Pittard J. M., 2009, MNRAS, 396, 1743

Pittard J. M., 2010, MNRAS, 403, 1633

Pittard J. M., Dougherty S. M., 2006, MNRAS, 372, 801

Pittard J. M., Dougherty S. M., Coker R. F., O'Connor E., Bolingbroke N. J., 2006, A&A, 446, 1001

Pittard J. M., Stevens I. R., 2002, A&A, 388, L20

Pollock A. M. T., Corcoran M. F., Stevens I. R., Williams P. M., 2005, ApJ, 629, 482

Pope M. H., Melrose D. B., 1994, PASA, 11, 175

Reimer A., Pohl M., Reimer O., 2006, ApJ, 644, 1118

Stevens I. R., Blondin J. M., Pollock A. M. T., 1992, ApJ, 386, 265

Stevens I. R., Pollock A. M. T., 1994, MNRAS, 269, 226

Varicatt W. P., Williams P. M., Ashok N., 2004, MNRAS, 351, 1307

Vishniac E. T., 1983, ApJ, 274, 152

Vishniac E. T., 1994, ApJ, 428, 186

Walder R., 1998, Ap&SS, 260, 243

Walter R., Farnier C., Leyder J.-C., 2010, arXiv:1008.2533

White R. L., Becker R. H., 1995, ApJ, 451, 352

Williams P. M., van der Hucht K. A., Pollock A. M. T., Florkowski D. R., van der Woerd H., Wamsteker W. M., 1990, MNRAS, 243, 662

Zhekov S. A., Skinner S. L., 2000, ApJ, 538, 808

Mike Corcoran & Julian Pittard

Spectroscopic madness—A golden age for amateurs

Thomas Eversberg

Schnörringen Telescope Science Institute (STScI), Am Kielshof 21a, 51105 Köln, Germany

Abstract: Today, professional instrumentation is dominated by heavily oversubscribed telescopes which focus mainly on a limited number of "fashionable" research topics. As a result, time acquisition for massive star research, including extended observation campaigns, becomes more difficult. On the other hand, massive star investigations by amateur astronomers performing spectroscopic measurements are on a level which can fulfil professional needs. I describe the instrumentation available to the amateur, their observational skills and the potential contribution they can make to the professional community.

1 Introduction

The so-called "Golden Age of Astronomy" not only influences professional scientific work but also the amateur domain. Large instrumentation such as 1m class telescopes have reached the amateur domain (Fig. 1) and optics and CCD detectors are available off-the-shelf for relatively low prices. Today amateurs can accomplish extraordinary spectroscopic results, which would have been impossible a few decades ago. For instance, a typical amateur deep sky observer with a small home telescope can achieve results comparable to modern professional instrumentation, as shown in Fig. 2 for the *Hubble* Deep Field. Only about two decades ago amateur astronomers began with serious spectroscopic measurements of relatively bright objects, guided by professional needs. Today a worldwide network of spectroscopists with hot spots in France and Germany has been established. It includes instrumental experts who build their own equipment, scientists by education and pure beginners. Information exchange is done via internet (mailing lists, discussion forums, websites) and regular international conferences. It culminates in various professional-amateur (ProAm) projects, mainly on hot stars.

2 State-of-the-art amateur spectroscopy

In the past few years, various spectrographs have been successfully designed and constructed by dedicated amateur astronomers using off-the-shelf optics and blazed gratings, and have been properly adapted to respective telescopes. Two examples using standard photographic optics are shown in Fig. 3. The first generation of instruments delivering a spectral resolution of more than 10.000 are now also available commercially. The most popular device is the LHIRES III Littrow spectrograph by the company Shelyak in France (Fig. 4). Because of its simple plug-and-play design for typical amateur telescopes like Celestron and Meade it is widely used for different campaigns (see below). Above this, skilled amateurs now start to design their own Echelle spectrographs. Two examples are shown in Fig. 5. Today, the first off-the-shelf Echelle spectrographs are also available, including a

Figure 1: The 1.2m Melle telescope is the largest amateur instrument in Germany.
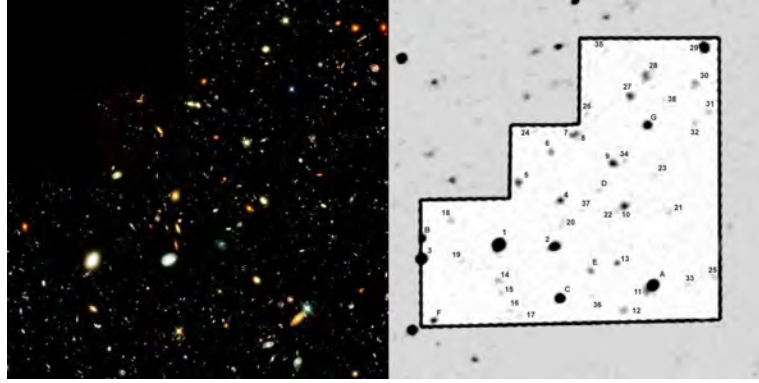

Figure 2: The *Hubble* Deep Field. Left: *HST*. Right: C14, 18 h exposure time, 10 km outside Cologne. The faintest objects have about 23 magnitudes in V. Courtesy Jörg Zborowska.

complete and tested software routine for a "plug-and-play" data reduction chain (Fig. 6)[1]. Amateur and off-the-shelf Echelle spectrographs have the same performance but are often cheaper than similar professional prototypes for small telescopes. This is mainly due to commercial off-the-shelf serial production.

3   Long-term campaigns, surveys, monitoring

Amateur spectroscopic equipment can easily be used for scientific investigations of stellar physics, particularly the study of bright emission line stars where line profile analysis of their often fast vary-ing spectra can be performed. For instance, using a standard 10 inch telescope, a signal-to-noise ratio (S/N) of about 100 can be achieved within 30 minutes for a star of about 8 magnitudes in V and for a two pixel resolution of about 1 Å. Objects of the order of $V = 10$ mag and fainter are generally ex-cluded due to limited amateur telescope apertures, although with longer exposure times and/or lower S/N this limit can be extended to even fainter stars. Hence, amateur spectroscopists can fill specific gaps for detailed investigations. These are **A) spectroscopic long-term campaigns** monitoring line profiles for periods of the order of months or even years, **B) surveys** to support detailed observations by large or space-based telescopes and **C) monitoring** of specific spectroscopic parameters over many years.

---

[1]www.shelyak.com

Figure 3: Typical amateur self-made spectrographs. *Left*: Device by Bernd Marquardt (Germany). *Right*: The maximum efficiency device by the author and Klaus Vollmann (Germany).
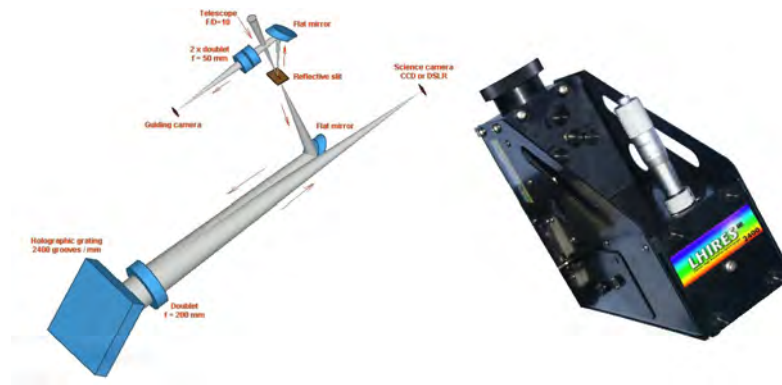

Figure 4: Off-the-shelf standard Littrow spectrograph LHIRES III from Shelyak.

3.1 The long-term ϵ Aurigae campaign

A prominent example of a long-term amateur campaign is the eclipsing binary ϵ Aurigae (F0Ia + companion) with an orbital period of about 27 years[2]. The respective campaign group[3] is internationally acting for the 2009 - 2011 eclipse of the star system. A periodic campaign newsletter regularly highlights recent events. Hα time series, obtained by Christian Buil from his balcony in Marseille using a Shelyak Echelle spectrograph (Fig. 6) is shown in Fig. 7. Because of its long period of 27 years ϵ Aurigae is simply a prototype object for amateur observations, impossible to perform by pro's on such a timescale (see also R. Leadbeater, these proceedings).

3.2 The long-term Mons campaign

The archetype of colliding-wind binary systems is the 7.9-year period and highly excentric WR+O binary system WR 140 (HD193793). Twenty-six amateurs and professionals from eight countries observed the prominent CIII wind line and its excess during periastron passage from Tenerife and from various home observatory in Europe to estimate the ephemeris of the system. All stations used the LHIRES III spectrograph. As part of this global campaign, Robin Leadbeater obtained spectra during periastron passage from his home observatory (Fig. 8). Figure 8 also shows his two spectra of

---

[2]http://www.threehillsobservatory.co.uk/epsaur_spectra.htm
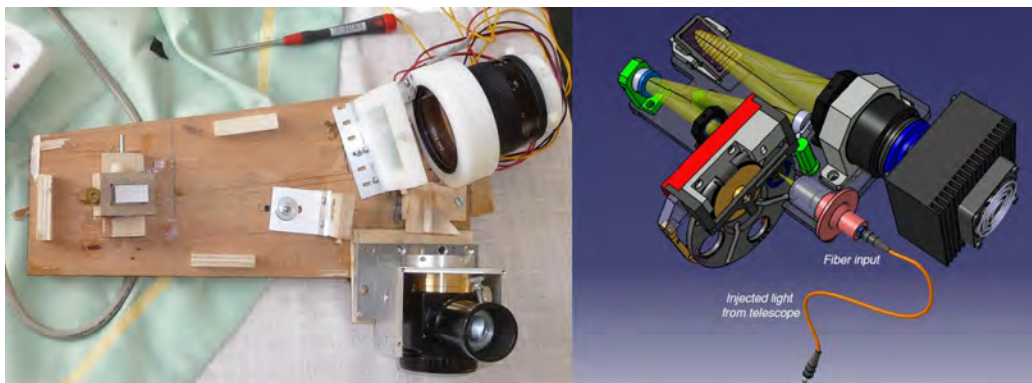[3]http://www.hposoft.com/Campaign09.html

57

Figure 5: Two Echelle prototypes both with grating cross-dispersers designed by the amateurs Berthold Stober (*left*) and Tobias Feger (*right*). The final device will be mounted in a solid casing. Note the wooden rack (*left*) for easy and fast geometrical improvements.
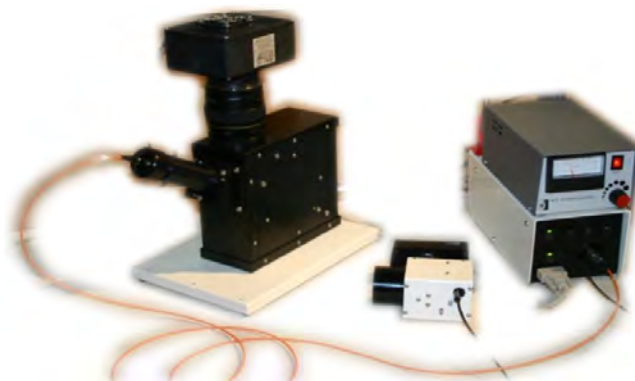

Figure 6: Off-the-shelf fiber-fed Echelle with prism cross-disperser from Shelyak.

CIII/CIV before and during periastron passage obtained with his configuration. The inset shows the resulting excess emission due to the wind-wind interaction shock cone.

3.3   Surveys

A "classical" example for an astronomical survey, supported by amateur observers, has been the astrometric *High Precision Parallax Collecting Satellite* (*Hipparcos*), launched in 1989. Amateur astrometry has been performed for centuries and dedicated amateurs had already the respective experience to obtain high precision data. As a result, many observers contributed their measurements to perform a successful satellite project. Such ProAm surveys are today possible in spectroscopy, as well. The presently most popular spectroscopic survey is the *COROT* Be Stars Survey[4] project for the astroseismology satellite *COROT* (*COnvection, ROtation and planetary Transits*). A respective amateur *COROT* survey of bright stars (e.g., Be stars), as performed under professional supervision can help understanding spectral variability like non-radial pulsations or oscillations in the respective Be star disks. Example spectrA, obtained by a French amateur group around C. Buil, are shown in Figs. 9 and 10.
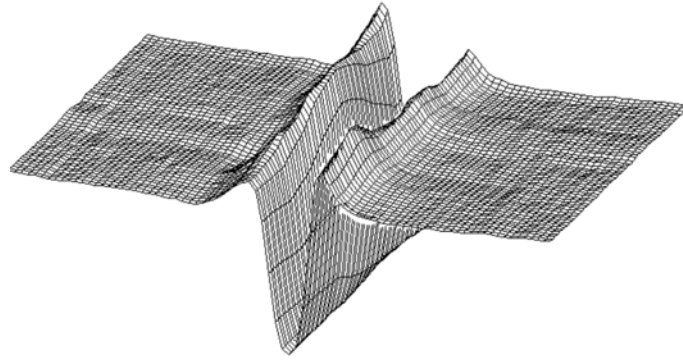
---

[4]http://www.astrosurf.org/buil/corot/data.htm

Figure 7: Hα time series for the eclipsing binary ϵ Aur between July 21, 2009 and March 10, 2010 with 3-days increment. Celestron C11, Shelyak Echelle spectrograph, average spectral resolving power R = 11000.
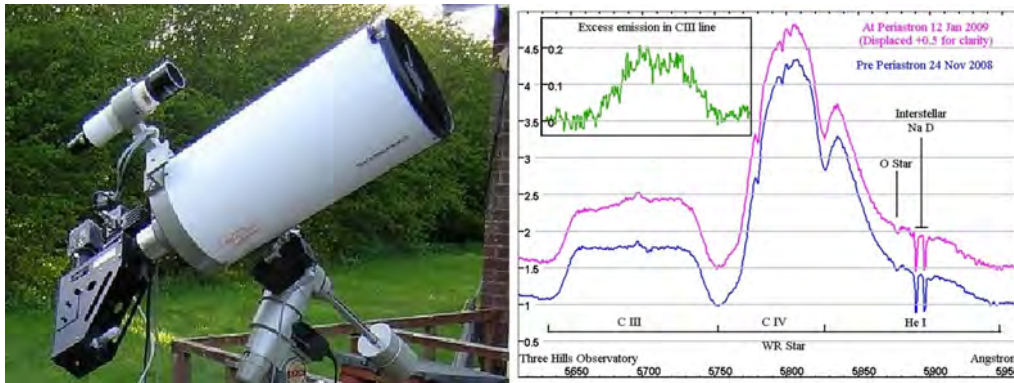

Figure 8: *Left*: The private Three Hills Observatory of Robin Leadbeater in Cumbria, England, consisting of a Vixen 20 cm Cassegrain and an off-the-shelf LHIRES III Littrow slit spectrograph. *Right*: Spectral variability of WR 140 within seven weeks obtained with the left instrument.

3.4   Monitoring

The most problematic task for professional spectroscopy is probably extremely long-term monitoring of specific spectral parameters. Only snapshots within relatively short time-scales are usually possible, resulting in large time gaps. The true long-term description of the physical behaviour remains hidden. Delays in publishing results, sometimes for several years, do not match the regular needs of a pro. Continuous monitoring is not a priority in professional spectroscopy. This, however, is one of the cornerstones of amateur work using simple standard procedures (e.g., equivalent width and radial velocity measurements) combined with well-known equipment and good routines. An example is shown in Fig. 11 for the Be star δ Scorpii. This Be star binary with an orbital period of about 11 years is one of the key targets of amateur work and for numerous observations. The next periastron passage will take place in July 2011 and is already in the focus of an extended ProAm campaign, including observations from Teide observatory, as for WR 140 (see Section 3.2).

4   How to establish a ProAm campaign

If the professional community wants to take advantage of amateur measurements one should keep some basic issues in focus. Instrumental knowledge and observational hands-on skills are already
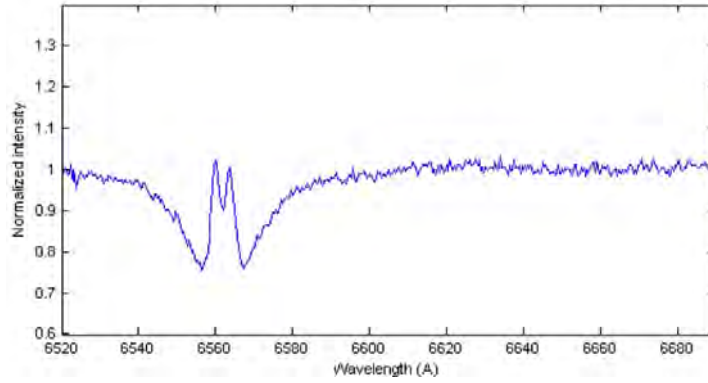
Figure 9: Hα amateur *COROT* survey spectrum of the $V =6.14$ B9Ve star HD194244, obtained with a Celestron C11 and an LHIRES III spectrograph with 2700 s exposure time.
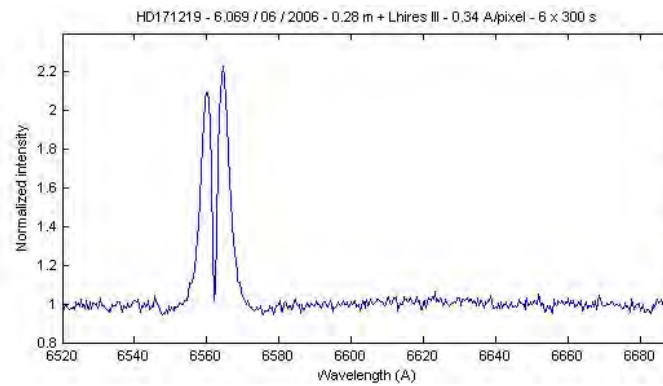

Figure 10: Hα amateur *COROT* survey spectrum of the $V =7.65$ B5IIIe star HD171219. Instrumental setup as above, but 1800 s exposure time.

present in the amateur domain. On the other hand, scientific knowledge (e.g., physics, procedures, data interpretation) need to be contributed by those who have a complete university education in this field and already have the relevant experience. The professional community can not expect complete campaign proposals from amateur astronomers but should first take their specific spectroscopic needs to the amateurs and discuss them. For instance, the Mons campaign on WR 140 took only place because of a close contact between a professional scientist (Tony Moffat) and one of his previous students who is now active in the German amateur community. The *COROT* Be stars survey project is mainly driven by a professional group[5] working closely together with amateurs in France[6], Germany[7] and elsewhere. Potential ProAm campaigns need some basic details. After an announcement in the respective communities it is essential to give information about the physical background and basic parameters (e.g., S/N, spectral resolution, etc.) to all interested observers. This is best done by a respective website. Unfortunately, there are only two well established communities of significant size, namely in France and Germany. In these two communities, respective discussion forums are available and it is recommended to use them for proper discussion. For the campaign management it is also recommended to separate science from administration issues. A highlight of each campaign is potential observing time at a professional observatory. Amateurs regularly do not have such access but are generally highly interested to go for it—often even at their own expense (if limited), as
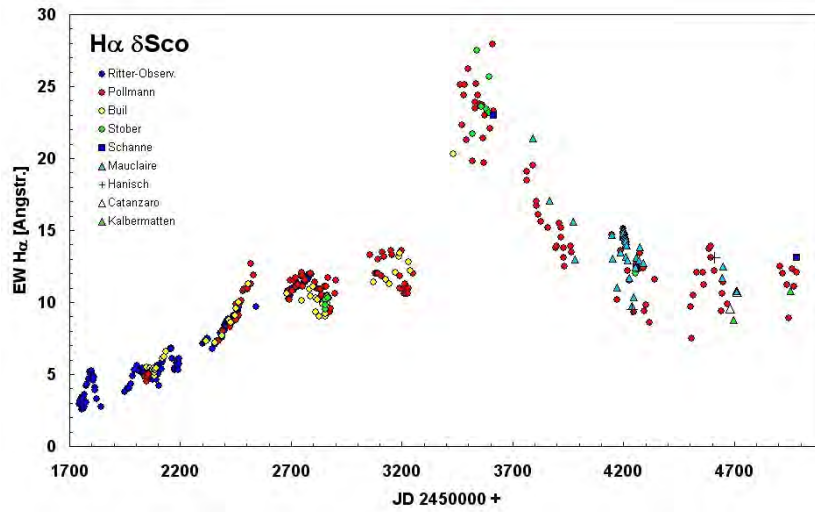
---

[5]http://www.ster.kuleuven.be/ coralie/members.htm

[6]http://astrosurf.com/aras

[7]http://spektroskopie.fg-vds.de

Figure 11: Hα equivalent width measurements for the Be star δ Scorpii over about nine years. Note that the first measurements taken by professionals (blue circles) have been dramatically extended by a group of amateur astronomers.

happened for the Mons campaign. Finally one should find some minimum financial resources (depending on the observatory site) to cover potential financial deficits (higher equipment transportation costs, unforeseen events, etc.).

5   Future plans and Summary

In May 2010 most of the key players in the WR 140 MONS campaign organised a wrap-up meeting at Convento da Arrábida[8] close to Lisbon, of which these are the proceedings. The group, now called "ConVento", will establish an informal website covering future ProAm campaigns, respective information about specific stellar targets and a mailing list / discussion forum. Every interested spectroscopist and photometrist is invited to join the group. The link to this website will soon be found at www.stsci.de. Considering the present situation in astronomy it seems obvious that skilled and sophisticated amateurs equipped with state-of-the art instrumentation in their domain, can successfully contribute their knowledge and enthusiasm to modern spectroscopic campaigns, either at their home observatories or at professional sites. The only obstacle to making continuous observations like those at professional sites is the local weather and the fact that amateur astronomer usually have to work in their daily job. This however can be circumnavigated by joint campaigns, as shown above. It is up to the professional community to uncover this valuable treasure.

Acknowledgements

I thank Tony Moffat, Thierry Morel and Gregor Rauw for their lasting support.

---

[8]http://astrosurf.com/joseribeiro/e_arrabida.htm

Thomas Eversberg

Recent ProAm Campaigns:
Be stars, *COROT* and others

Jose Ribeiro

jmscrib@gmail.com - ConVento Group

1   Introduction

The ProAm effort in modern astronomy and astrophysics is now a reality. The achievements of amateur astronomers throughout the early history of astronomy are well known. However, during the 20th century, the high specialisation and the technology required for dealing with the astronomical issues of that epoch, forced a natural separation of the professional activities from the amateur ones. Nowadays, technology has become much cheaper. Amateur astronomers have equipment capable of producing scientific results within their reach. Good equipment pushes some amateur astronomers to learn more, recovering their dialog with professionals. ProAm activities may be fruitful in data mining, in database feeding, in long-term campaigns and even in casual observations.

2   The French Effort

The French effort in the development of ProAm collaborations is paradigmatic. In 2003, the CNRS and the amateur association AUDE organised a school of astrophysics for amateurs with the aim of preparing collaborators for some of their projects, namely the ground-based support for a mission of *COROT* on the physics of Be stars'. This school resulted in the development of an affordable spectrograph, able to do science. At the end of 2005, 76 spectrograph kits of the LHIRESIII type were distributed. LHIRESIII is of a Littrow design and achieves a resolution of 17000 in Hα. In May 2006, a new school was organised in order to teach the use of the spectrograph, as well as all the reduction and calibration procedures. At this school, two long-term collaborations were launched, one on RR Lyrae, and another on Be stars. A database on Be stars was in preparation. In December 2006, *COROT* was launched. During the first trimester of 2007 the database of Be Star Spectra (BeSS, http://basebe.obspm.fr/basebe/), led by the Paris-Meudon Observatory, was available on the web for both professionals and amateurs who wished to deliver Be star spectra. In August 2007, at a practical spectroscopy course at the Observatoire de Haute-Provence (OHP), some brainstorming was done in order to organise the Be star observations. Issues as observing frequency, activity alerts, and observer night preparation were discussed. At the OHP course in June 2008 a very useful tool, the Arasbeam, was born (http://arasbeam.free.fr/?lang=en). It is a web site that each observer consults in order to choose the most urgent stars to be observed. This way, the community maximises the coverage of these stars. Thanks to that, the results speak for themselves:

- Eight Be activities were detected since then.

- 10640 amateur spectra in BeSS.

- 476 different Be stars $m(V) < 9$, dec > -25 (since 6/2008, after ArasBeam implementation).

- Only 144 different Be stars were in BeSS before 5/2008!

- Only 60 Be stars of $m(V) < 9$ don't have any spectrum.

- All stars of $m(V) < 7$ have at least one spectrum.

- From the *COROT* mission on Be stars, two refereed papers resulted with amateur co-authors (Gutiérrez-Soto et al. 2009; Neiner et al. 2009).

- The French site ARAS[1] also organised some long-term observational campaigns on several other targets.

- Another refereed paper used BeSS data, and includes an amateur as co-author (Štefl et al. 2009).

3 The Czech ProAm Collaborations

Some scientists from the Astronomical Institute of the Czech Republic and from the Astronomical Institute of the Charles University in Prague accept collaborations with amateurs in spectroscopy. Here, some long-term observations such as the follow up of upsilon Sagittarii are being performed. As of 2007, the phase curve of the radial velocity of the blue side of the Hα line was not well defined, with many missing points. Today, the behaviour of that line is well established, at least in the present state of the system. The Pleione system has been followed by the Czech group for nine years, recurring to the Czech Ondrejov and to the Canadian DAO telescopes. The orbital period of the system was already established by other teams. However, some doubts existed about the orbital eccentricity, and it was important to take some RV measurements during the superior conjunction of the system. At that date, it was overcast in Ondrejov and in Canada. It was clear in Lisbon, and four spectra were taken, three of them in three consecutive nights. This casual and independent observation was helpful for the study, resulting in a refereed publication (Nemravová et al. 2010). Many other examples of ProAm collaborations with the Czech scientists can be found in ADS (e.g., papers co-authored by C. Buil).

4 Conclusions

Better equipped and skilled amateur astronomers can make valuable scientific contributions. Today, amateurs have at their reach Echelle spectrographs. By applying algorithms that before were only at the reach of professionals, amateurs can obtain RV results unthinkable a year ago! A 28 cm telescope equipped with an Echelle, in the suburbs of Toulouse, reached 75 m/s radial velocity!![2] The recent campaigns for the coverage of the WR 140 periastron and the still ongoing epsilon Aurigae eclipse are paradigmatic examples of the importance of coordinated work. The role of the secular AAVSO in photometry and of ARAS in spectroscopy are good examples of this. In future, an organization coordinating all ProAm activity across all astrophysical techniques and all wavelengths, aiming for long-term campaigns, is needed. Recently the first steps in that direction were set by the creation of the

---

[1] http://www.astrosurf.com/aras/

[2] http://www.astrosurf.org/buil/extrasolar/obs.htm

ConVento group during the workshop "Colliding Winds in Interaction", held in Portugal[3]. Although exclusively dedicated to stellar astrophysics, it is the first ProAm international group covering all the astrophysical wavelengths and all astrophysical techniques (http://www.stsci.de/convento/).
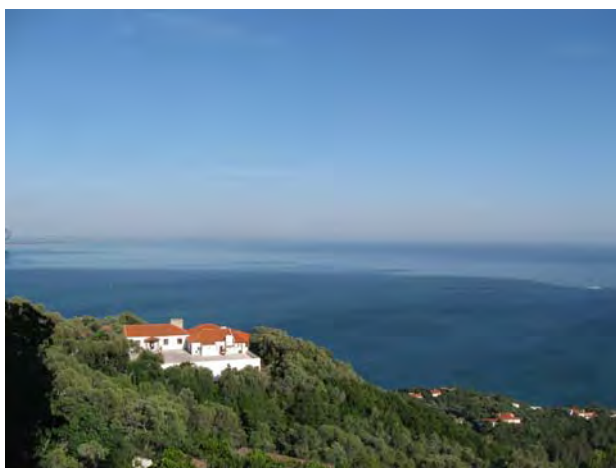
References

Gutiérrez-Soto, J., et al. 2009, A&A, 506, 133
Neiner, C., et al. 2009, A&A, 506, 143
Nemravová, J., et al. 2010, A&A, 516, A80
Štefl, S., et al. 2009, A&A, 504, 929

---

[3]http://astrosurf.com/joseribeiro/e_arrabida.htm

Robin Leadbeater & José Ribeiro

Convento da Arrábida

The International
Epsilon Aurigae Campaign 2009-2011.
A description of the campaign
and early results to May 2010

Robin Leadbeater

Three Hills Observatory, UK
robin@threehillsobservatory.co.uk

1 Background

In early 2009, immediately following the end of the WR140 periastron campaign (see these proceedings), I turned my telescope back to ϵ Aurigae in time for the start of the eclipse. As well as being an interesting object in its own right, the Pro-Am campaign being run on ϵ Aurigae during the current eclipse is a good example of how amateur spectroscopists can make a useful contribution. ϵ Aurigae is a naked eye magnitude 3 star and was first noted to be variable by Johan Frisch in 1821. It was subsequently found to be an eclipsing binary with a period of 27.1 years which undergoes an approximately 2 year long flat-bottomed eclipse with approximately 0.8 magnitude drop in V (Fig. 1, note also an apparent brightening around mid eclipse in this light curve from the last eclipse.)
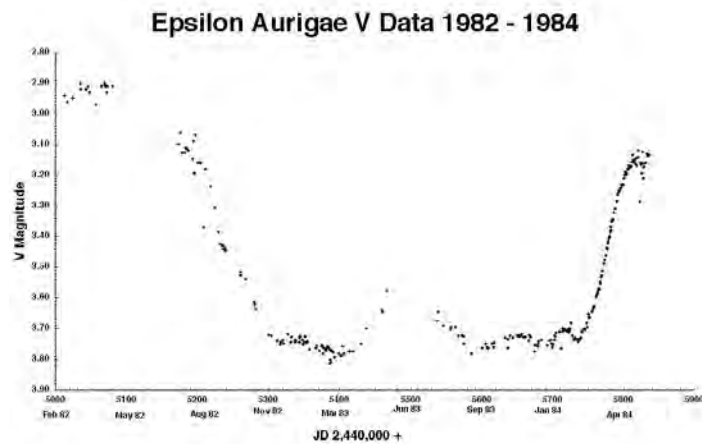

Figure 1: V-band light curve of ϵ Aurigae during the last eclipse (Hopkins 1987; R. Stencel, private communication).

All the visible light from the system appears to come from one component (an F-type star) with no visible light from the eclipsing object, which clearly cannot be a normal star given the large size and

very low luminosity in the visible part of the spectrum. Since we see only one component, there is not enough data for a complete orbital solution so there has been plenty of room for speculation over the years as to the size, mass and nature of the components and the scale of the system. To make life more difficult, the F star also shows variability outside eclipse both in brightness and in its spectral lines. Every 27 years a new generation of astronomers with a new generation of instruments try to solve the mystery. This time amateurs equipped with high resolution spectrographs are joining in the fun.

2 Review of early results from the current eclipse

- Eclipse began - 17th Aug 2009

- "2nd contact" - 9th Jan 2009

- Mid-eclipse - 4th Aug 2010

- "3rd contact" - 19th Mar 2011

- Eclipse ends - 13th May 2011?

The star is currently (May 2010) in eclipse, with 1st contact having occurred 17th August 2009 and mid eclipse due in about 2 months time (4th August 2010). Already during this eclipse there have been some announcements which have changed our thinking on the system. The so called "high mass" model was the common consensus model up to the end of last year (2009), with an F supergiant eclipsed by a disk of opaque material with possibly at least 2 B stars hidden at the centre to take care of the mass-luminosity discrepancy (Fig. 2).

This view has now been challenged following publication of a combined UV/Visual/IR spectrum by Hoard, Howell, & Stencel (2010; hereafter HHS) in which components from a single B5 star in the UV, a cool disk in the IR and the F star in the visible have been identified. The inference from this is that the F star is not a supergiant but a highly evolved object (post AGB?) with low mass but large diameter. The disk would then contain a single main sequence B star. The scale of the system is also reduced by about 40% compared with the high mass model (Figs. 2 and 3).
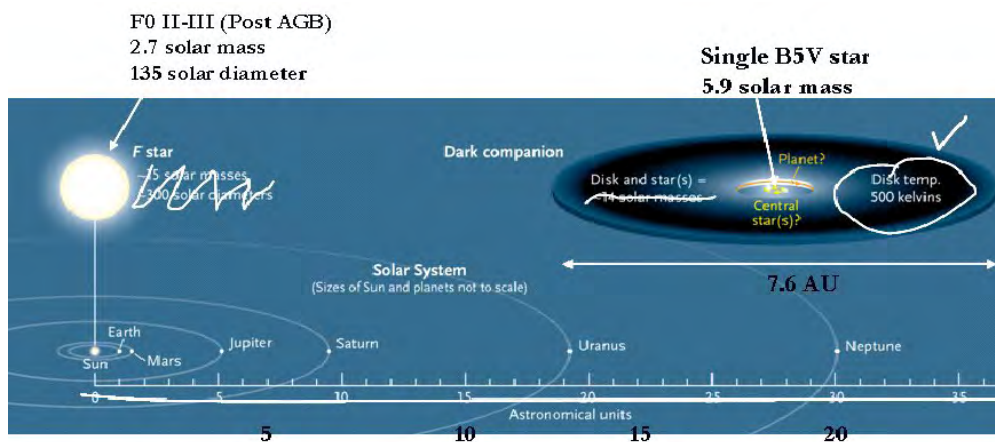

Figure 2: Modifications to the consensus model following the HHS paper.

Also just announced in Nature this April (2010) are remarkable direct observations of the disk crossing the F star made by Kloppenborg et al. (2010) using the CHARA interferometry system
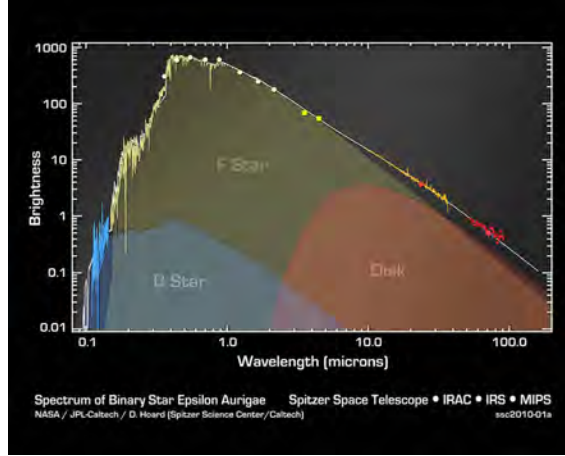
Figure 3: Taming the Invisible Monster: System parameter constraints for ϵ Aurigae from the Far-ultraviolet to the Mid-infrared (Hoard et al. 2010).

(Fig. 4). The scale of the system and rate of movement measured from the interferometry is consistent with the HHS low mass model.
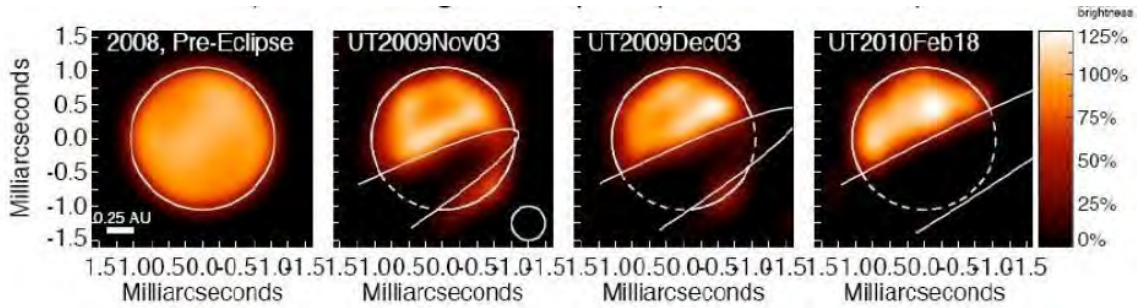

Figure 4: Infrared images of the transiting disk in the ϵ Aurigae system (Kloppenborg et al. 2010).

3 The role of amateurs—Photometry

So what part are amateurs playing during this eclipse? An international campaign is running to provide information exchange and to collect amateur data. This is being organised by professional Bob Stencel and amateur Jeff Hopkins, who also collaborated during the last eclipse, Jeff Hopkins coordinating the collection of photometric data. I have joined them in the past few months to coordinate the amateur spectroscopy side of things. (There is also an international outreach/education project "Citizen Sky" being run by AAVSO, aimed at non-specialists interested in finding out how scientific research is done but I will be concentrating on the work being done by experienced amateurs in this paper.)

By filtering out the medium-timescale brightness variations which are also seen outside eclipse, an estimate of 2nd contact can be made from the V mag curve for the eclipse to date (Fig. 5).

If the CHARA images are superimposed, however, it is immediately clear that the point identified as 2nd contact is not the traditionally defined point when the disk reaches the far edge of the star. Instead it likely corresponds to the point when the bottom half of the star is completely obscured. This explains the anomalously long ingress period ($\sim$140 days from the photometry compared with $\sim$90 days based on the star diameter and the orbital velocity of the system).
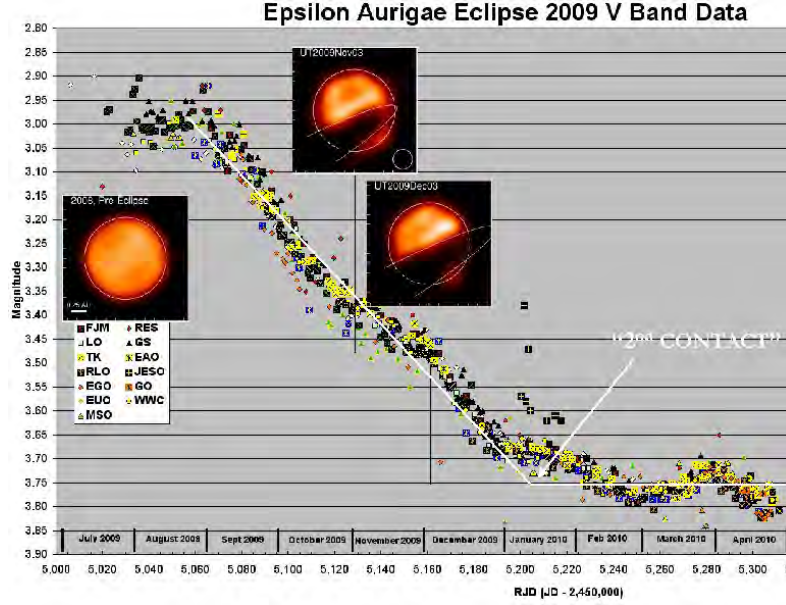
Figure 5: Hopkins et al. - International epsilon Aurigae campaign 2009-11 (http://www.hposoft.com/Campaign09.html)

4 The role of amateurs—Spectroscopy

What about ϵ Aur spectroscopically during eclipse? There are currently 12 amateur observers from five countries contributing spectra (Table 1). Most are following specific lines at $R \sim 18000$ using the LHIRES III spectrograph but two observers are providing wide wavelength coverage at $R \sim 12000$ using the new eShel fibre fed echelle spectrograph (see T. Eversberg, these proceedings).

I have recently set up a web page giving access to the spectra[1] and to date (May 2010) there are over 330. All the amateur data are made freely available for research purposes with conditions similar to those of the AAVSO, i.e., the campaign should be mentioned in papers and the observers included as co-authors if their data form a significant part of the paper. Figure 6 shows the coverage to date.
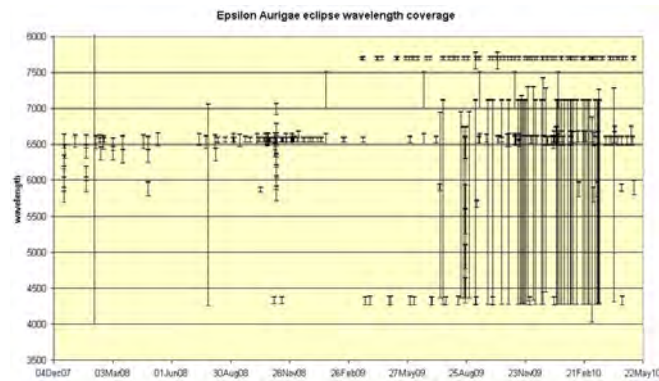

Figure 6: Spectroscopic coverage by amateurs during the current eclipse.

The wide coverage of the observations made using the eShel echelle spectrograph stand out compared with the narrow range of the LHIRES. The main lines covered are Hα and Sodium D. The set of results at 7700Å are mine and I will talk about them in more detail.

---

[1] www.threehillsobservatory.co.uk/espsaur_spectra.htm

Table 1: List of amateurs involved in the ε Aur campaign.

Lothar Schanne	Germany	LHIRES III
Jose Ribeiro	Portugal	LHIRES III
Robin Leadbeater	UK	LHIRES III
Christian Buil	France	eShel
Olivier Thizy	France	eShel
Benji Mauclaire	France	LHIRES III
Thiery Garrel	France	LHIRES III
Francois Teyssier	France	LHIRES III (low res)
Brian McCandless	USA	SBIG SGS
Jeff Hopkins	USA	LHIRES III
Stan Gorodenski	USA	LHIRES III
Jim Edlin	USA	LHIRES III

My observatory (Three Hills - Fig. 7) is located in the far north west of England and is housed in small plastic shed. The top half hinges off to reveal the telescope. It is controlled remotely from the house by wireless link. (There is no eyepiece and no room for a human observer!)

Figure 7: LHIRES III spectrograph at Three Hills Observatory.

The location is good for observing ε Aur which is circumpolar from my latitude. I also have a good horizon to the north which is important as ε Aur is only 8 deg altitude in June. The LHIRES III spectrograph is attached to the 280 mm aperture Celestron C11 telescope (this is an upgrade from the WR140 campaign when I used a 200 mm aperture telescope.). During eclipse the F star acts like a searchlight revealing different parts of the eclipsing object in silhouette as it moves past. This is depicted in Fig. 8.

As well as the opaque regions which are responsible for producing the light curve, the eclipsing object also has semi-opaque gaseous regions which produce an absorption spectrum when in front of the F star. By measuring the intensities and radial velocities of lines in the spectrum it is potentially possible to track the distribution and velocity profile of the gas component throughout the eclipsing object as it transits in front of the F star. The absorption features from the eclipsing disk are superimposed on the spectrum of the F star. Because the F star spectrum is variable and most of the lines are common between F star and disk, the removal of the F star features can only be approximate, but the result is a spectrum of narrow lines from the disk. By measuring the radial velocities (RVs) of

Figure 8: Sketch of opaque and semi-opaque regions in the rotating eclipsing disk just after second contact (the actual distribution of material in the disk is currently unknown).

the disk lines it is possible to identify the rotation of the disk. This was done during the last eclipse, for example, by Lambert & Sawyer (1986; hereafter L&S) who tracked the neutral potassium line at 7699 Å. The change in RV from positive to negative from ingress to egress is clear (Fig. 9).

The Hα line is an obvious line to follow but analysis is further complicated by variable emission wings which are seen outside eclipse, assumed to come from circumstellar material around the F star (a disk or outflowing wind?). The red and blue emission components swing up and down in intensity quasi-periodically and occasionally the absorption line has been seen to diminish significantly (Schanne 2007). Despite this, the emergence of an additional increasingly redshifted absorption component during this eclipse is clear (Fig. 10).
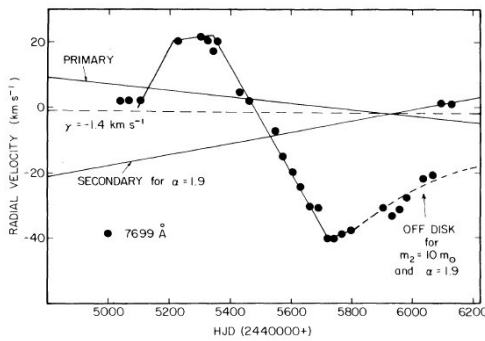

Figure 9: KI 7699 line radial velocity during 1982-84 eclipse (Lambert & Sawyer 1986).
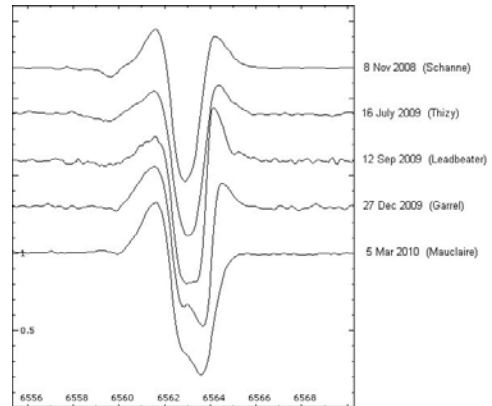

Figure 10: Hα line profile evolution during ingress.

I decided to concentrate on the KI 7699 Å line that L&S had studied. The main reason for choosing this line is that it is absent from the spectrum outside eclipse, so the effect of the eclipsing object can be observed directly (there is a small constant interstellar component which can be removed). It is surrounded by O_2 telluric lines, but fortunately they are far enough away not to interfere. In fact, they make useful calibration markers. To reach 7699 Å at maximum resolution I had to modify the grating adjustment on the spectrograph. At this wavelength the 2400 l/mm grating is set at a very low angle which gives good dispersion but low efficiency. My aim was to look in more detail at the evolution of the line profile by taking many more spectra than L&S had been able to do (89 spectra to date, one every 4-5 days on average compared with 8 by L&S in the same period. The false colour contour plot shows the evolution of the line (Fig. 11).

Note that the eclipsing object appeared in the spectrum over 2 months before the brightness started dropping. The line gets wider and the core of the line first moves slightly to the red and is currently (May 2010) moving to the blue. A preliminary analysis of what has been happening in this line has been published (Leadbeater & Stencel 2010). By measuring the maximum radial velocity at the red

edge of the line we can measure the orbital velocity of the fastest rotating component in front of the F star during the eclipse (Fig. 12).
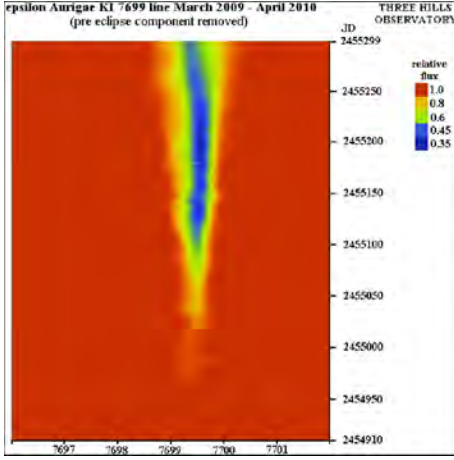

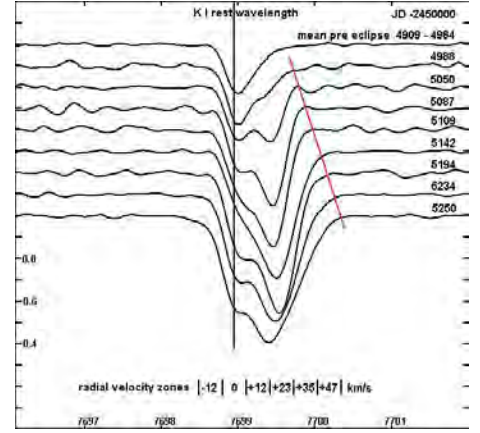Figure 11: 7699 Å line profile evolution during ingress.

Figure 12: Neutral Potassium 7699 Å line profile evolution during ingress.

As expected for a Keplerian disk, this velocity is low at the outer edge of the disk but increases as the smaller-radius parts of the disk move in front of the F star. These data can be used to estimate the central mass, giving a result which is consistent with the value published in the HHS paper (Fig. 13).
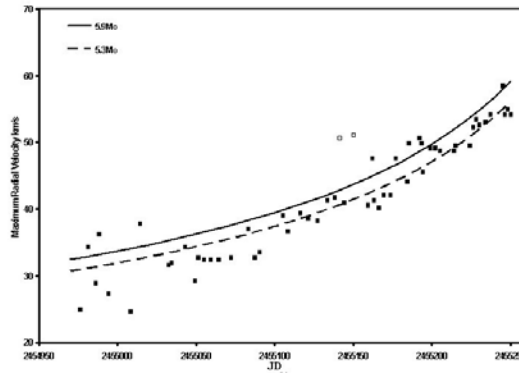

Figure 13: Radial velocity of the red edge of the 7699 Å line during ingress compared with that predicted for a Keplerian disk.

By plotting the equivalent width of the eclipsing object component of the line, we see that the development is not smooth but takes place in a series of steps, marked by letters (Fig. 14, the first two of which occur before the decrease in brightness).

These steps were confirmed by some observations made by Apache Point Observatory using the 3.5 m ARC telescope (W. Ketzeback, private communication), though they were unable to cover the initial emergence of the KI component. The steps are assumed to represent changes in density in the disk profile and it is difficult to resist speculating that the disk might have a ring-like structure, though these may be spiral arms or arcs (Fig. 15).
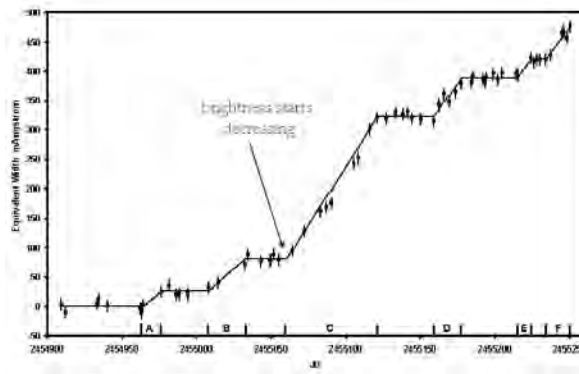
Figure 14: Excess equivalent width of 7699 Å line during ingress (out of eclipse component removed).
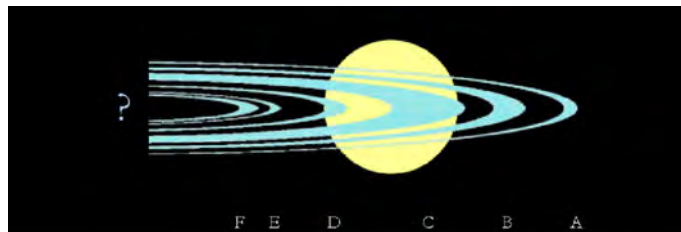

Figure 15: Schematic of the postulated density variations in the eclipsing disk.

5   Latest results

There have been differences in the behaviour of the lines on the approach to mid eclipse. The KI 7699 line started moving to the blue in March followed by the Na D lines in May but as of May 2010 the Hα line continues to move to the red (Figs. 16 to 18).

6   Prospects for the rest of the eclipse

To bring the story right up to date, there are also reports that the brightness is now increasing but caution is needed to make sure the correct extinction corrections have been applied now ϵ Aur is at low elevation (not a problem with the spectra which are normalised to the continuum.) The next month or two will be difficult observing conditions owing to the low elevation and twilight. The picture shows an actual observing run at Three Hills at solar conjunction last June (Fig. 19). There are fewer tree branches this year!

References

Hoard, D. W., Howell, S. B., & Stencel, R. E. 2010, ApJ, 714, 549
Hopkins, J. L. 1987, IAPPP, 27, 30
Kloppenborg, B., et al. 2010, Nature, 464, 870
Lambert, D., Sawyer, S., 1986, PASP, 98, 389
Leadbeater, R., & Stencel, R., 2010, arXiv:1003.3617
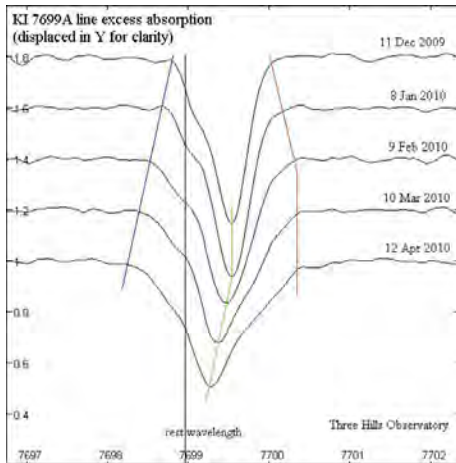Schanne, L., 2007, IBVS, 5747, 1
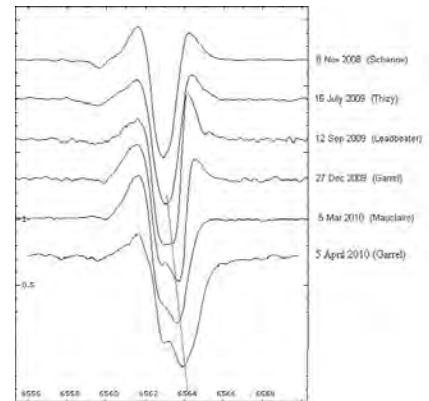
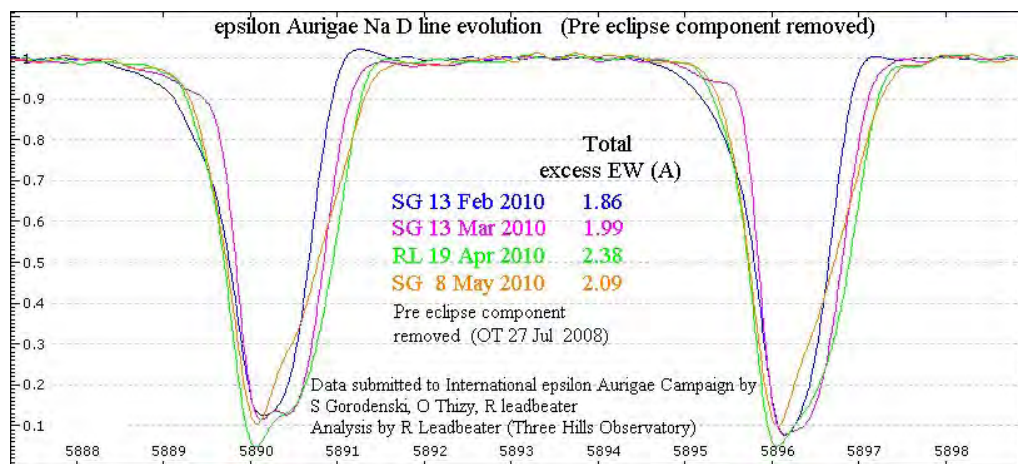Figure 16: Latest KI 7699 spectra.

Figure 17: Latest Hα spectra.

Figure 18: Latest Na D spectra.

Figure 19: Observing ε Aurigae at Three Hills Observatory during solar conjunction 2009.

Robin Leadbeater

Scientific collaborations in astronomy between amateurs and professionals

Johan H. Knapen[1,2]

[1] Instituto de Astrofísica de Canarias, E-38200 La Laguna, Tenerife, Spain
[2] Departamento de Astrofísica, Universidad de La Laguna, E-38205 La Laguna, Tenerife, Spain

Abstract: As our successful Mons campaign to observe WR140 has shown, there is a strong interest among both amateur and professional astronomers to collaborate on specific scientific questions. I highlight here some recent examples of successful collaborations, and outline a number of areas of astronomy where Pro-Am collaborations are making a difference.

1 Introduction

Both professional and amateur astronomers have been studying the skies for centuries. Their respective rôles, however, have changed considerably. In the 18$^{\text{th}}$ and 19$^{\text{th}}$ century, for instance, one of the main tasks of professional astronomers was to calculate astronomical data to be used by the merchant fleet and the military, and to provide the society at large with important data such as the times of sunrise and sunset and, in fact, time itself. Amateur astronomers meanwhile entertained themselves with what most astronomers might now consider more interesting activities, such as discovering planets and comets, and observing nebulae. Well-known amateurs include Caroline Herschel (1750-1848) who discovered several comets, and her brother William (1738-1822) who discovered Uranus, several moons of that planet and of Saturn, created a catalogue of nebulae (a term used at the time to describe any extended object), and observed double stars. He constructed hundreds of telescopes, and made a number of important discoveries related to light and radiation. Needless to say, amateur astronomers at the time were wealthy individuals.

While in the 19$^{\text{th}}$ century the interests of professional and amateur astronomers started to overlap more and more, they diverged again during the 20$^{\text{th}}$ century. One of the main reasons for this is that professionals started to use expensive and exclusive telescopes, such as the ones used by Hale and Hubble in California, which were out of reach of all amateurs.

We are now at the start of the 21$^{\text{st}}$ century, and one of the characteristics of our modern times is the almost ubiquitous availability of high-quality yet relatively cheap technology. So whereas professional astronomers now use very advanced instruments, including very large optical and radio telescopes, and massive supercomputer power, interested amateurs can start to use technologically advanced telescopes, cameras, and computers at a cost which is accessible to many millions of citizens around the world. In the next Section of this paper, I will summarise some of the areas in which amateurs can, and do, use these tools to help advance professional astronomy.

2 Professional-Amateur Collaborations

There are various areas of astronomy where amateurs can and do play a role. Almost without exception, these are based upon either the large amount of time that amateurs can dedicate, or the large amounts of independent observations or calculations they can collectively generate. I will give examples of some of these areas in the following subsections.

2.1 Ultra-deep exposures

In an era where professional astronomy keeps producing spectacular images of "deep-space" objects (galaxies, planetary nebulae, etc.), it is perhaps surprising that amateur astronomers can still help by obtaining ultra-deep exposures. This is mainly due to the combination of two factors, namely, first, that the level of surface brightness reached in an image does not depend much on the aperture of a telescope, and, second, that professionals rarely can spend a night, or longer, on obtaining a deep image of one single target. When amateurs do precisely that, the results can be spectacular.

An example of this is the ProAm collaboration between R. Jay Gabany and D. Martínez-Delgado and their colleagues. They use the private, robotic, Blackbird Observatory in New Mexico with a 20 inch RC Optics telescope to take deep images of nearby galaxies—reaching up to ten times fainter than images from the Sloan Digital Sky Survey (SDSS). This is achieved through a combination of a large field of view (a small telescope with a large CCD), long exposures, of typically 5-20 hours, and the use of a luminance filter which allows the maximum amount of light to pass to the camera. This is done at a very dark observing site.

As an example of their work, I reproduce in Fig. 1 their deep optical image of NGC 5907, a nearby galaxy with a set of conspicuous outer stellar streams. As described in detail in their paper (Martínez-Delgado et al. 2008), these stellar streams are thought to originate in a past encounter of NGC 5907 with a smaller companion galaxy, and yield very interesting constraints on cosmological models of galaxy evolution. This team has subsequently published more results on such beautiful amateur images of nearby galaxies, and several of their images can be found on their website (www.cosmotography.com) or on the Astronomy Picture of the Day (APOD) site (apod.nasa.gov). They serve as an excellent illustration not just of what amateur astronomers with dedication and state-of-the-art equipment can achieve, but also of how a successful ProAm collaboration can lead to scientific progress.

2.2 Meteors and Meteorites

When a debris particle (a small or large rock called a *meteoroid*) enters the Earth atmosphere, it burns and leaves a light-emitting trail (a *meteor*) which can be easily observed from the ground. If the particle was large enough, part of it can survive its descend through the atmosphere and fall on the ground, in which case the remnant is called a *meteorite*. Meteorites are interesting because they can shine light on the chemical and physical conditions outside the Earth, and on the past history of the Solar System.

Observations of meteors and the recovery of meteorites depends on many different observers, mainly because the events are short-lived, not generally predictable, and very much localised geographically. These observers (and recoverers, to a lesser extent) cannot possibly all be professionals, and amateurs thus play an important role. Many different reports of a meteor can be collected and lead to the calculation of a rather detailed three-dimensional orbit trajectory. In case of a very bright meteor, or fireball, one can then deduce whether, and if so where, a meteorite may have fallen. A search operation can then be mounted to recover the meteorite(s).

Figure 1: Stellar streams outside the main disk of the edge-on galaxy NGC 5907, as seen on this deep optical image obtained at the amateur Blackbird Observatory. Reproduced from APOD (2008 June 19); image credit and copyright: R. Jay Gabany (Blackbird Observatory)—collaboration; D. Martínez-Delgado (IAC, MPIA), J. Peñarrubia (U.Victoria), I. Trujillo (IAC), S. Majewski (U.Virginia), & M. Pohlen (Cardiff).

A rather spectacular case was reported last year by Jenniskens et al. (2009). This team studied the impact of a small asteroid, called 2008 TC3, over northern Sudan on October 7, 2008. After collecting reports of the meteor sighting, the team calculated a trajectory and deduced the most likely place of impact of the resulting meteorite(s). A search party was then organised with the help of local residents and students, and a total of 47 meteorites with a total mass of 3.95 kg were later recovered in this very sparsely populated desert region. Scientific results deduced from the meteorite recovery include the classification of the asteroid as F-class, most probably made up of a material so fragile that it had not previously been recovered from meteorites.

2.3   Asteroid Shapes

Even though they are small, asteroids moving in their orbits occasionally occult a star which is bright enough to be observed by amateur astronomers with modest optical equipment. Because many asteroid orbits are known to significant precision, as are the positions of bright stars, accurate predictions are available of when a certain asteroid will occult a star, and from where on Earth this should be observable. The observer sees the star reduce in brightness when it is occulted by the asteroid, for a certain duration of time depending directly on the linear size of the asteroid as it covers the sightline from the observer to the star.

If large enough numbers of observers collaborate by observing the same occultation from a
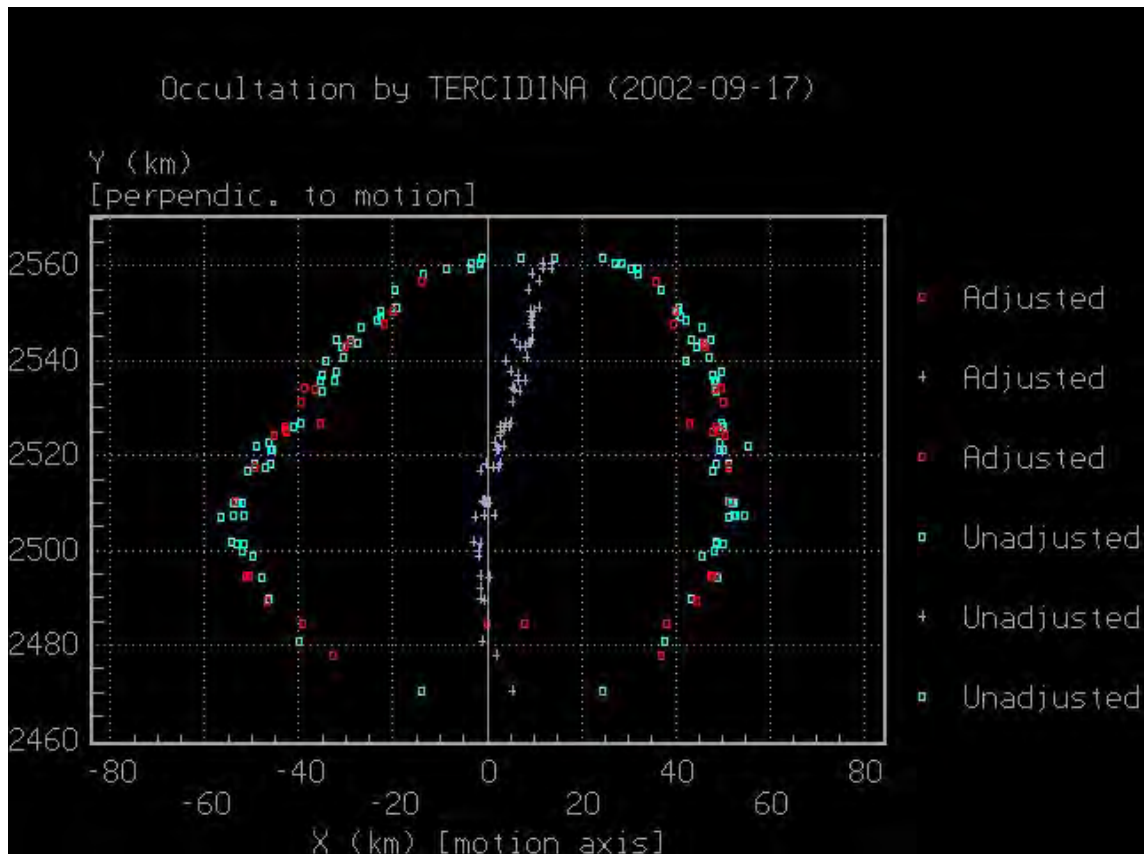
Figure 2: Projected image of the asteroid Tercidina obtained from over 100 individual observations of the occultation by this asteroid of the star HIP 19388. From http://euraster.net/results/2002/20020917-Tercidina.html.

densely populated region of the world and then combining their data, an accurate map of the asteroid can be calculated. This is illustrated in Fig. 2, which shows a detailed image of the asteroid Tercidina, based on the collective observations of 105 European amateur observers in 17 countries, 75 of which measured the occultation (the remaining "negatives" are equally useful to constrain the extent of the asteroid). The calculated image of Tercidina shows it to measure 92×106 km in size, and irregularities in its shape can be easily seen. Again, this is an example of many different amateur observers collaborating to reach a result that is impossible to obtain from one single viewpoint, even with the largest telescopes.

2.4 Comets and Bright Supernovae

The discovery of comets or bright supernovae has traditionally been a prime area for amateurs to contribute to astronomical scientific progress (also historically, e.g., Caroline Herschel). Nowadays, new asteroids and outer Solar system bodies are too faint to be discovered by amateurs, and are found through deep wide-area searches with professional observing programmes. But other "new" objects, particularly comets and supernovae, are still waiting to be discovered, and some of those discoveries continue to be made by amateurs.

Before roughly 1996, of order ten new comets were discovered per year, and between 10 and 60% of those were discovered by amateurs. New comets continue to be named after their discoverers, and some people become rather famous because of this.

Nowadays, some 200 new comets are being discovered every year, around 1% of which by am-

ateurs (so in absolute numbers not much has changed: a few new amateur comets per year). The increase in numbers is thanks to new ways of observing. In particular, the *Solar and Heliospheric Observatory* (*SOHO*) satellite, which has been observing the Sun for over 15 years now, has discovered roughly half of all known comets, a total of up to 1900. This is because in its observations, it blocks out the direct light of the Sun, and as a by-product its images can reveal small comets passing close to the Sun. It is interesting that a fraction of *SOHO*'s comets have in fact been discovered by amateur astronomers, looking through the vast data sets produced by the satellite. Several amateurs have discovered more than 100 of these comets each...

With supernovae the story is similar. Once a matter of chance discovery by amateurs carefully observing the night sky, most supernovae are now found with automated, professional, observing experiments. This development has specifically been driven by cosmological studies, which use supernova statistics to constrain parameters such as the fraction of dark energy in the Universe, and thus our cosmological understanding of the Universe. Bright supernovae can still be discovered by amateurs by finding "new" stars in galaxies or in certain regions of the sky. For instance, in 1987 the New Zealand amateur Albert Jones co-discovered the bright supernova 1987A in the large Magellanic cloud, which was the closest supernova for several hundred years.

2.5 Time Series and Variability

Although the introduction of queue scheduling helps to some extent, obtaining complete series of images or, especially, spectra of variable objects over long periods is becoming harder as telescopes get larger and access more competitive. One way out for some professionals is to build private dedicated telescopes, which are often robotic. But these are by their nature limited in the observing modes available, in access, and in the number and nature of objects that are observed.

Here is thus an interesting niche for enterprising amateur astronomers. They can nowadays make real contributions to scientific progress, mainly thanks to improvements in technology. This has lowered the cost and increased the availability of high-quality telescopes, spectrographs, CCD cameras, and data processing software. To make this efficient, amateurs should collaborate amongst themselves and with one or a few professionals who can provide scientific guidance, and lead the analysis and publication of the results obtained.

A very good example of such a collaboration is explained in detail in other contributions to these proceedings, which explain the various aspects of the Mons WR140 campaign. Such campaigns are technologically and intellectually challenging for those involved, and lead to scientific progress, as judged by contributions to the professional literature (e.g., Leadbeater & Stencel 2010; Fahed et al. 2011; Morel et al. 2011).

2.6 Classifying and Computing

A relatively new way of amateurs directly contributing to progress in science (not just astronomy) has been facilitated by the widespread availability of computers in people's homes and broadband internet connectivity. This has led to two new kinds of endeavours, namely amateurs classifying huge numbers of scientific images, and large scientific computing projects being executed on individuals' home computers.

2.6.1 Classifying by Amateur Volunteers

Amateur classification in astronomy started off in 2000 with the Stardust@home project, where volunteers could register to help NASA find impacts from interstellar dust particles on large series of

images taken by the Stardust spacecraft. That was followed in 2007 by the extremely successful GalaxyZoo project (galaxyzoo.org; Lintott et al. 2008). The team of professional astronomers who developed this set up a website where volunteers could look at images of galaxies from the SDSS and answer a number of simple questions, such as whether the galaxy had discernible spiral structure or not. This was hugely successful, probably because contributing to the project could be done from the comfort of one's home, at any time of the day, because participating was simple and did not require any investment in terms of purchasing equipment, or training, and because not only did one contribute to "real" science, there was also the chance to make significant discoveries. The fact that a volunteer might well be the first person ever to look in detail at a specific galaxy no doubt contributed to the success.

In the first year, GalaxyZoo collected some 50 million classifications from around 150000 volunteers around the world (many of these classifications were repeat observations, allowing the team to reach reliable results). By now, the team of professional astronomers behind GalaxyZoo has published around 20 scientific papers in the professional literature.

Undoubtedly the most famous GalaxyZoo participant is a Dutch school teacher named Hanny van Arkel. In 2007, she noticed a small blue-green patch of light below an SDSS galaxy and posted a message asking whether anyone knew what it was. No one knew, and it was called "Hanny's Voorwerp" (Hanny's Object). She has since collaborated with a number of professional astronomers who have concluded from additional observations that the patch is most probably a cloud of gas illuminated by a quasar (Józsa et al. 2009; Lintott et al. 2009; Rampadarath et al. 2010). Hanny's Voorwerp has made her famous, and her many media appearances make her an excellent ambassador of astronomy and of "citizen science" in general.

The GalaxyZoo project has since evolved into the "Zooniverse" (www.zooniverse.com), where thousands of volunteers continue to classify images of astronomical interest ranging from the surface of the Moon to supernovae and galaxy mergers.

2.6.2 Distributed Computing

Distributed computing uses a distributed system of computers which communicate through a network as a way of using spare computing capacity on many individual machines. In a number of areas of science, including astronomy, this is now being used very successfully to enlist the help of volunteers. The volunteer can contribute to a scientific computing project by registering as a participant on the web, and then allowing the project to execute calculations on his or her home computer. This is done when the computer has spare capacity, and often people leave their computers on at night. Volunteers thus contribute a bit of their time, and some electricity costs.

The area started in 1996 with prime number searches. In the field of astronomy, we can consider the SETI@home (setiathome.berkeley.edu; SETI stands for Search for Extra-Terrestrial Intelligence) project to be the pioneer. Starting in 1999, it has been using massively distributed computing to analyse large amounts of radio data on volunteers' home computers. To date, no signatures from life in space have been detected, but SETI@home is listed in the Guinness book of records as the largest computation in history. It has over 5 million participants world-wide, who no doubt all hope to own the computer that will process the first sign of extraterrestrial life.

The PlanetQuest programme (www.planetquest.org) tries to find extrasolar planets by reducing stellar imaging from major telescopes on home computers made available by volunteers. In other areas of science, the Folding@home (folding.stanford.edu) project is noteworthy: it uses massive amounts of computing power provided by volunteers to study protein folding and molecular dynamics.

3 Concluding Remarks

In astronomy, as in other areas of science, "citizen science" is important because it allows dedicated amateurs to contribute directly to scientific progress in collaboration with professionals, but also because it is a great way to popularise science. Many amateurs collaborate from the comforts of their home through computer-based projects such as the Zooniverse or SETI@home. Others are more traditional observers, some of whom have teamed up to provide valuable meteor, comet, or asteroid observations. Yet others, including the authors of other papers in these proceedings, use spectroscopic monitoring of interacting stars to provide professionals with data which are hard to obtain with professional telescopes.

Joining existing ProAm collaborations is sometimes possible for interested amateurs. Starting new ones depends on meeting the right professional astronomer, and may not be easy because there must be a good match between the quantity and quality of the data that the amateur can offer and what the professional needs to advance his or her scientific research. In general, such collaborations can be very fruitful, as the examples described above clearly illustrate.

References

Fahed, R., et al. 2011, in Proc. IAUS272 Active OB Stars: Structure, Evolution, Mass Loss and Critical Limits, in press

Jenniskens, P., et al. 2009, Nature, 458, 485

Józsa, G. I. G., et al. 2009, A&A, 500, L33

Leadbeater, R., & Stencel, R. 2010, arXiv:1003.3617

Lintott, C. J., et al. 2008, MNRAS, 389, 1179

Lintott, C. J., et al. 2009, MNRAS, 399, 129

Martínez-Delgado, D., Peñarrubia, J., Gabany, R. J., Trujillo, I., Majewski, S. R., & Pohlen, M. 2008, ApJ, 689, 184

Morel, T., et al. 2011, in Proc. IAUS272 Active OB Stars: Structure, Evolution, Mass Loss and Critical Limits, in press

Rampadarath, H., et al. 2010, A&A, 517, L8

Johan Knapen & Andy Pollock

Eva Santos & Johan Knapen

Nelson Viegas

Filipe Dias

Thomas Eversberg

Tony Moffat

Filipe Dias

Mike Corcoran

Remi Fahed   Mike Corcoran
        Andy Pollock   Tony Moffat

José Ribeiro   Luis Carreira